SEMIANNUAL REPORT
For the Period
1 May 1966 to 1 November 1966

LITERATURE SEARCH OF PHYSICAL PROPERTY DATA AND OF COMPOSITE SURFACE WORK FUNCTION MODELS

By

L. W. Swanson
A. E. Bell
C. H. Hinrichs
L. C. Crouser
B. E. Evans

Prepared for

Technical Management
NASA Lewis Research Center
Cleveland, Ohio
Electric Propulsion Office

15 December 1966

CONTRACT NAS3-8910

Field Emission Corporation
McMinnville, Oregon

Semiannual Report
For the Period
1 May 1966 to 1 November 1966

LITERATURE SEARCH OF PHYSICAL PROPERTY DATA AND OF COMPOSITE SURFACE WORK FUNCTION MODELS

By

L.W. Swanson
A.E. Bell
C. H. Hinrichs
L.C. Crouser
B.E. Evans

15 December 1966

CONTRACT NAS3-8910

Technical Management
NASA Lewis Research Center
Cleveland, Ohio
Electric Propulsion Office

FIELD EMISSION CORPORATION
Melrose Avenue at Linke Street
McMinnville, Oregon

TABLE OF CONTENTS

PREFACE

This is the 6 month report of a 12 month effort to (1) compile and review existing experimental facts relating to adsorption on the transition metals, (2) review pertinent theoretical descriptions of certain aspects of adsorption (e,g. binding, mobility, dipole moment formation etc.) and (3) develop from these reviews new empirical and theoretical views of adsorption phenomena. This interim report which summarizes the progress thus far is presented in two major divisions: Task I deals with the compilation and description of experimental results thus far reviewed and Task II contains critiques of several existing theories pertaining to various aspects of adsorption phenomena. The final report will contain a third section relating to new models and theoretical insights. It is hoped that the final version of this report will give the reader an up-to-date and comprehensible picture of adsorption phenomena on metallic substrates.

TASK I - LITERATURE SEARCH OF SURFACE PHYSICAL PROPERTY DATA

INTRODUCTION

During this report period, a search has been made for the significant literature up to August, 1966. The majority of the significant work comes from the period following about 1955 when ultra-high vacuum techniques began to extend the range of surface studies into the monolayer coverage region. A few exceptions occur, where the nature of the experiment minimizes the need for U.H.V. techniques. From this extensive exploratory work comes a large body of qualitative observations and an appreciable amount of theoretical speculation, both of which have been progressively refined, along with experimental techniques, to yield a rapidly growing bulk of basic quantitative information on surfaces.

Although experimental investigations of metal surface-adsorbate interactions have been conducted for many years, very few experiments carried out prior to the advent of ultra-high vacuum technology may be regarded as having meaning. This may be understood readily if reference is made to the length of time required for a monolayer of residual gas to be formed on a freshly-cleaned metal surface. If the pressure is of the order of 10^{-4} torr, a pressure within the capabilities of mechanical pumps, a monolayer is formed in less than 0.01 seconds. At 10^{-7} torr, a region commonly referred to as the high vacuum region, 10 seconds are required while in the ultra-high vacuum region of 10^{-10} torr or better a monolayer is formed only after about 3 hours. Thus, it becomes clear that one of the first considerations in evaluating the merits of an experimental technique is that of the vacuum conditions prevailing during the course of the experiment. This factor also established a reasonable starting point for a literature search since it was not until 1953 that the methods of measuring pressures in the ultra-high vacuum region were known. This is not to say that ultra-high vacuum had not been obtained prior to this date, but only that the number of reliable experiments is very small. No effort has been made here to describe the vacuum techniques since a number of excellent reviews are already in existence.

A second consideration which bears heavily upon the reliability of the experimental results is that of the condition of the surface. Since the interaction of the adsorbate with the surface is affected strongly by the presence of a contaminant, it is important that the surface be clean prior to adsorption. Thus, methods must be available for cleaning the surface if the experimental technique is to be acceptable. While the most direct method of cleaning the surface is by heating, it is not possible to clean some metals this way and other methods must be devised such as sputtering,

In most cases, the interpretation of the experimental results is complicated by the uncertainty associated with the structure of the surface, For example, if the surface is polycrystalline, it is difficult to identify the relationship between the experimental results and the surface structure. Total current field emission measurements of work function yield only weighted averages over all the crystal faces present. Therefore, priority is given to experimental techniques which permit studies to be made on single crystallographic plane.

A clear understanding of metal surface-adsorbate interactions can come only after an adequate store of experimental data have been collected. The quality of the experimental data depends in an important way upon the techniques used to obtain them. Indeed, the slow progress in understanding surface interactions may be attributed to the lack of sensitive techniques with which to obtain the experimental data.

SECTION A-EXPERIMENTAL TECHNIQUES

Objectives

The objectives of this section of the report are to outline the acceptable methods of acquiring the data listed in Task I, Section B of this report. An attempt has been made to present each experimental technique clearly enough that a reader may be able to read the pertinent papers with understanding. In each instance, the description has been treated in as elementary a fashion as possible. Because of the elementary nature of the descriptions, it is anticipated that the reader may wish to refer to some of the original papers or the several excellent reviews which have been written on the respective topics.

Presented in this section are the descriptions of five experimental techniques which have found favor among experimental surface scientists and which are considered to be among the more important techniques currently in use. These techniques have in common the features mentioned above and have been used extensively.

Attention has been given to the mathematical methods used in experimental analysis, particularly for those experimental techniques which require the use of kinetic equations for the interpretation of the results. One must understand the way in which the kinetic equations have been derived in order to fully appreciate the benefits and shortcomings of an experiment,, Only a general discussion is given on details of the experimental apparatus since these vary from experiment to experiment and the original papers should be consulted for further clarification.

Future Work

Future effort will be devoted to completing the descriptions of experimental techniques. In addition, it is considered beneficial to include a discussion of the various ways in which certain physical quantities are measured. Work has already begun on descriptions of methods of measuring work function and heat of adsorption. Other topics which will be included are the methods of determining sticking probability and coverage.

LOW ENERGY DIFFRACTION

Introduction

When a beam of low energy electrons (usually between 25 and 200 eV) is incident upon a crystal surface, a back reflected diffraction image is formed which, when properly analyzed, yields information concerning the atomic structure of the surface. The use of low energy electron diffraction to investigate surfaces had its beginning in 1927 when Davisson and Germer substantiated the wave nature of electrons and has been pursued by Farnsworth during the past 30 years. Recent improvements in vacuum practice and experimental techniques have inspired others to use this technique in the study of surface structure.[1,2,3] Basically, two approaches have been developed. In the first, a Faraday collector is used to analyze the diffraction image. This technique is time consuming and a major improvement in the design of the experimental apparatus was the incorporation of a phosphor screen and post acceleration of the diffracted electrons to allow direct viewing of diffraction pattern. A schematic of a low energy diffraction tube utilizing the latter method is shown in Figure 1.

To a first approximation, the electron diffraction centers have the periodicity of the substrate lattice parallel to the surface, and hence the surface becomes a two-dimensional diffraction grating. Actually, the diffraction pattern is influenced by the second and third layers so that the concept of two-dimensional grating in the case of low energy electron diffraction is not entirely appropriate. Furthermore, examples may be found, particularly in the case of certain crystals with diamond structures, in which the surface structure is different from the bulk of the substrate lattice.

Diffraction effects become important when the wave length of the incident beam is of the order of the spacing of the diffraction centers. The wave length for electrons accelerated through a potential difference of V volts is computed from

$$\lambda = 150.4/V^{1/2}\ \text{Å}$$

and if d_{hk} is the interrow spacing of atoms in a two-dimensional array, the conditions for diffraction maxima (Figure 2) are given by the Bragg condition

$$n\lambda = d_{hk} \sin \theta_{hk}$$

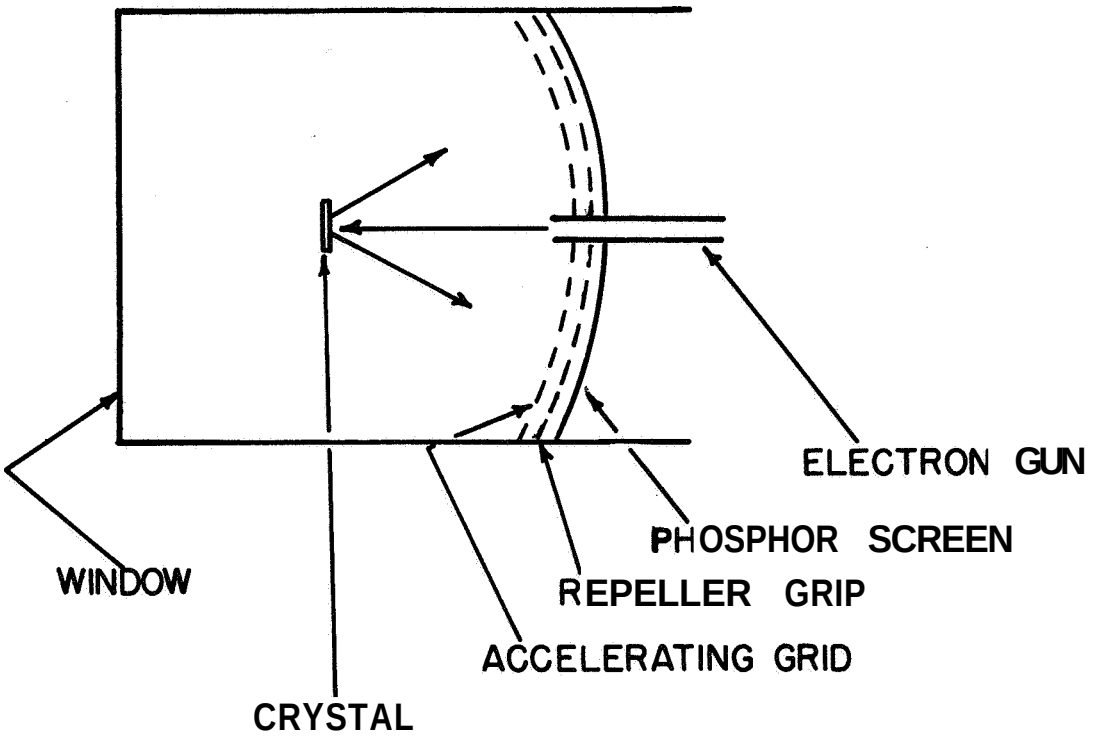

Figure 1. Basic components of a postacceleration display low energy electron diffraction tube.

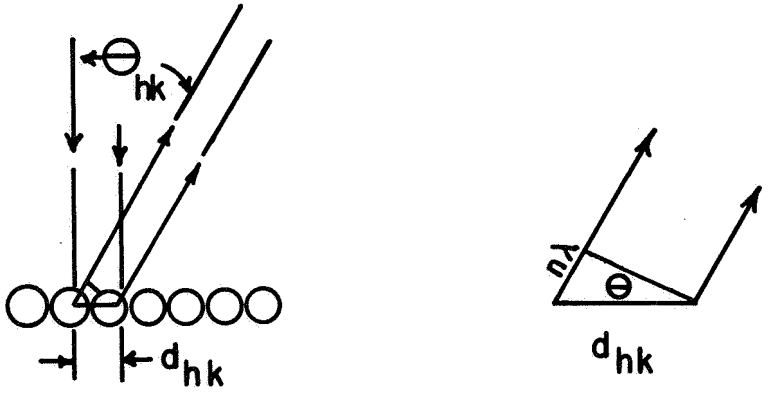

Figure 2. Illustration of conditions for diffraction image maxima.

where θ_{hk} is the diffraction angle measured relative to the surface normal and n is the order of the image. Diffraction images for two different cases of a surface parallel to a (100) plane and one parallel to a (111) plane are illustrated in Figure 3, The interpretation of these patterns is discussed in some detail below.

The scattering of the incident electrons occurs as a result of charge sensitive interactions at the surface; therefore, low energy electron diffraction effects are sensitive to perturbations in the surface charge distribution due to the presence of foreign atoms on the surface or other influencing factors. For example, it is possible, under favorable conditions to detect the presence of roughly 1% of a monolayer of adsorbate. In addition, it is possible to observe the effects temperature on the lattice vibrations of the surface atoms by a measurement of the Debye-Waller effect in which the intensity of the diffracted beam is found to depend upon temperature, Although the primary value of the method of low energy electron diffraction has been in providing information concerning surface structure, improvements in technique promise to make possible the investigation of such phenomena as catalysis, adsorption, epitaxy, chemical reactions, and order-disorder transitions.[1,2,3] Furthermore, low energy electron diffraction is a useful method for a wide variety of surface materials, provided a method of cleaning is available other than heating, e.g., ion bombardment. In fact, it is even possible to make measurements on dielectric surfaces if the surface is first sprayed with electrons to prevent surface charging during the experiment.[4]

Although low energy electron diffraction is a highly sensitive method, it is difficult to arrive at a completely fool-proof interpretation of the observed diffraction pattern which can be more complex than in the three-dimensional case because of the larger number of permissible structures.[5] Furthermore, the problem of interpretation is complicated by the fact that diffraction does not occur from the top layer of atoms alone but second and third atomic layers may contribute also. In addition, there are numerous other factors which add to the complexity of the diffraction image such as secondary electrons, interference effects due to scattering from steps in the surface layers, temperature effects, and uncertainty in the contact potential.[6] At present, these inherent complications make quantitative analysis of the diffraction image virtually impossible; however, it is possible to make corrections for many of the adverse effects and as these problems become better understood, more precise measurements are to be expected.

Surface Crystallography

As with three-dimensional crystallography, certain conventions have been established for the description of two-dimensional crystal structures. Actually, the conventions Lased in three-dimensional crystallography have been carried over to two dimensions with only minor modifications or extensions being required. These conventions have been discussed in detail by E.A. Wood[7]

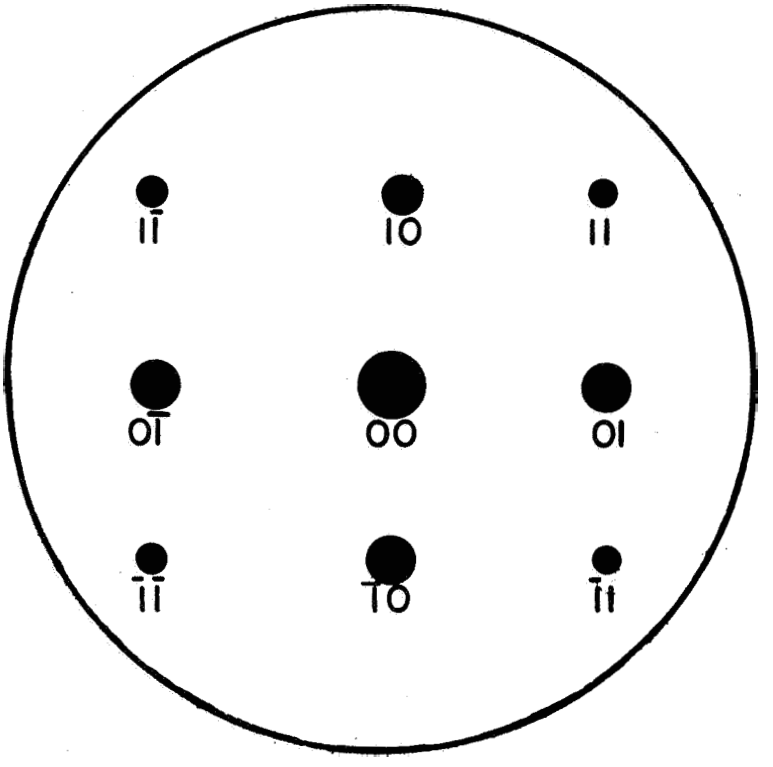

Figure 3a. Diffractionpattern characteristic of (100) plane.

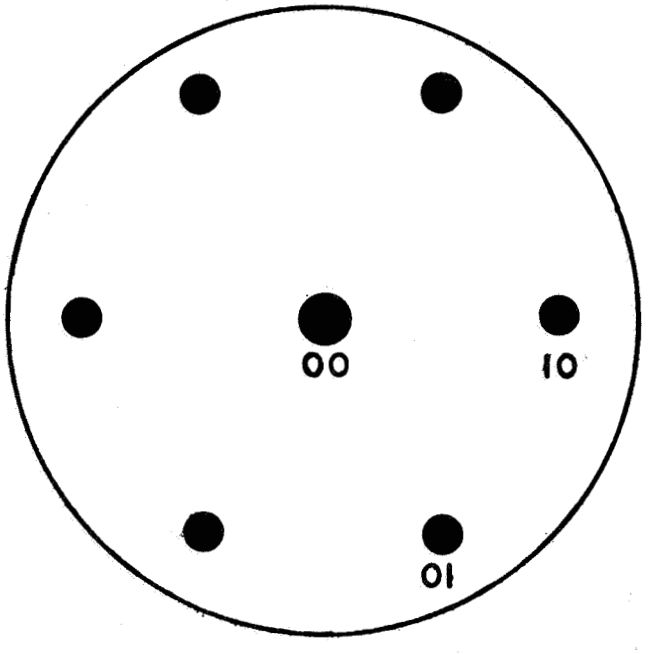

Figure 3b. Diffraction pattern characteristic of (111) plane.

and will be introduced here for the convenience of the reader.

In discussing two-dimensional structures, it is convenient to use the term diperiodic to describe any structure, not necessarily with all atoms lying in a plane, which has only two-dimensional symmetry (i.e., no symmetry in the direction normal to the surface). It has been suggested that the transition from the symmetry of the bulk lattice to the extreme of the surface be called the selvedge. The selvedge may be very thin as in the case of metal surfaces or may be three or more atomic layers thick as in the case of certain semiconductors and compounds.

The terms lattice and unit cells are reserved for three-dimensional symmetry and the corresponding terms to be used in the two-dimensional case are the net and unit mesh respectively. Here, a net is a two-dimensional array of points such that each has an identical environment. Note this is different from a diperiodic array which may be composed of atoms lying in more than one plane; diperiodic structures are formed by associating with each net point an assembly, or basis, of atoms. In two-dimensional crystallography five nets may be distinguished and are shown in Figure 4. The letter c denotes the use of a centered mesh while p indicates that the net is a primitive mesh. In all cases the convention requires that $a < b$.

Listed below is a set of standard symbols, based on the work of Wood, which appear frequently in the literature.

a, b: Lengths of unit-mesh edges such that $a < b$. Subscript s may be used to distinguish surface structure from underlying structure where necessary.

$\bar{a}$, $\bar{b}$: Unit-mesh vectors.

γ: Interaxial angle xy, ab.

x-, y-: Directions of crystallographic axes of coordinates.

x, y: Coordinates of any point within the unit mesh, expressed in terms of a and b units.

z-: Direction normal to x- and y- directions.

z: Coordinate of any point in this direction.

u, v: Coordinates of any net point, expressed in terms of a and b as units.

uv: Indices of a direction in the direct net.

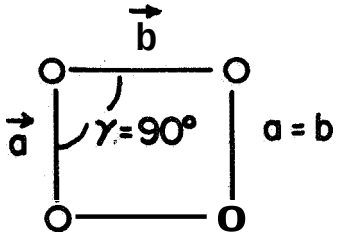

(a) SQUARE

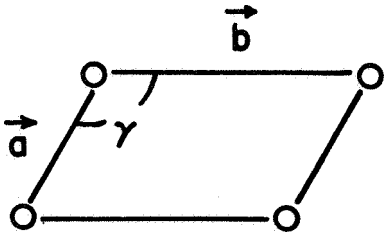

(b) OBLIQUE

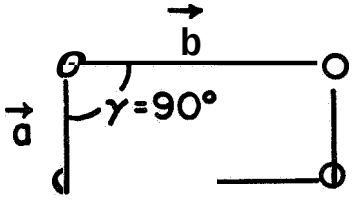

(c) RECTANGULAR

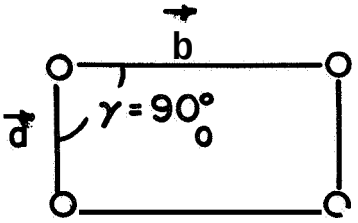

(d) CENTERED RECTANGULAR

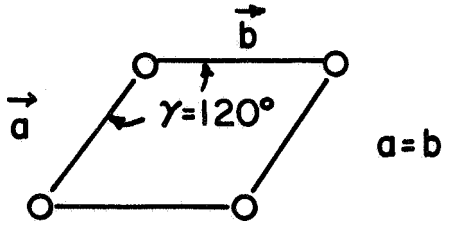

(e) HEXAGONAL

Figure 4. The five two-dimensional nets.

h, k: Two-dimensional Miller indices of mesh points.

(hk): Indices of a set of parallel rows.

hk Indices of the reflection from a set of parallel rows; coordinates of a line or "rod" in the reciprocal-lattice as measured on any plane normal to the lines.

hk: Indices of equivalent rows with different indices.

*: Starred quantities refer to quantities in reciprocal space.

$d_{(hk)}$: Interrow spacing of rows hk.

p, c: Primitive and centered nets.

The interrow spacings for the five nets are:

Oblique:

$$1/d^2_{(hk)} = (h^2/a^2\sin^2\gamma) + (k^2/b^2\sin^2\gamma) - (2hk\cos\gamma/ab\sin^2\gamma)$$

Rectangular: p and c

$$1/d^2_{(hk)} = (h/a)^2 + (k/b)^2$$

Hexagonal:

$$1/d^2_{(hk)} = 4/3\left[(h^2 + hk + k^2)/a^2\right]$$

Square:

$$1/d^2_{(hk)}$$

As in the triperiodic case, it is convenient to introduce the concept of a reciprocal lattice in the analysis of diperiodic structures. This, coupled with the Ewald sphere, provides a powerful aid in the reconstruction of the surface structure or net. The Ewald sphere is a sphere of radius $1/\lambda$ intersecting an arbitrarily chosen origin of the reciprocal net such that the incident beam passes through the geometric center of the sphere and the origin of the reciprocal net. In the diperiodic case, the requirements for diffraction are not quite so severe as for the triperiodic lattice so that the reciprocal lattice goes over from a set of lattice points to a set of lines or one-dimensional "rods" extending indefinitely normal to the plane. The various spots of the diffraction image may then be found from use of the Ewald sphere as shown in Figure 5, for the case of an electron beam incident normal to the (100) surface of a cubic crystal. Notice that in this case, spots corresponding to the 00, 10, 01, $\bar{1}0$ and $0\bar{1}$ reciprocal lattice lines will be present in the diffraction pattern,

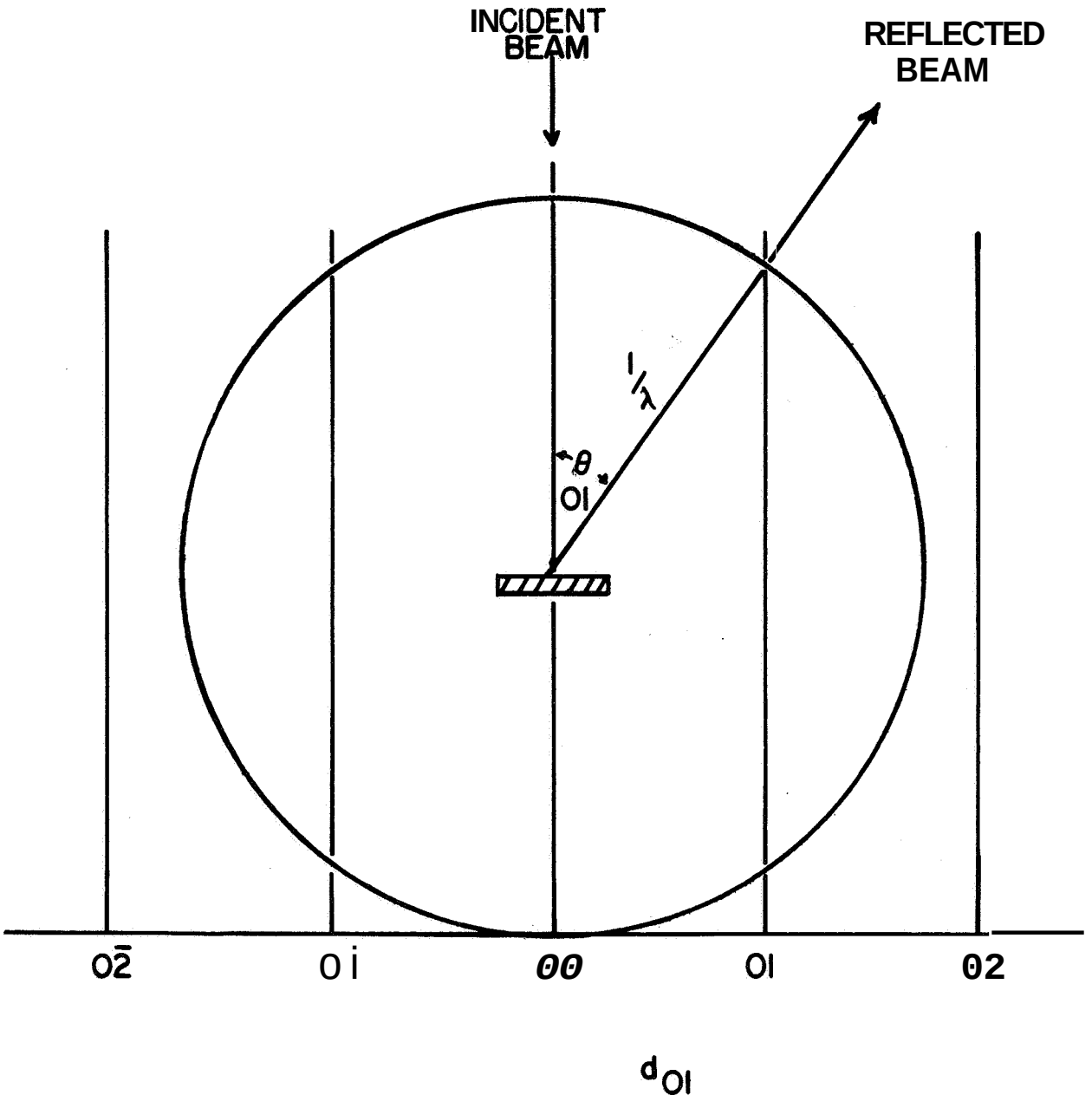

Figure 5. A section of the reciprocal lattice of a dipfriodic structure with the Ewald sphere. For the special case of normal incidence and $\lambda = d_{hk} \sin \theta_{hk}$.

but the 02, 20, $0\bar{2}$ and $\bar{2}0$ spots will be absent.

It sometimes happens that the surface mesh and the mesh of the corresponding plane in the bulk are different and it is useful to refer the surface mesh to that of the substrate. This situation arises in at least two ways; when the clean surface structure differs from the bulk and also as a result of adsorption. It is customary to describe the surface mesh in terms of the known substrate mesh. Here the reference net is the net parallel to the surface. Thus, if the substrate net is a square array and the surface is a square array with dimensions twice as large, the surface mesh will be designated 2 x 2 (See Figure 6a). Or in the case of the hexagonal structure shown in Figure 6b, the surface mesh is 3 x 1. The information contained in this short hand notation can be extended by including both the substrate material and the adsorbate. Thus, oxygen adsorbed on the (110) face of nickel is found to have the structure described by Ni(110) 3 x 1-0, meaning that when oxygen is adsorbed on the (110) face of nickel the resulting diperiodic surface structure has a mesh with edges parallel to the edges of the clean surface net but with a_s equal to 3a. If a centered mesh is chosen, the designation would be c(2 x 2) and is shown in Figure 6c. When a simplification results from consideration of a mesh whose sides are turned at an angle with respect to the substrate structure, then the designation 3 x 1-R(30°) has been used. This would indicate that the surface mesh with the indicated dimensions is rotated 30° with respect to the substrate mesh.

Summary

Low energy electron diffraction techniques have done much to further our knowledge of the surface-adsorbate interaction. In particular, low energy electron diffraction may be used to study adsorption, yielding information about adsorption sites, as well as coverage, and sticking probabilities. This technique is especially powerful when used in conjunction with other techniques such as flash desorption or work function measurements. In addition, valuable information concerning epitaxy, lattice vibrations, chemical reactions, catalysis and order-disorder transitions may be obtained, Although much may be learned from such studies, quantitative measurements are not yet possible due to the complexity of the electron scattering process at the surface,

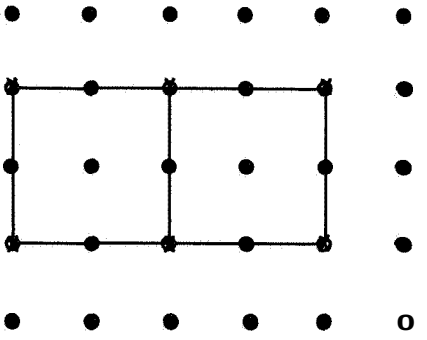

(a) 2x2 SQUARE MESH
o substrate mesh
x surface mesh

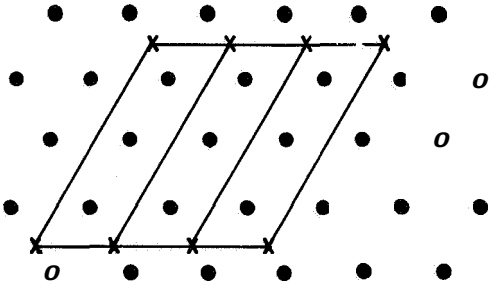

(b) 3x1 HEXAGONAL MESH
o substrate mesh
x surface mesh

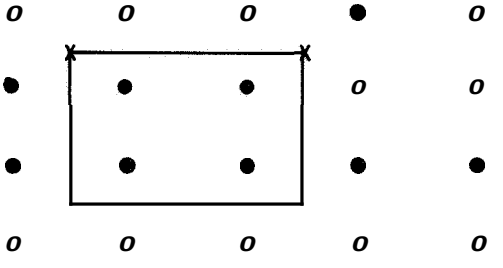

(c) c(2x2) RECTANGULAR
o substrate mesh
x surface mesh

Figure 6. Illustrations of shorthand designation of relationship between surface mesh and substrate mesh.

FLASH FILAMENT TECHNIQUES

Introduction

Measurements of adsorption-desorption phenomena involving the use of a heated solid surface play an increasingly important role in the investigation of the physical and chemical properties of surfaces.[8] The flash filament technique consists of using a test cell of known volume (one to two liters), containing a temperature controlled surface (usually, but not always in the form of a filament or ribbon) and some means of measuring pressure changes as the adsorption and desorption processes take place. Although the most widely used pressure detector has been the Bayard-Alpert ionization gauge whose advantages and disadvantages have been discussed in the literature,[9] considerable refinement comes with the use of a partial pressure analyzer because it removes much of the uncertainty in the identification of the species being adsorbed or desorbed. In addition, mass spectrometers have made possible such measurements as the study of replacement,[10] isotopic mixing on the surface,[11] and coadsorption.[12] As with all reliable surface measurements, considerable care must be exercised to insure the cleanest possible conditions during the experiments.

The advantages of the flash technique are that the system is relatively inexpensive and simple to construct and, most importantly, it permits the measurement of a number of important parameters such as binding energy, sticking probability, the pre-exponential factor which is related to the entropy of adsorption, as well as information concerning replacement and coadsorption.

In spite of these advantages, there are certain limitations to the flash method. By its very nature, it must be possible to heat the surface to a relatively high temperature, thus confining the measurements to the refractory metals. The most widely used method of heating the surface has been resistive heating of a filament or ribbon and, because these surfaces are inherently polycrystalline, the interpretation of experimental results is always somewhat doubtful. It is possible to make flash measurements on single crystals if special considerations are given to the design of the desorption tube.[13] It should be mentioned that surfaces of ribbons have been found to approximate single crystal planes (often (113) or (114)), but in general, the orientation depends upon prior treatment of the ribbon.[14,15] The physical quantities of interest are not measured directly but must be derived from the kinetics of the process, requiring that special consideration be given to the derivation of the kinetic equations for adsorption and desorption.[8]

Kinetics of the Flash Technique

In developing the kinetic equations for the flash technique, the following symbols will be chosen:

n - density of molecules in the gas phase in molecules/cm^3

σ - surface coverage density in molecules/cm^2

V - volume of the sorption chamber in cm^3

A - total surface area in cm^2

S - system pumping speed in cm^3/sec

q - rate of gas influx into the system in molecules/sec

t - time in sec

T - temperature in degrees Kelvin

k - Boltzman's constant in appropriate energy units

s - sticking probability

E - metal-adsorbate binding energy

ν - pre-exponential frequency

The rate of increase in the number of molecules per volume in the gas phase may be written generally as

$$V\frac{dn}{dt} = -Sn - S_a n \; t \sum_{i=o}^{n} q_i \qquad (1)$$

where the q_i take into account all sources of gases, including the desorption from the surface of the filament under investigation. Only three types of sources need be considered, q_o, q_1, and q_2, corresponding respectively to the influx of gas responsible for the background pressure (i.e., wall effects, gauge interactions, virtual leaks, etc.), the influx of adsorbate gas externally admitted to the system, and the gas evolving from the surface. In the following discussion, it will usually be assumed that q_o is negligibly small and special consideration must be given to those situations for which this condition is not met. The gas evolution from the surface may be written as $q_2 = A(d\sigma/dt)$, while the quantity S_a is the pumping due to adsorption on the surface, Specifically,

$$S_a = As(\sigma)K(m,T)$$

where from kinetic theory

$$K(m,T) = \frac{kT}{2\pi m}^{1/2}$$

The general expression for the kinetics then becomes

$$V\frac{dn}{dt} = -Sn - sAKn + A\frac{d\sigma}{dt} + q_i \qquad (2)$$

As it stands, the above expression does not lend itself to easy analysis; however, considerable simplification results by suitable choice of experimental procedure. Both adsorption and desorption experiments are conducted by the flash filament technique and since they involve slightly different procedures as well as kinetics they will be described individually.

Adsorption kinetics have been investigated by two methods referred to as the closed system and the continuous flow methods.[8] As implied, the closed system method is one in which gas (or vapor) is admitted to the test chamber while the filament is too hot for adsorpiton to occur, When the gas has reached the desired pressure, the volume is sealed off and the filament temperature is dropped suddenly to some prescribed value. As the temperature of the filament begins to decrease, the gas is pumped by the filament, leading to a characteristic decrease in the pressure within the test cell. (Figure 7). For this case, with S and q_i set equal to zero, Equation (2) reduces to

$$V\frac{dn}{dt} = -sAKn \; t \; A\frac{d\sigma}{dt} \qquad (3)$$

If re-evaporation of the adsorbed gases is ignored (i.e., $d\sigma/dt = 0$), then the sticking probability may be found from

$$s = -\frac{V}{KA}\frac{d\ln\left[n(t)\right]}{dt} \qquad (4)$$

The surface coverage density at any time is given by

$$\sigma(t) = V\left[n(o) - n(t)\right] / A \qquad (5)$$

In the event that re-evaporation is not negligible, it is still possible to analyze the pressure vs time curve as follows: It is usually assumed that the sate of decrease in coverage is governed by an Arrhenius law of the form

$$\frac{d\sigma}{dt} = \sigma^x \nu_x e^{-E/kt} \qquad (6)$$

where x = 1 or 2 (for monatomic and diatomic molecules) is the order of the

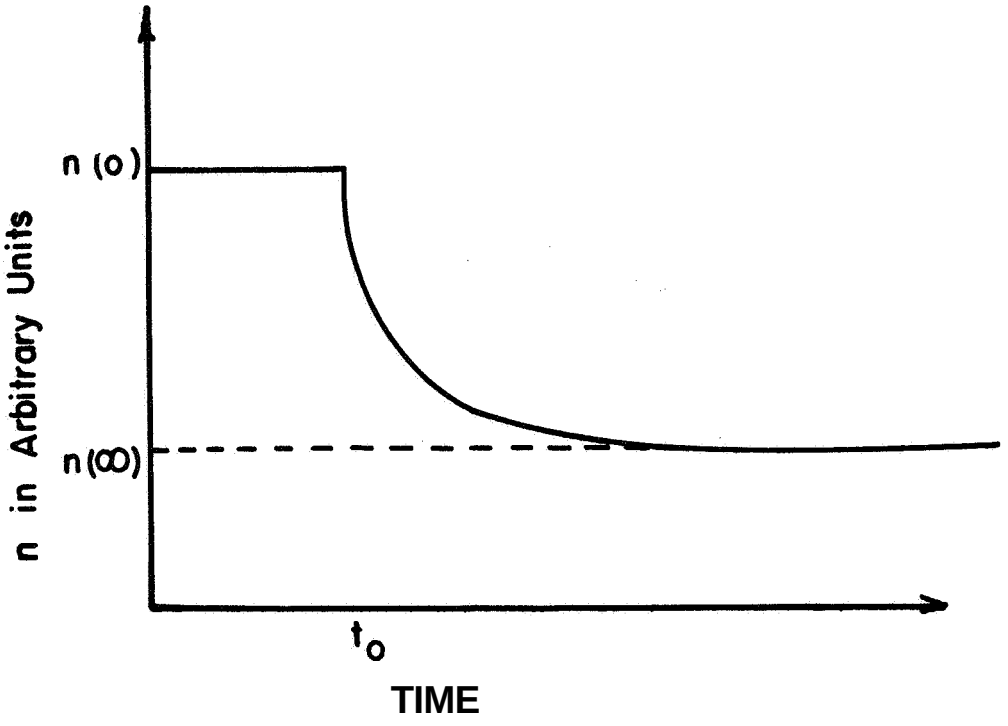

Figure 7. A typical n vs t curve for adsorption in a closed system in which the surface was suddenly cooled at time t_o.

desorption process. Rewrite Equation (3) in the form

$$\frac{dn}{dt} = \frac{-skAn}{V} \; t \; \frac{1}{V} \; \frac{d}{dt}(Ab) \tag{7}$$

then by measuring dn/dt for various values of n(o) and plotting a family of curves of dn/dt vs n for a constant number adsorbed (i.e., A 6 = constant) it is possible to obtain s from

$$s = \frac{-V}{kA} \left[\frac{d}{dn} \left(\frac{dn}{dt} \right) \right]_{A\sigma} \tag{8}$$

and in addition, extrapolation of the curves through n = o yields for first order desorption

$$\left(\frac{dn}{dt} \right)_{n=o} - \frac{A}{V} \frac{d\sigma}{dt} = \frac{A\sigma\nu e^{-E/kT}}{V} \tag{9}$$

which permits E to be determined as a function of $A\sigma$ assuming a value of ν.*

Unfortunately, it is difficult to achieve the conditions of the ideal closed system. One important problem is that gases adsorbed on the walls of the test volume may evolve as the pressure in the cell decreases thereby leading to an erroneous interpretation of the pressure vs time curve. In addition, ion gauge pumping can be considerable although precautions can be taken to reduce this effect substantially. In addition, impurities can build up rather rapidly. Impurity problems such as CO buildup due to hot filament degassing can be minimized by using continuous flow techniques, where gas is continually passing through the system.

Continuous flow studies have been performed both by maintaining the flow rate constant and the pressure constant.[16,17] In the constant flow method, the adsorbing vapors are allowed to flow at a constant rate through the system as determined by the rate of input through a suitable leak and the rate of removal by the pumping system and by adsorption on the surface. With the filament initially hot, a reference pressure is reached by careful adjustment of the leak and pumping rates which, once adjusted, remain constant for the duration of the experiment. The filament is then allowed to cool leading to a sudden decline in the pressure due to the onset of adsorption. (Figure 8).

*Usually one assumes $\nu = 10^{13} sec^{-1}$

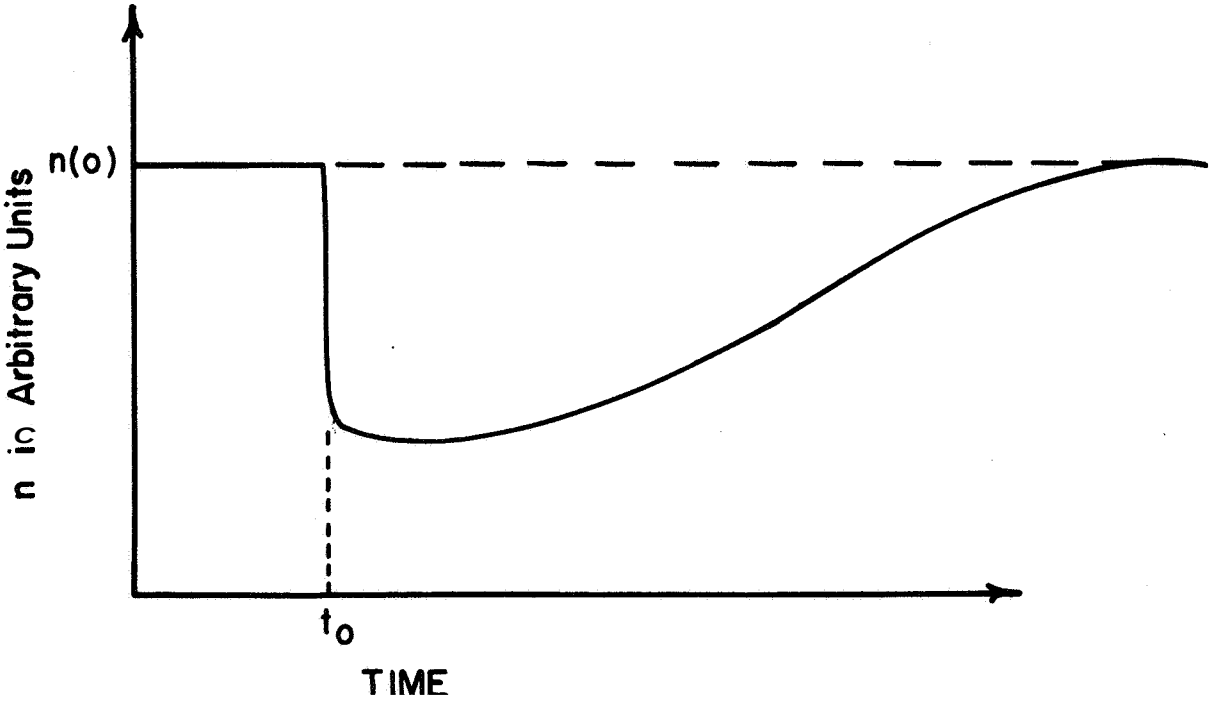

Figure 8. Typical n vs t curve for adsorption at constant flow rate.

As the filament becomes covered, the rate of adsorption decreases until finally the pressure returns asymptotically to the initial steady state value. For this case, the rate equation is

$$V \frac{dn}{dt} = -Sn - sAKn + q_1 + A \frac{d\sigma}{dt} \qquad (10)$$

Now the pumping speed may be readily found by introducing a small quantity of gas with conditions such that no filament pumping (i.e., with a monolayer adsorbed) or readsorption occurs and then plotting ln p vs t, as gas is pumped from the system,, In this case

$$\frac{S}{V} = \frac{-d\ln(n)}{dt} = -\frac{d\ln(p)}{dt} \qquad (11)$$

The value of q_1 is determined by considering the steady state situation for which

$$q_1 = Sn(o) \qquad (12)$$

so that if re-evaporation is negligible,

$$\frac{dn}{dt} = \frac{S}{V} \left[n(t) - n(o)\right] - \frac{sKA}{V} n(t)$$

or

$$s = \frac{V}{KA} \frac{d\ln(n)}{dt} - \frac{S}{KA}\left[\frac{n(t)-n(o)}{n(t)}\right] \qquad (13)$$

$$\sigma_o = \frac{V}{A} \left[n(o) - n(\infty)\right] \qquad (14)$$

Use of a constant pressure flow system minimizes problems of gauge and wall interactions and provides a means of direct measurement of pressure dependent parameters.[17] In this system, gas flows from a reservoir through a servo-controlled leak valve into a small chamber containing an ion gauge, then through a capillary whose conductance is calculated from the geometry and into the sample chamber, The flow rate into the sample chamber is regulated in such a way as to maintain constant pressure in the sample chamber.

The flow rate through the system is represented by the expression:

$$q_1 = Sn + V\frac{dn}{dt} + q_o + sAKn - A\frac{d\sigma}{dt} \qquad (15)$$

By using high flow rates, Vdn/dt is negligible. Interactions of the walls and gauges are small because impurities are continuously pumped out. By allowing the system to equilibrate at constant pressure, errors due to gauge pumping and degassing can be eliminated. The net sorption rate by the sample is proportional to the upstream pressure, since Sn is a constant in this system.

Kinetics of Flash Desorption

The kinetics of flash desorption may be studied by heating a sample at a controlled rate and analyzing the resulting p vs t curves as gas evolves from the surface. The type of system used is shown schematically in Figure 9. The general rate expression is

$$V\frac{dn}{dt} = -Sn + A\frac{d\sigma}{dt}, \qquad (16)$$

provided readsorption and gas influx from the reservoir is negligible during the heating time.

Again, it is found that analysis of the desorption kinetics may be simplified by making the proper design considerations. Desorption experiments are normally conducted in systems operating under one of two possible extremes, namely the conditions of $Sn \ll Vdn/dt$ and $Sn \gg Vdn/dt$. Since both of these approaches are used commonly, it is worthwhile to consider each in some detail.

Pumping Speed Small Compared to Rate of Gas Evolution. - When the pumping rate is slow compared to the rate of gas evolution,[18] $Sn \ll Vdn/dt$ and Equation (16) reduces to

$$V\frac{dn}{dt} = A\frac{d\sigma}{dt} = A\sigma^{x}\nu_x e^{-E/kT(t)}$$

A typical pressure vs time curve for this situation is shown in Figure 10. It will be observed that at points of maximum evolution rate, $d^2n/dt^2 = 0$, which leads to the result

$$\frac{E}{kT_P} = \ln x \cdot x - 1 + \ln\left[\nu_x T_p / (dT/dt)\right] - \ln E/kT_P \qquad (17)$$

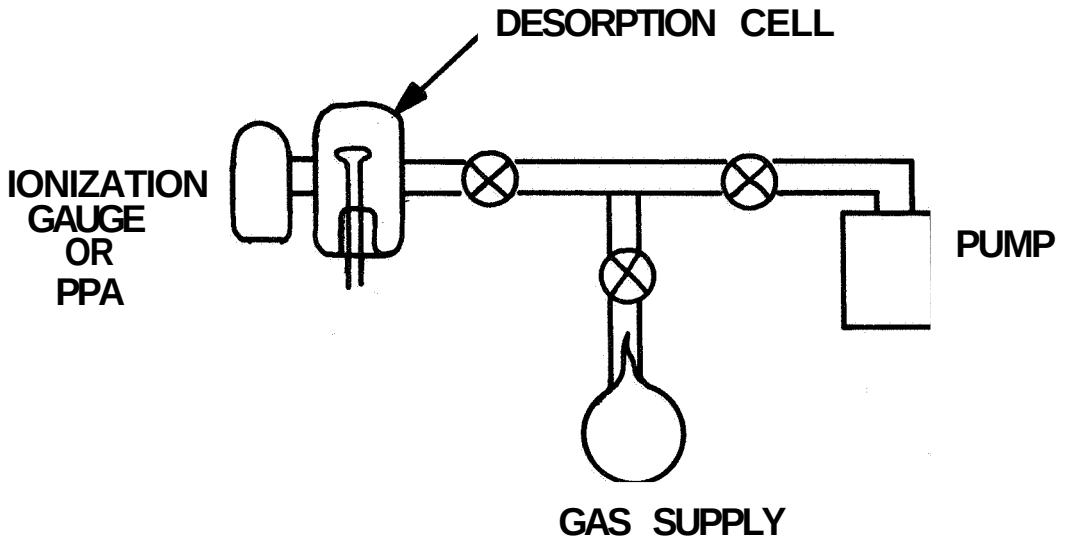

'Figure 9. Schematic representation of closed flash desorption system.

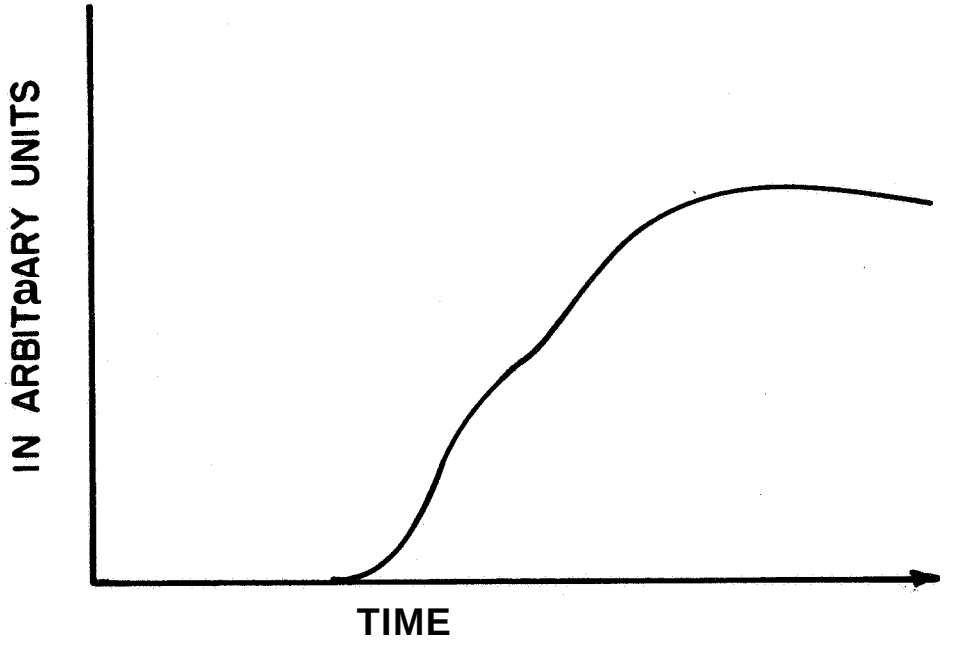

Figure 10. Hypothetical n vs t curve for flash desorption in a closed system from two adsorbed states.

Before carrying this development further, it is convenient to consider the second case:

Pumping Speed High Compared to the Rate of Gas Evolution. - In this case,[19] $Sn >> V dn/dt$ and the Equation (16) simplifies directly to

$$Sn = A\frac{d\sigma}{dt} = -A\nu_x \sigma^x e^{-E/kT(t)}$$

Here the pressure vs time curve assumes the structure shown in Figure 11 and the peaks occur at times (temperatures) for which

$$\frac{dn}{dt} = 0$$

which leads to

$$\frac{E}{kT_P} = \ln x\,\sigma^{x-1} + \ln\left[\nu_x T_p / dT/dt\right] - \ln E/kT_P$$

This is identical to the result obtained above for the opposite extreme and so the analyses for both situations are identical. It is well at this point to continue the analysis for first and second order kinetics separately. For the case, x=1, Equation (17) becomes

$$\frac{E}{kT_P} = \ln\left[\nu_1 T_p / (dT/dt)\right] - \ln E/kT_P$$

The last term is small which permits one to rewrite the above expression in the form

$$\frac{E}{kT_p} = \ln\left[\nu_1 T_p / (dT/dt)\right] - \ln\left\{\ln\left[\nu_1 T_p/(dT/dt)\right]\right\}$$

If a linear heating schedule is used, i.e., $T = T_o + \beta t$ then $dT/dt = \beta$ and

$$\frac{E}{kT_p} = \ln\frac{\nu_1 T_p}{\beta} - \ln\left[\ln\left(\frac{\nu_1 T_p}{\beta}\right)\right]$$

or for $10^8 < \nu_1/\beta < 10^{13}\,{}^oK^{-1}$

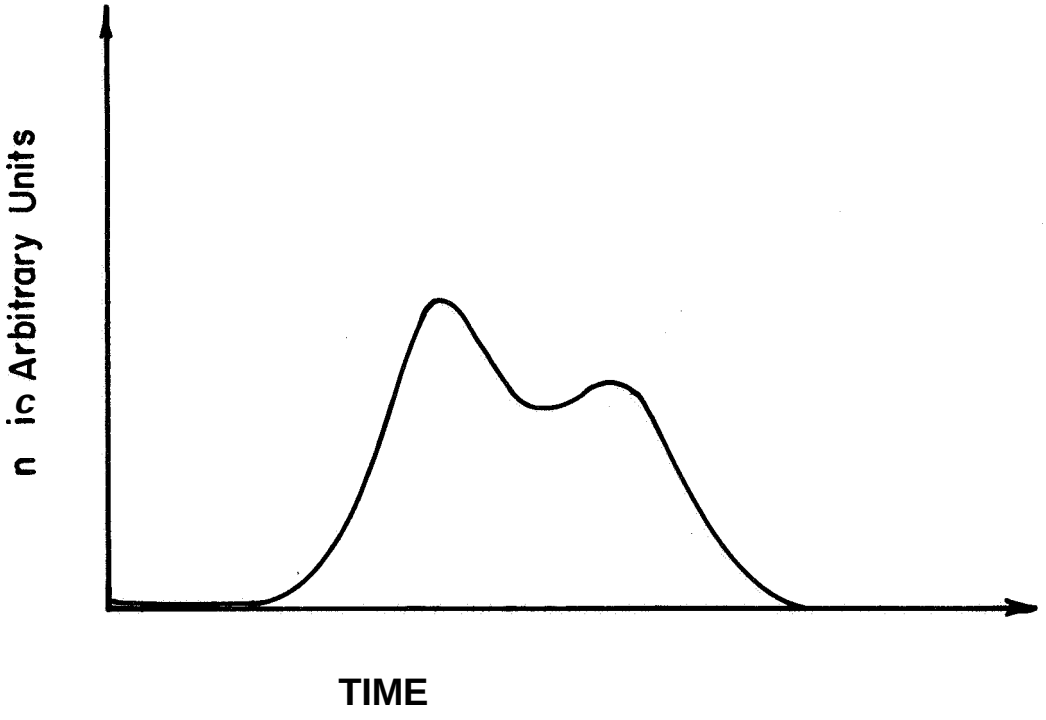

Figure 11. n vs t curves for flash desorption from two adsorbed states for the case of large pumping speed.

$$\frac{E}{kT_P} = \ln\frac{\nu_1 T_p}{P} - 3.64 \pm 1.5\% \qquad (18)$$

This may be used in this form if a value for ν_1 is assumed (usually $\nu_1 = 10^{13}\,sec^{-1}$ is assumed). It is still possible to obtain a value of E without assuming a value for ν_1 by varying the heating rate β, in which case it is found that

$$\frac{E}{kT_P} = \frac{d \ln \beta}{d \ln T_P} - 2$$

If the desorption process is second order, Equation (17) must be rewritten in the form

$$\frac{E}{kT_P} = \ln 2\sigma_P \pm \ln\frac{\nu_2 T_p}{dT/dt} - \ln E/kT_P$$

With a linear heating schedule the desorption is found to be characterized by

$$\frac{d \ln \sigma_o T_p^2}{d(1/T)} = \frac{E}{k} \qquad (19)$$

where σ_o is assumed to be equal to $2\sigma_p$. Thus, a linear plot of $\sigma_o T_p^2$ vs $1/T$ may be used to demonstrate second order kinetics. The intercept gives ν_2.

Summary

Experiments using flash filament techniques provide a highly sensitive means of acquiring information necessary for the complete identification of states of adsorption. From such measurements, it is possible to determine the binding energy, the entropy of adsorption, the molecular form of the adsorbate, the sticking coefficient, and the maximum coverage in each state. Recent improvements in technique make possible the separation of states differing in binding energy by only a few eV. However, in spite of its usefulness, the flash filament technique is limited to the refractory metals and is not possible to relate the information gained directly to the microscopic structure of the surface,

ELECTRON IMPACT DESORPTION

Introduction

Under certain conditions, desorption is induced by the interaction of incident low energy electrons with molecules adsorbed on a metal surface. The earliest reports of electron impact desorption were made by workers using mass spectrometers in which desorption of gases from various electrodes by the ionizing electron beam produced spurious effects in their measurements.[20] Since these early findings, many have observed and reported similar effects, all of which have considerable practical importance. J.R. Young[21] and G.E. Moore[22] made mass spectrometric investigations of electron impact desorption of gases from various anode materials and at least partially confirmed the long-held belief that gases desorbed from anodes were responsible for the observed poisoning of thermionic oxide cathodes. Later studies by Degras, et al,[23] and by Redhead[24] led to the conclusion that electron impact desorption affected the operation of an ionization gauge, while more recently, electron impact desorption has been recognized as an important contributor to gas contamination in high current electron storage rings[25] and controlled fusion chambers.[26] In spite of the extensive number of observations of electron impact desorption, relatively few investigations have been made to determine the basic nature of the effect, and credit must be given to Redhead[24] and Menzel and Gomer[27] who appear to have concluded independently that the desorption is a direct result of electronic excitation to repulsive surface states.

Basically, the experimental arrangement for studying electron impact desorption consists of a specimen on which gases are adsorbed, a source of electrons with which to bombard the specimen, and some means of detecting the desorption products, all in an ultra-high vacuum environment maintained at pressures at least in the 10^{-10} torr range. In general, the techniques of different investigators differ only in the method of detecting the desorption products and four methods have been used., For example, in the work of Degras, et al,[23] an ionization gauge was used to measure the total pressure change resulting from bombarding the surface with electrons. Moore22 and Petermann[28] used mass spectrometric techniques to identify the desorbed species. Redhead[24] utilized the fact that under certain conditions the desorption products are ions which can be measured directly, and Menzel and Gomer[27] used the field electron microscope, which permits visual observation of the desorption process on a microscopic scale.

While it seems possible that desorption of very loosely bound adsorbates may result from direct momentum transfer, it appears that in the majority of cases electron impact desorption must be explained in terms of electronic excitation of the adsorbed molecule to the repulsive portion of an excited

molecular or ionic state on the surface. This is made clearer by referring to the potential energy curves shown in Figure 12, which represent various quantum states of a hypothetical metal-adsorbate system. The curves shown correspond respectively to the ground state (M *t* A), the antibonding state (M *t* A)* , an excited state of the ground state species $(M + A)^*$, and an ionic state $(M^- + A^+)$. It is assumed that transitions from one state to another occur vertically within the shaded or Franck-Condon region. Observe that transitions to the states $(M + A)^*$ and $(M^- + A+)$ are to repulsive portions of the respective potential energy curves and consequently result in desorption, either as a neutral for the former case or as a positive ion for the latter. The probability for desorption of the ion will be reduced in this example because it must cross the potential energy curve corresponding to the $(M + A)^*$ binding state where it can become bound and subsequently return to the ground state, Although a number of modes of desorption can be visualized, it should be pointed out that only desorption from an ionic state has been positively identified at this time. However, it seems quite unlikely that ionic desorption accounts for all the electron impact desorption. There is some evidence suggesting that excitation to a loosely bound state followed by thermal desorption might be possible also.[29]

If the energies of the desorption products can be analyzed, it is possible to acquire additional information about the ground state of the adsorbed species. This may be seen by referring once again to Figure 12. Suppose desorption from the ionic state, preceded by electron impact ionization, is considered. Since there is a certain spread in the positions of the ground state atoms, depending upon their vibrational energies and the shape of the potential well for this state, there will be a corresponding spread in the energies of the desorbed ions. In other words, knowledge of the energy distribution of the desorbed ions permits one to approximate the square of the ground state vibrational eigenfunction for the adsorbed species. Similar arguments hold for the desorption of neutral molecules as well, but such information is not easily obtained due to the difficulty with which energy measurements are made on neutral atoms.

Although the electron impact desorption process has not been placed on a firm theoretical basis, a few qualitative remarks are possible in light of earlier work by Redhead[24] and by Menzel and Gomer.[27] Menzel and Gomer argue quite convincingly that the cross section for excitation to the repulsive state cannot differ by more than a factor of ten from the cross section for excitation to the corresponding state of the molecule in the gas phase, which is of the order of $10^{-16} cm^2$. This conclusion is arrived at by approximating ground and excited state wave functions for the bound molecule by a linear superposition of a set of carefully chosen basis states. The transition probabilities calculated in this way seem to be at least as large as the corresponding transitions in the gaseous state. Thus, in view of the fact that observed cross sections for electron impact desorption are often several orders of magnitude lower than the cross sections for the corresponding

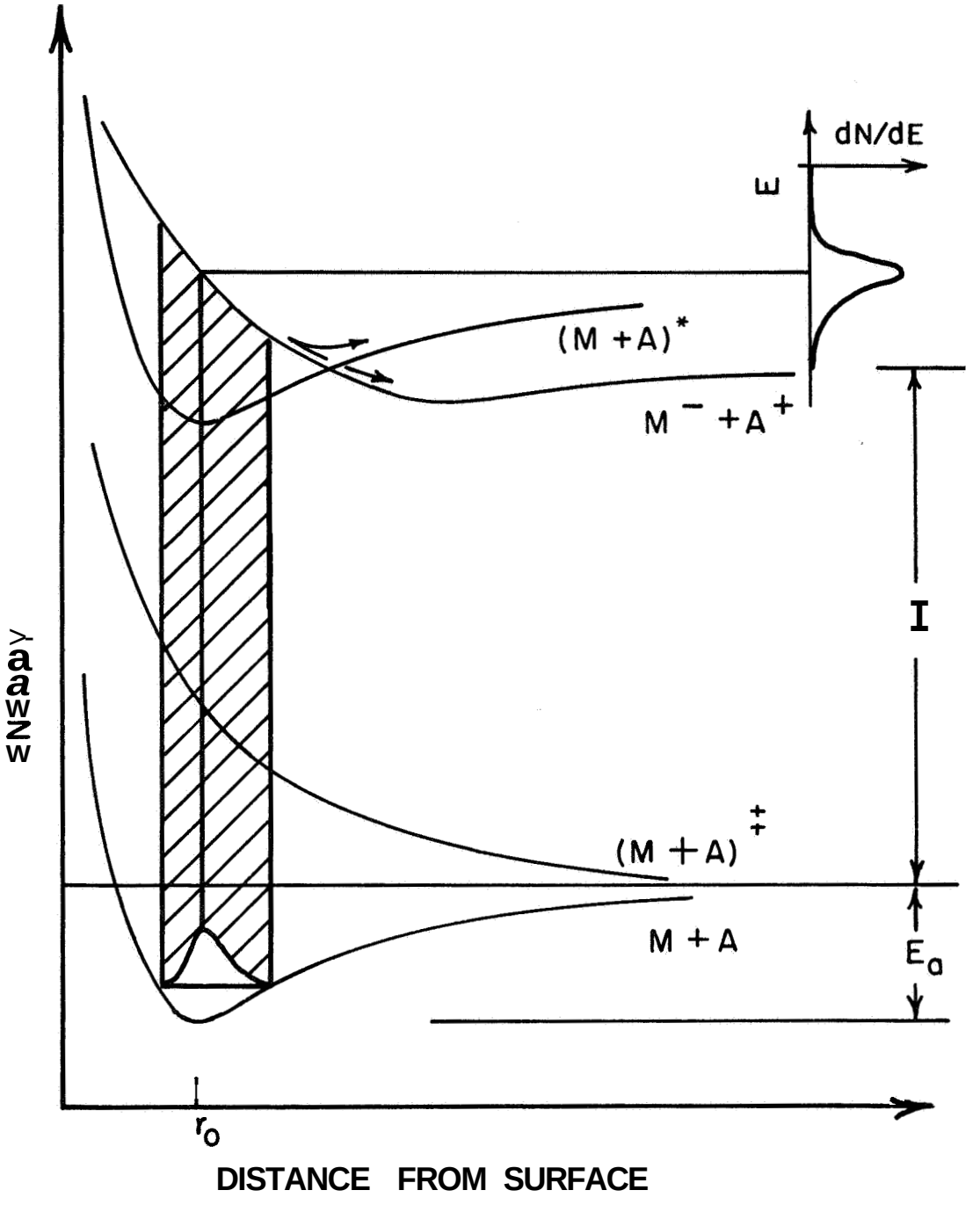

Figure 12. Potential energy curves for metal-adsorbate states at a hypothetical surface.

transitions in the gas phase, it would appear that the competing process of readsorption plays an important role.

Further conclusions are that the probability for desorption will increase with increasing lifetime of the adsorbed molecule in the excited state and will decrease with increasing mass and binding energy of the adsorbed species. In addition, the probability for desorption will depend rather sensitively on the equilibrium position of the adsorbed molecule, the probability decreasing with decreasing distance.

In his investigation of the electronic desorption of oxygen adsorbed on molybdenum, Redhead found that ions and neutrals were desorbed in the ratio of one ion for every 50 neutrals. Furthermore, it was noted that the energy threshold for the onset of desorption was the same for both the ions and the neutrals which led him to propose, with excellent experimental verification, that the desorption for both species occurred from the same ionic state but that the ions were neutralized by Auger transitions as they moved away from the surface.

The Kinetics of Desorption

As with flash filament desorption, the important parameters for electron impact desorption are obtained from the kinetic equations for the desorption process. Here one must take into account the kinetics for the three methods of measurement, namely, measurement of pressure change, measurement of work function change, and detection of desorbed ions.

The following symbols will be used:

n = the number of molecules per unit volume in the gas phase.

S = the pumping speed of the vacuum system in cm^3/sec.

V = the volume of the system in cm^3.

q = the influx of gas into the gas phase due to electron desorption.

q_o = the influx of gas into the gas phase in molecules/sec, responsible for the background pressure.

σ = surface coverage density in $molecules/cm^2$.

J = electron current density (assumed uniform over the surface) in $charge/cm^2\text{-}sec$.

A = target area in cm^2.

e = electronic charge.

Q = the total electron desorption cross section in cm^2.

ϕ = work function of the metal in electron volts.

In addition, the following assumptions will simplify greatly the calculations appearing below:

(1) The electron current density is uniform over the surface.

(2) The desorption rate is proportional to current in the first order.

(3) Diffusion of gas out of the bulk or along the surface is considered to have a negligible effect on the results.

(4) Readsorption from the gas phase is neglected, a valid assumption for pressures in the 10^{-10} torr range.

(5) Thermal desorption is not considered.

Pressure Change. -The time rate of change in the number density of molecules in a vacuum system is described by

$$V\frac{dn}{dt} = -Sn\,t\,q_o\,t\,q \tag{20}$$

If first order electronic desorption processes are assumed, then

$$q = \sigma QJA/e \tag{21}$$

The surface coverage density will change with time according to the expression

$$\frac{d\sigma}{dt} = -\sigma QJ/e \tag{22}$$

which has the immediate solution

$$\sigma = \sigma_o \exp(-QJt/e) \tag{23}$$

Combining Equations (20), (21) and (23) one obtains the differential equation

$$\frac{dn}{dt} = -Sn/V + q_o/V + (\sigma_o QJA/eV) \exp(-QJt/e) \tag{24}$$

A solution to this equation is readily obtained and, if $n_o = q_o/S$, the final result is

$$n(t) = n_o + \frac{\sigma_o AQJ}{eS - QJV}\left[\exp(-QJt/e) - \exp(-S/V)t\right] \quad (24)$$

This may be simplified; for example, if S/V is much larger than QJ/e, one obtains

$$n(t) = n_o + \frac{\sigma_o AQJ}{eS}\exp(-QJt/e) \quad (25)$$

From this equation, the following information is derived

$$Q = -\frac{e}{J}\frac{d\ln\left[n(t) - n_o\right]}{dt} \quad (26)$$

and

$$\sigma_o = \left[n(0) - n_o\right] eS/AQJ \quad (27)$$

which may be used to compute the cross section and initial coverage respectively. Note that the quantity, n, may be related at room temperature to the pressure, p, in torr, by the kinetic theory expression

$$n = 3.3 \times 10^{19} p$$

On the other hand, if S/V is very small compared to QJ/e,

$$n(t) = no\ t\frac{\sigma_o A}{V}\left[1 - \exp(QJt/e)\right] \quad (28)$$

from which

$$Q = -\frac{J}{e}\frac{d}{dt}\ln\left[\frac{n(t) - n_o + \frac{\sigma_o A}{V}}{\frac{\sigma_o A}{V}}\right] \quad (29)$$

and

$$\sigma_o = \frac{V}{A}\left[n(\infty) - n_o\right] \quad (30)$$

Work Function Change.-For small coverage changes, it is reasonably valid to assume that the work function is related linearly to coverage through the expression

$$\phi = \phi_\infty + c\sigma$$

where c is a constant and ϕ_∞ is the value of ϕ when $\sigma = 0$. With this assumption then, Equation *(23)* may be rewritten to yield

$$Q = -\frac{ed}{Jdt} \ln\left[\frac{\phi(t) - \phi_\infty}{\phi(0) - \phi_\infty}\right] \tag{31}$$

Detection of Tons.- The ion current arising from electron impact ionization on the surface of the metal follows the rule

$$I^t = \sigma Q^t i \tag{32}$$

where I^t is the positive ion current, i is the electron current and Q^t is the cross section for an adsorbed molecule to be desorl-ed as an ion, Application of Equation *(23)* then leads to

$$I^t = I_o^t \exp(-QJt/e) \tag{33}$$

where $I_o^t = \sigma_o Q^+ i$. From this expression the total cross section for electron desorption may be obtained:

$$Q = -\frac{ed\ln I^t}{Jdt} \tag{34}$$

The ionization efficiency is

$$\text{Eff} = I_o^t/i = \sigma_o Q^t \tag{35}$$

Knowledge of the initial coverage allows one to use the latter expression to compute Q^+.

Experimental Considerations

It must be emphasized, that in the application of the kinetic equations derived in the preceding section, care must be taken to ensure that the conditions specified by the assumptions are satisfied for the particular experimental circumstances in question. An important consideration is that of

readsorption which is inherently connected with the vacuum conditions; for, since the cross sections for electronic desorption are quite small, it is often necessary to carry out the measurements over extended periods of time in order to desorb an appreciable amount of gas. In addition, it seems almost certain that desorption occurs from more than one state, a fact which manifests itself in nonlinear In I^+ vs t curves, for example. With proper analysis, however, it is usually possible to separate the effects of more than one state without undue difficulty.

The designs of three experimental electron impact desorption tubes are shown in Figures 13, 14, and 15. The tube shown in Figure 13 was used by Redhead[24] to measure the electronic desorption of oxygen and carbon monoxide adsorbed on molybdenum. Here, the surface being studied was in the form of a polycrystalline ribbon which could be heated, both resistively and by electron bombardment. The desorbing electrons were emitted by a thoria coated tungsten filament with a spread in energy of about 0.8 eV, and the desorption process was studied by means of the ions reaching the collector. Heating of the molybdenum ribbon permitted evaluation of the binding energies for the adsorbed molecules.

Figure 14 shows a tube used by the research group at Field Emission Corporation to investigate the electron impact desorption of coadsorbed alkali metal and electronegative adsorbates on various refractory metals. In this tube, the elecron beam is directed axially onto the apex of the emitter tip on which the adsorbate resides. With the arrangement shown, it is possible to select parts of the field emitted electron beam in order to determine changes caused by electron impact on single crystallographic planes. In field emission studies, use is made of the extreme sensitivity of the emission current on the work function of the surface so that the cross sections are determined using Equation 31. The field emission technique does not lend itself to the detection of ions nor to the identification of the desorbed species. However, it is highly sensitive method of measuring cross sections as low as $10^{-23} cm^2$.

The tube shown in Figure 15 was used in an investigation of the electron impact desorption of carbon monoxide adsorbed on nickel.[29] A mass spectrometer was incorporated in the design of the all stainless steel desorption chamber, which, along with the ion collector, permitted detection of both neutrals and ions.

Summary

Electron impact desorption techniques yield information about excited and ionic states of the surface-adsorbate bond, By means of carefully taken threshold data, it is possible to deduce the binding energy of the ground state of the adsorbed species, thereby supplementing information derived from flash filament experiments. Finally, if the energy distributions for the desorbed ions are measured then the shape of the ground state potential energy curve may be estimated.

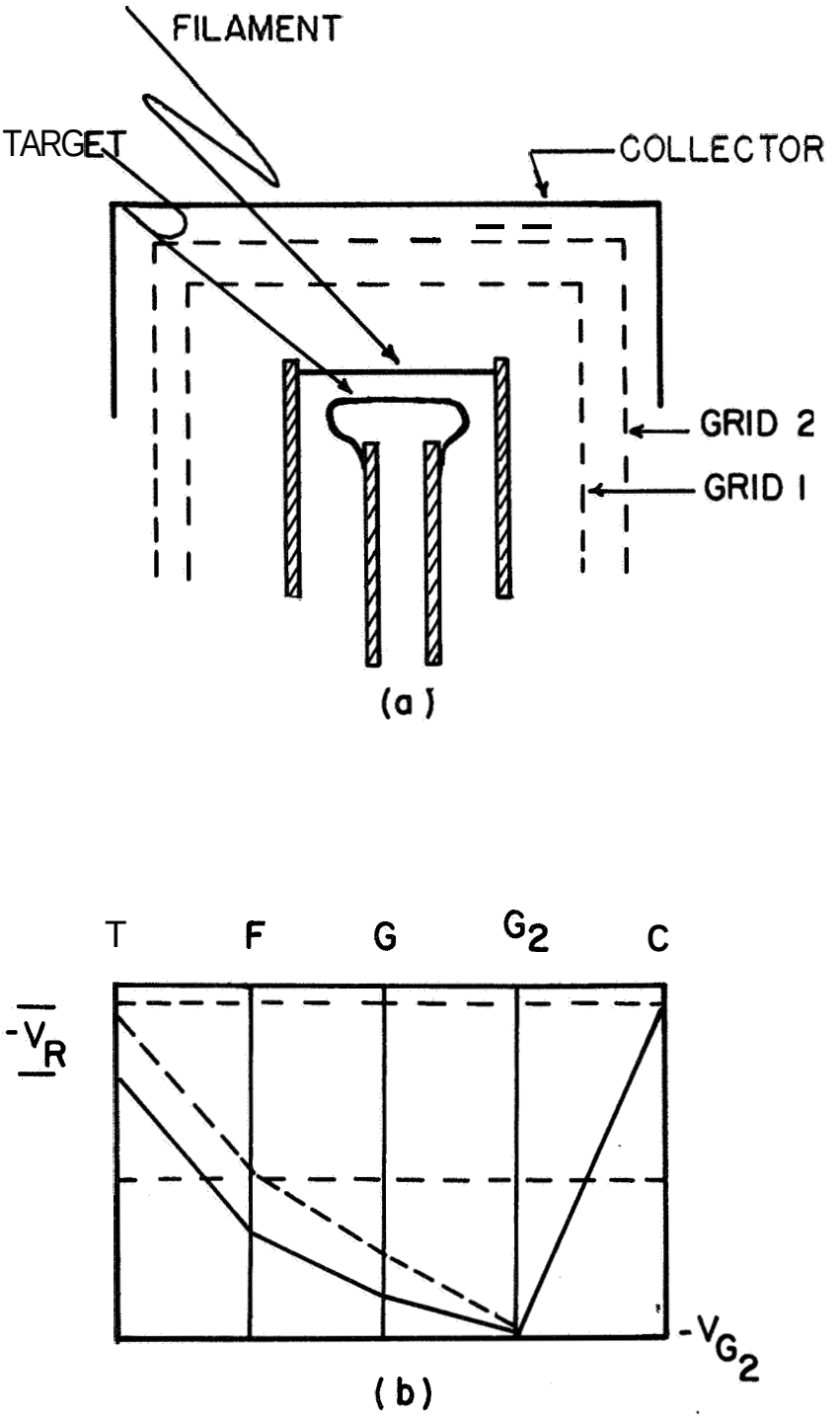

Figure 13. (a) Schematic diagram of experimental electron impact desorption tube used by Redhead. (b) Representation of electrode potential configuration used in Redhead's tube.

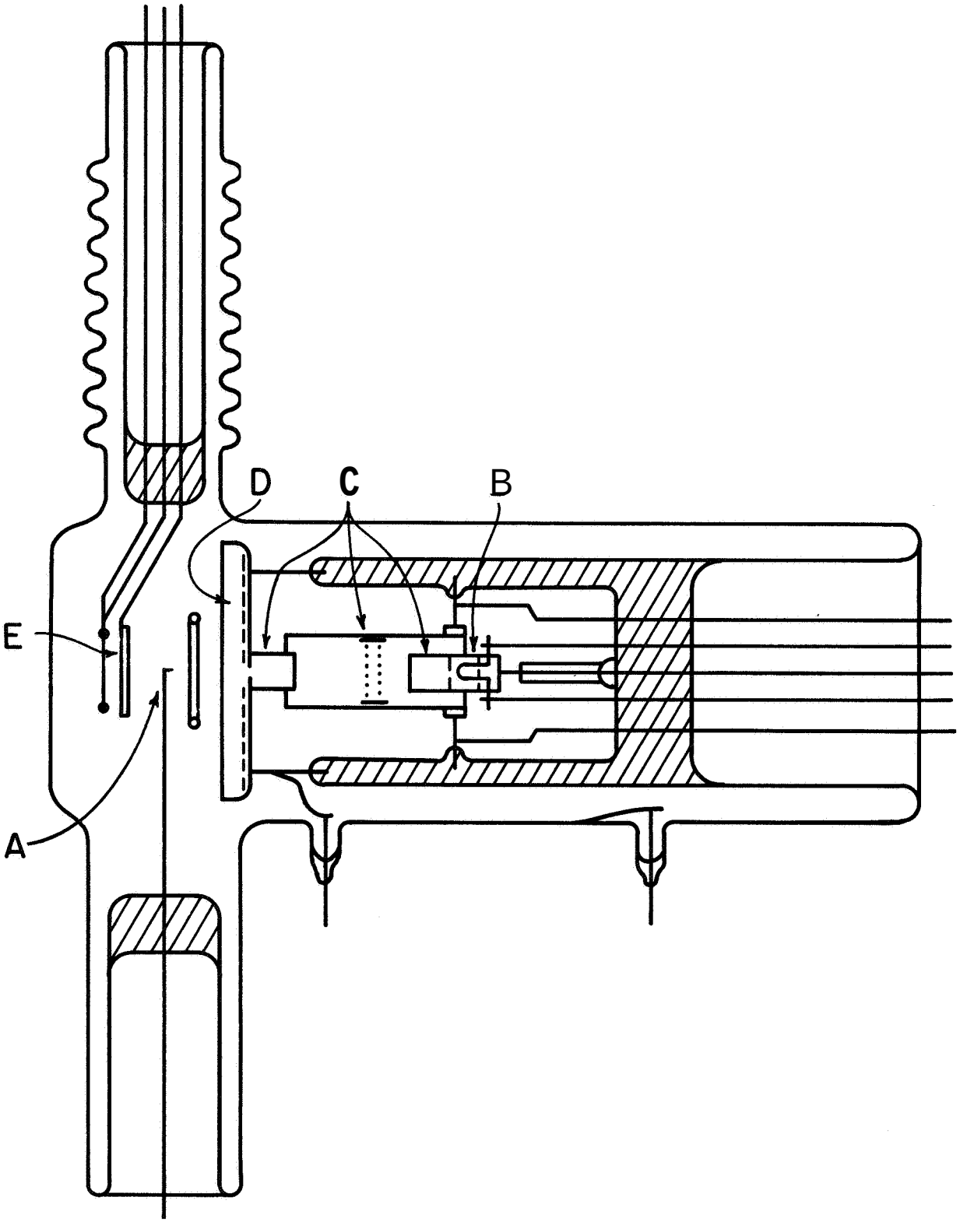

Figure 14. Field emission tube used by L. W. Swanson, et al., for electron desorption studies. A is a tungsten field emitter, B is a tungsten filament used as the electron source, C is a lens arrangement that can be used either to focus the electron beam or as a Faraday collector, D is a phosphor screen, and E is a collector.

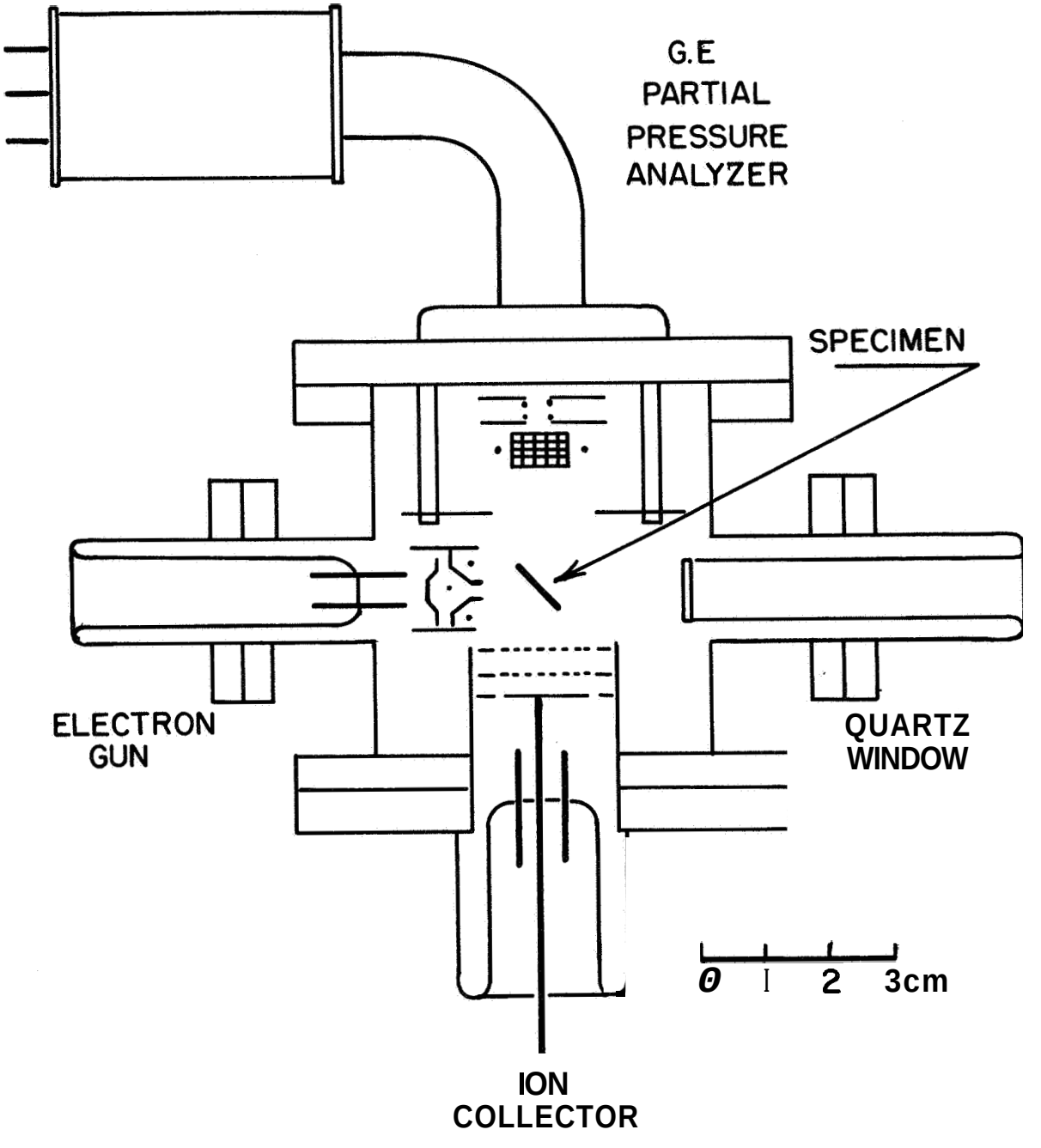

Figure 15. Electron impact desorption tube used by Hinrichs.

FIELD ELECTRON MICROSCOPY

Introduction

Field electron emission was discovered as early as 1897 by R.W. Wood of Johns Hopkins University, but it was not until after 1928 when R.H. Fowler and W. Nordheim of the University of Cambridge developed the wave mechanical concepts of field emission that earlier experimental results could be clarified. Although various aspects of the Fowler-Nordheim theory of field emission were confirmed in the 1930's, the reproducibility and reliability of these early experiments were clouded by the inability to control and measure the vacuum conditions within the tube and the uncertainty as to the geometry of the emitting sites. The invention of the field electron projection microscope by Erwin W. Müller overcame many of these difficulties by providing a single crystal emitting surface of well-defined geometry and visual read-out of the work function topography of the emitting surface. The field electron microscope, which permits visualization of the effects of various phenomena at the surface of metallic crystals on what is nearly an atomic level, became an increasingly useful tool for analyzing physical and chemical phenomena that affect the work function or surface configuration. Subsequently, various investigators, principally Robert Gomer of the University of Chicago,[30] exploited the microscope to study such phenomena occurring at metal surfaces as catalysis› adsorption, desorption and epitaxy.

The extreme sensitivity of field emission process on the degree of surface contamination provided early impetus for the obtaining and measurement of high vacuum, as well as the first visual demonstration of atomically clean surfaces. Perhaps the most important contribution field electron microscopy provided for surface physics and chemistry was to make available a tool for obtaining and demonstrating Well-defined surface conditions in performing investigations of surface adsorption and related phenomena.

Theory of Field Emission

Field emission is a quantum mechanical phenomenon with no classical analogue. When a sufficiently high electric field is applied to the surface of a metal or semiconductor the surface potential barrier is deformed to provide a finite length through which electron within the metal can "tunnel". This phenomenon (See Figure 16) can be formulated mathematically by considering a Fermi sea of electrons within the metal impinging on the surface.[31] Multiplying this impingement rate by the appropriate quantum mechanical transmission coefficient leads to the following expression for the number of field emitted electrons whose energy E (relative to the Fermi level) lies between E and $E + dE$:

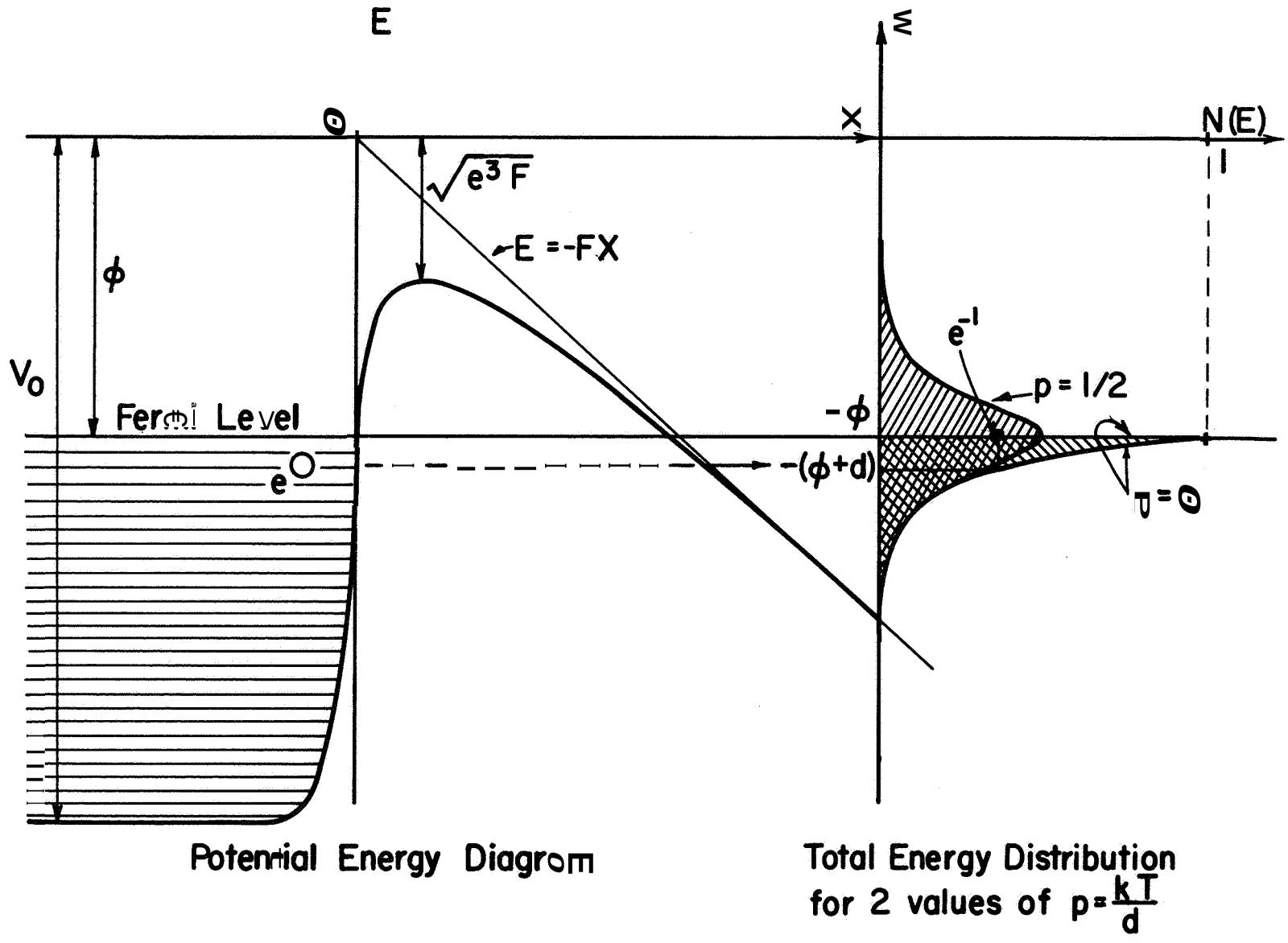

Figure 16. Potential energy diagram and total energy distribution for field of T-F emitted electrons.

$$P(\epsilon)d\epsilon = \frac{4\pi m d e^{-c_e \epsilon/d}}{h^3(e^{\epsilon/kT}+1)}\, d\epsilon \qquad (32)$$

where

$$c = \frac{4}{3}\,\frac{(2m\phi^3)^{1/2} v(y)}{\hbar e F}$$

and

$$d = \frac{\hbar e F}{2(2m\phi)^{1/2} t(y)}$$

and $t(y)$ and $v(y)$ are slowly varying functions of the work function ϕ and applied electric field F which have been published in tabular form.

Multiplying Equation (32) by the electronic charge, then integrating over the limits $-\infty$ to ∞, yields an expression for the current density of the field emitted electrons. This integration is conveniently accomplished by defining a dimensionless parameter $p = kT/d$ which leads to an expression for the current density J_{TF} of T-F (thermal-field) emission of the following form:

$$J_{TF} = \frac{\pi p}{\sin \pi p}\,\frac{F^2 e^{-c}}{8\pi h \phi t^2(y)} = \frac{\pi p}{\sin \pi p}\, J_{0F} \qquad (33)$$

which breaks down completely at $p = 1$ but is approximately valid up to $p \tilde{=} 2/3$. For small values of p (i.e., low temperatures or high fields) $\pi p/\sin \pi p \tilde{=} 1$ and one obtains the zero degree approximation of the Fowler-Nordheim formula for J_{0F} which may be rewritten in terms of the directly measurable field emission current I and applied voltage V, as

$$I = A_f V^2 e^{-m/V} \qquad (34)$$

In view of this relation, it follows that a "Fowler-Nordheim plot" of the current-voltage relationship ($\ln I/V^2$ vs. $1/V$) yields a straight line having a slope m and an intercept A_f with the vertical axis at $1/V = 0$. The linearity of a Fowler-Nordheim plot is normally regarded as adequate proof that the emission is due to stable field emission. When the Fowler-Nordheim law is satisfied, it can be shown that ϕ is related to the slope m by the expression:

$$m = 2.96 \times 10^7\, \frac{\phi^{3/2}}{\beta}\, s(y) \qquad (35)$$

where s(y) is a tabulated function which is equal to 0.951 ± 0.009 over the range of current densities normally encountered. Using the work function ϕ_1 for a clean surface as a reference, the work function ϕ_2 of the surface when coated with an adsorbate can then be determined from

$$\phi_2 = \phi_1 \left[\frac{m_2 \, s(y_1)}{m_1 \, s(y_2)} \right]^{2/3} \tag{36}$$

where m_1 and m_2 are the slopes of the corresponding Fowler-Nordheim plots. Absolute determinations of the work function require a knowledge of the geometric factor β (where $F = \beta V$), which can be determined from an electron micrograph of the emitter profile with an accuracy of about 15%; however, when the work function of the uncoated surface is well known, both β and the work function of the coated surface can be determined with good accuracy.

Techniques

General discussions of field electron microscopy and details on construction and processing have been presented in the literature.[30,31] Briefly, the field electron microscope is a diode in which field emitted electrons are drawn from the single crystal hemispherical tip of a very sharp needle (tip radius usually below 1 micron) mounted in an evacuated bulb with a phosphor screen concentric with the cathode surface. When a sufficiently positive "viewing voltage" is applied to the phosphor screen, the field emitted electrons travel along nearly radial paths and form on the phosphor screen a visible, highly magnified emission image of the emitter surface. Such an image is shown in Figure 17 for a clean (110) oriented emitter. The field electron microscope is characterized by a high magnification (typically 105 to 10^6 x) a high resolving power for smooth surfaces, typically 30A, limited by the initial energy spread of about 0.25 eV of the field emitted electrons (and a still higher resolving power(2.2A in certain cases) for surface irregularities). Pattern detail arises from local variations in field and work function at the tip surface, and the pattern has a symmetry characteristic of the crystal structure of the tip material. Observation of the emission pattern of the uncoated tip provides a sensitive criterion for checking the smoothness and cleanliness of the substrate.

Emitter tips are easily fabricated from most refractory metals and many semiconductors. Thermal heating is normally employed for cleaning surfaces, although other methods, such as field desorption, must be used for low melting metals. Nearly all metals and semiconductors can be fabricated into clean emitters by vapor grown whiskers.[32]

Adsorption, desorption and migration of adsorbates are measured through observation of the rate of change of the field electron pattern or current,

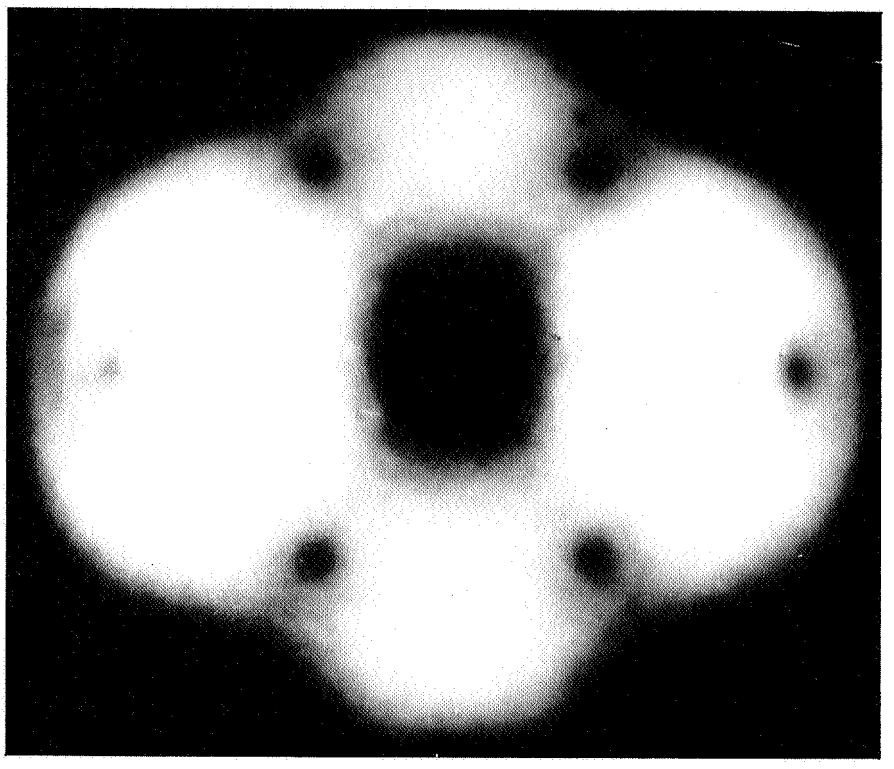

Figure 17. Field emission pattern of a cl'ean (110) oriented tungsten emitter.

which in turn, permits a determination of the associated physical constants (sticking probability, rate constants, and activation energies). However, at the high values of electric field required for emission, there is a possibility that the large electrostatic forces accompanying these fields may alter the processes under study and, at high temperatures may even alter the shape of the substrate. To avoid this, the "viewing field" required for field emission may be applied in the form of very short pulses at low duty factor (e.g., 1 microsecond pulses at a rate of 30 to 200 pulses per second), and the emission pattern is then viewed as a motion picture. This technique, introduced by Dyke[33] and co-workers, minimizes the perturbing effect of the viewing field on the event under study and allows almost complete freedom in the selection both of the tip temperature (from 0°K to the melting point of the emitter) and of the magnitude and polarity of the dc voltage which, in addition to the pulsed viewing voltage, may be applied at the tip surface.

Besides a high voltage supply for pattern viewing, additional equipment necessary far most field emission investigations include sensitive current and voltage measuring meters and provisions for measuring and controlling the emitter temperature. The latter is usually accomplished by resistively heating the supporting filament onto which the emitter is spot welded and accurately measuring the resistance of a small section of the filament, The resistance measurements can be related to temperature by precalibration or making use of the known variations of resistivity with temperature.

The vacuum requirements for performing meaningful investigations of surface phenomena by field emission are such that the surface must remain free of foreign contamination over the period of time the measurements are being performed. Residual gas pressures not only affect the particular surface phenomenon under investigation, but also lead to sputtering of the emitter surface by positive ions formed by electron impact ionization when steady field emission currents are drawn from the emitter. Residual helium pressures are particularly effective in leading to cathode sputtering during field emission but this problem is readily eliminated in sealed-off tubes by using glass of low helium permeability or immersing the tube in cryogenic liquids, Depending on the type of experiment contemplated, field emission investigations can be performed with evacuated sealed-off tubes or tubes attached to the vacuum system, but in either case it is desirable to have residual gas pressures well below 1×10^{-9} torr. Investigations of the adsorption of volatile gases, such as hydrogen or neon, can be accomplished by immersing the tube in liquid helium and utilizing chemical or sublimation sources to deposit the desired adsorbate onto the emitter. A typical design of a field electron microscope used in adsorption studies is shown in Figure 18.

Work Function-Coverage Relationships

The properties of the clean or contaminated emitter surface become apparent only through their effect on the electron emission. The precise

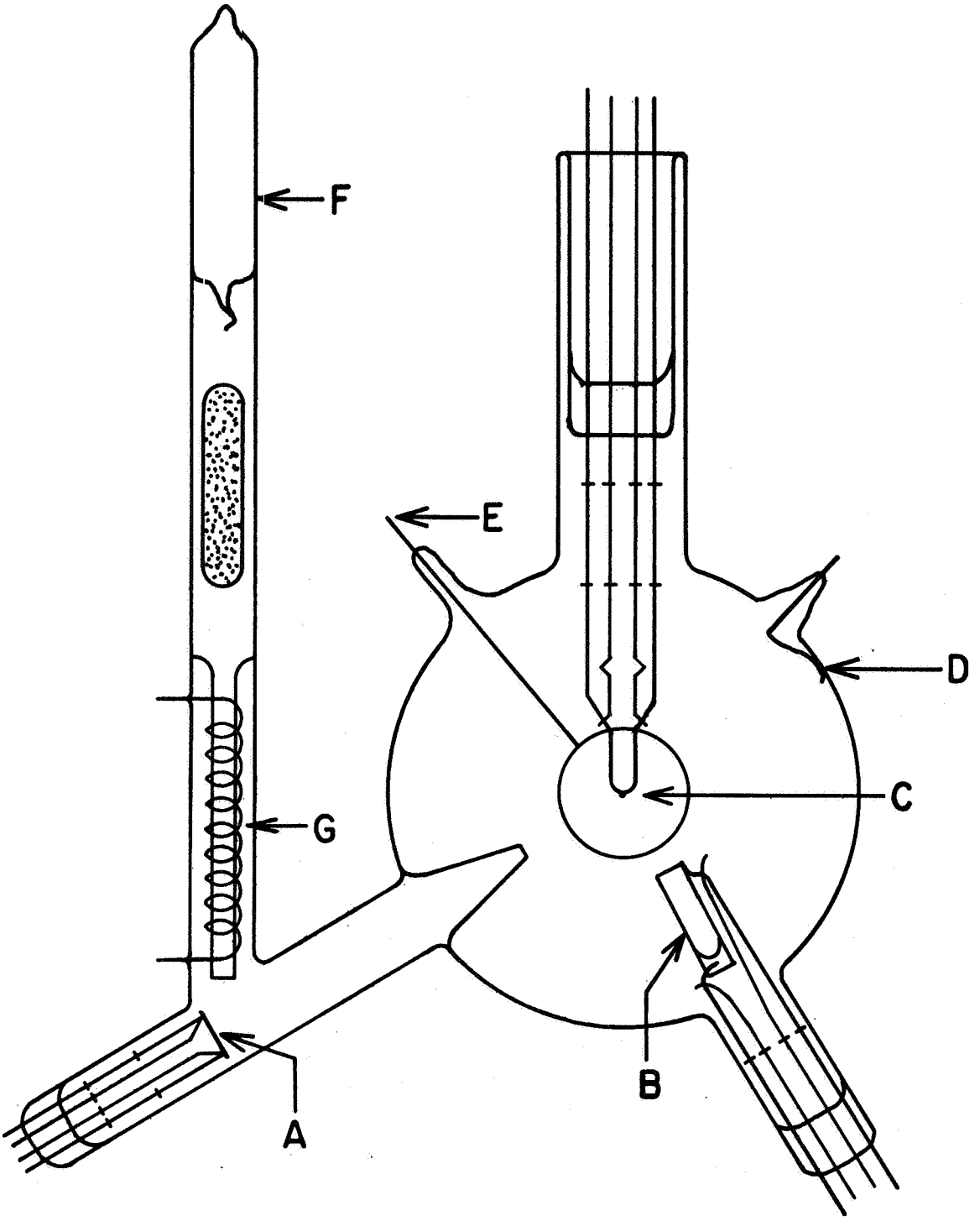

Figure 18. Front view diagram of field emission microscope for investigation of cesium and oxygen on tungsten. **A,** cesium source; B, oxygen source (heatable platinum crucible containing copper oxide); C, emitter assembly; D, electrical connection to conduction coating; E, anode ring; F, cesium reservoir; G, secondary cesium source.

evaluation of the work function is therefore of primary importance in the interpretation of the patterns observed in the field electron microscope. The variation in the electron emission over the surface of a smooth, atomically clean tungsten emitter is caused by variation of the work function with crystallographic direction. The use of Equation (36) to obtain the work function change due to adsorption is strictly correct only if F and ϕ are constant over the emitting region, which is seldom the case. In general the electron emission is averaged over a variety of crystal faces with widely varying work functions. It can be shown that the slope of a Fowler-Nordheim plot yields an average value of $\phi^{3/2}/\beta$ which is related to the individual regions as follows:

$$\left(\phi^{3/2}/\beta\right) = \sum_i f_i \phi_i^{3/2}/\beta_i \qquad (37)$$

where f_i is the fraction of the total current carried by the ith emitting region.

In practice, the curvature of the Fowler-Nordheim plot over the voltage range is negligible, so that its slope yields a constant $\phi^{3/2}/\beta$. It can be seen from Equation (37) that the experimentally obtained value is weighted heavily in favor of the highly emitting, or low work function, regions and may in practice be taken almost identical to the lowest ϕ encountered on the emitter surface.

Thus, in utilizing Equation (36) to determine work function changes on adsorption it should be remembered that average values are obtained and when adsorption greatly alters the emission distribution from that of the clean surface, these values cannot always be related directly to contact potentials.

The dangers inherent in the determination of averages can be overcome by measuring the electron current from individual crystal planes by suitably designed current probes, A tube designed for this purpose is shown in Figure 19 which allows measurement of total energy distributions as well as the emission from a single plane.

Utilizing the average work function-coverage relationships and the results of probe tube measurements, it is possible to establish the relationship between the work function of individual. crystal planes and average coverage. Although the field electron patterns give some indication as to the distribution of the adsorbate over the various crystallographic planes, only probe tube techniques will provide unequivocal measurements as to the atom density on various planes throughout the coverage range.

Surface Migration

One of the early uses of field electron microscopy was the investigation of surface migration of adsorbed layers on various substrates. The activation

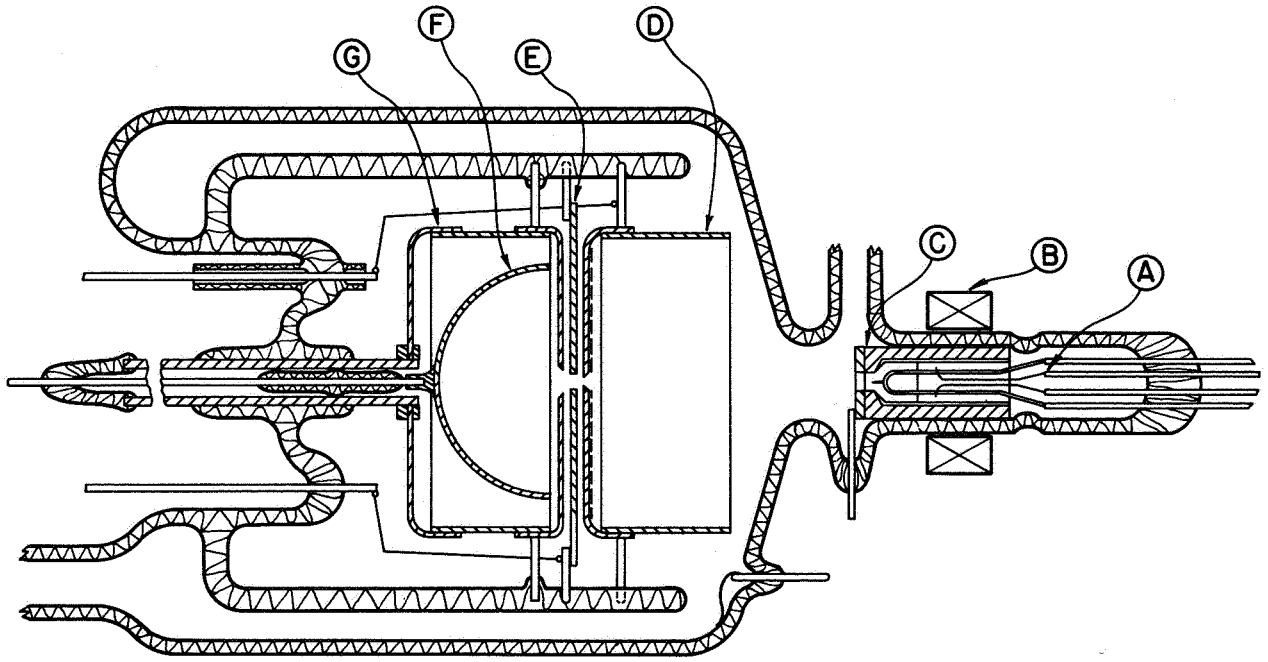

Figure 19. Energy analyzer tube designed to measure work function and energy distribution of single crystallographic planes. Provisions can be made for depositing adsorbates.

energy for surface migration on various crystallographic planes can be determined readily by measuring the temperature dependence of the rate of diffusion of the adsorbate as it migrates across the emitter surface. Recently, it has been determined that the electric field necessary for field emission viewing can alter the rate of surface migration.[34] By applying the viewing voltage in pulses of low duty factor the time average field is negligible and such field effect problems are eliminated without sacrificing viewing.

The determination of surface diffusion rates involves the measurement of the time necessary for the adsorbate to travel a given distance across the emitter surface. This can be accomplished by visually choosing the end point when the advancing boundary travels a specified distance on the surface. In cases where the adsorbate migrates across the surface without a sharp boundary visual end points cannot be easily employed. In this case one can make use of the fact that the field emission current (in this case the pulsed current) usually varies as the adsorbate migrates across the surface and can be utilized to establish the end point.

Thermal Desorption

Field electron microscopy lends itself to the measurement of thermal desorption rates and has been used in this connection for a variety of systems.[30] Typically, thermal desorption rates are determined by utilizing known relationships between work function and coverage. In this fashion, rates of work function change over a small coverage increment at various temperatures lead to the determination of activation energies of desorption.

Pulsed electron microscopy can also be used to good advantage for desorption measurements for the following reasons: (1) it allows visual inspection of the pattern during desorption and use of pattern changes for end points and (2), the variation of the pulse current I_p at constant voltage V_p at constant I_p can be followed and related to coverage-time plots for subsequent kinetic analysis. When using I_P or V_P to follow desorption rates care must be taken to allow for temperature effects on I_P as shown in Equation(33) and also the temperature variations of the work function of the particular adsorbate-substrate system.

It should be realized that activation energy measurements frequently involve some sort of average. For immobile layers the average is weighted toward the regions of lowest binding energy within the coverage increment, whereas for mobile layers in two-dimensional equilibrium the activation energy of desorption is often weighted towards the regions of highest binding energy.

Most adsorbate-substrate systems amenable to field electron microscopy lend themselves to the measurement of desorption rates by the above methods. It is only those systems which show no work function change on adsorption

that are not easily investigated by field electron microscopy. So far, few such systems are known to exist.

Coadsorption

Field electron microscopy has recently been applied to the investigation of two-component adsorbate-substrate systems (coadsorption). The systems potassium-hydrogen[35], cesium-fluorine[36] and cesium-oxygen[37] have been studied thus far. Of primary interest in these investigations was the effect of various amounts of the more strongly adsorbed electronegative component on the work function changes, surface diffusion and desorption rates of the alkali metal.

Although the results of utilizing field electron microscopy for the investigation of coadsorption are in the preliminary stages, it can be stated with some degree of confidence that this technique has great promise for providing a detailed understanding of the specific interactions involved in these more complex systems.

Field Effects

As mentioned earlier, the sometimes undesirable perturbation of the surface event under investigation by the high field required for field electron microscopy can be eliminated by the use of pulsed field electron microscopy. Moreover, the embodiment of the field electron microscope makes it uniquely suited for the intentional study of the field perturbations of various surface phenomena. The latter characteristic has been exploited recently[38] in order to investigate the effect of field on the surface kinetics and thermal dynamic stability of cesium on various refractory metals. In practice, the direct viewing of the surface event under study can be retained even with the application of dc fields of varying magnitude and polarity by superposition of the pulsed viewing voltage on the dc voltage through a suitable resistor-capacitor combination.

The temperature dependence of the surface diffusion rates of cesium on tungsten in the presence of an electric field has been measured[38] for two different but successive modes of surface diffusion with an initial cesium coverage of approximately 0.2 monolayer. Values of the field dependent activation energy of surface diffusion $E_d(F)$ for the two modes were determined by assuming a diffusion coefficient $D(F,T)$ of the form

$$D(F,T) = D_0 e^{-E_d(F)/kT} = \frac{x^2}{t} \tag{38}$$

where D_0 is a constant, and x is the distance traversed by the adsorbed

cesium in time t. The temperature dependence of the diffusion rates in the presence of an electric field was found to obey Equation (38), thus permitting the calculation $E_d(F)$ and D_0 as functions of applied field. Results of this nature could be fitted to a particular model involving the interaction of the applied electric field with the dipole moment formed by the adatoms, thereby giving considerable insight as to the electronic structure of the adsorbate.

The effect of positive field on thermal desorption (better known as field desorption) has been investigated for a variety of systems[39,40,41] and recently treated theoretically[42] for various types of adsorption. It is only through field electron microscopy techniques that field strengths sufficient to initiate field desorption can be generated at reasonable voltages and their effect on adsorbed layers conveniently studied.

According to Gomer and Swanson,[42] there are two basic mechanisms for field desorption, depending on whether I-ϕ is large or relatively small. Both cases involve a deformation of the potential energy of the ionic adsorbed state such that, beyond a certain distance x_c from the surface, the ionic state is both the ground state and a repulsive state. In general, the rate constant for field desorption is expressable as

$$\tau_F = (\nu s)^{-1} e^{E_a(F)/kt} \qquad (39)$$

where ν is a frequency factor ($\sim 10^{13}$ sec^{-1}), s is a transition probability or entropy factor which generally decreases with F. The quantity $E_a(F)$ is the activation energy for desorption, which may be written generally as

$$E_a(F) = \sum_n I_n - n\phi + E_a - \Delta(F) \qquad (40)$$

where I_n is the nth ionization potential, E_a the zero field binding energy, and $\Delta(F)$ is a field dependent correction factor, which is different for the various types of binding, Ionic, Metallic and Covelent, The first two fall under the category of small I-ϕ.

Case I. I-ϕ Small: Ionic Adsorption.-This situation is the simplest to consider for the field correction is easily computed by differentiating the total potential for an ion bound to the surface. The correction factor is found to be given by

$$\Delta(F) = (ne)^{3/2} F^{1/2} - F\,en(x_o - \lambda)$$

where λ is a Thomas-Fermi screening Length and x_o is the equilibrium distance

of the ion from the surface, In this case s = 1.

Metallic Adsorption.-In the case of metallic binding, I-Ø is still small and the atomic valence level, which becomes broadened as the atom approaches the surface, lies near the Fermi level, If this valence level lies only partly below the Fermi level

$$\Delta(F) = 3.8\ n^{3/2} F^{1/2} - \frac{1}{2}(\alpha_a - \alpha_i) F^2 - pF \qquad (42)$$

Where α_a is the effective polarizability at $x = x_o$, α_i is the ionic polarizability, and p is the effective dipole moment at $x = x_o$.

On the other hand, if the valence level falls completely within the conduction band of the metal, as would be the case of a metal atom adsorbed on a surface of identical atoms, the last term above is not effective so that

$$\Delta(F) = 3.8\ n^{3/2} F^{1/2} - \frac{1}{2}(\alpha_a - \alpha_i) F^2 \qquad (43)$$

For both situations, s is unity.

Case II. I-Ø large: Covalent Bonding. -When I-Ø is large,

$$\Delta(F) = \frac{(ne)^2}{4x_C}\ t\ F\ en\ x_C\ t\ \Delta(P) \qquad (44)$$

where $x_C = x_C + \lambda$ and $\Delta(P)$ refer to various polarization effects which are discussed in greater detail elsewhere.[42] Field desorption measurements not only provide knowledge as to the types of field interactions with the electronic structure of the adsorbate, but also provide considerable insight as to the detailed bonding of the adsorbate to the substrate and, in some cases[43], yield precise mapping of the one-dimensional potential energy curves of the adsorbate-substrate system.

Since field desorption is most conveniently studied by field electron microscopy techniques from an immobile layer, probe techniques can be used to great advantage to isolate the measurements to single crystallographic planes. This coupled with the ability to determine indirectly zero field activation energies of desorption from the existing field desorption theory, allows one in principle to determine the variation of the zero field binding energy as a function of adsorbate coverage on a single crystallographic plane.

Epitaxial Layers

Another recent application of field emission techniques has been the investigation of the nucleation and growth kinetics of epitaxial layers on various substrates. Results of this nature were first reported by Melmed[44] as an extension of earlier investigations of vapor phase grown metallic whiskers,[32] also by field emission techniques, to the investigation of two-dimensional epitaxial layers. Investigations of this nature, now reported for a variety of adsorbate-substrate systems[45], have provided considerable insight as to the detailed mechanisms involved in the nucleation process and the effect of substrate and surface contaminants on the epitaxial growth kinetics.

One particular interesting phenomenon regarding epitaxial growth discovered by Melmed that has some bearing on field electron microscopy technology concerns the apparent ability of certain low melting adsorbates such as copper, which are not readily amenable to field electron microscopy techniques, to be grown epitaxially on a tungsten substrate. In some instances it was observed that the epitaxial layer consisted of a clean, perfect single crystal structure of the face-centered copper structure grown across a tungsten field emitter surface and could be used for subsequent adsorption studies by field electron microscopy techniques.

Summary

Some of the recent applications of field electron microscopy to surface phenomena are as follows: (1) Work function-coverage relationships; (2) Zero field surface migration; (3) Thermal desorption; (4) Coadsorption; (5) Field effects on surface kinetics: (6) Investigations of epitaxial growth; (7) Electron impact desorption; and (8) Substrate surface rearrangement (e.g., self-migration and sputtering). It seems safe to conclude, therefore, that field electron microscopy has made important contributions to the understanding of various phenomena which occur at metal and semiconductor surfaces and will continue to make significant contributions as its use becomes more widespread,

FIELD ION MICROSCOPY

Introduction

It might be supposed that an ideal tool for acquiring the desired understanding of metal surfaces would be one permitting actual visualization of events occurring there on an atomic scale. Because of its ability to resolve single atoms, the field ion microscope very nearly achieves this ideal. Although similar to the field electron microscope, the field ion microscope image is formed with ions rather than electrons. Here advantage is taken of the shorter

wavelength of the ions and the fact that ions from a cooled emitter surface have smaller transverse energy, making it possible to distinguish adjacent atoms which have a separation of 2.74 Å or less.

The basic principle of the field ion microscope is that atoms can be ionized in a high electric field, an effect predicted by Oppenheimer[46] and verified experimentally by Müller.[47] In this process, known as field ionization, the potential energy curve of the atom becomes distorted to such an extent that an electron can tunnel from the atom into the metal with the formation of a positive ion as illustrated in Figure 20. In the field ion microscope, the tip is maintained at a sufficiently high electric field to ionize the impinging gas atoms which are present within the tube (usually helium at a pressure of approximately one micron). The electric field at the surface of the tip approaches 4 or 5 volt/Å, and is highest in the vicinity of the atoms which protrude beyond the average surface by virtue of the fact that the tip is crystalline in nature. The rate of impingement of the surrounding gas atoms is greater than expected on the basis of kinetic theory because of attractive field induced dipole forces, There is a critical distance, x_c, from the emitter surface within which field ionization is not allowed because the ground state of the imaging gas atom falls below the Fermi level so that tunneling of the electron is prohibited. Thus, best resolution is achieved by selecting a value of the electric field such that ionization occurs as near the critical distance as possible.

Most of the impinging gas atoms actually pass through the critical region without being ionized and as they collide with the surface they impart some of their kinetic energy to the substrate, being left with only enough energy to "hop" about on the surface. As they move about, they eventually hop over protruding surface atoms where the probability of ionization is greater because of the higher electric field and the ions thus formed are accelerated to the phosphor screen, creating an image of the surface as shown in Figure 21. Clearly, the resolution will be improved if the tangential velocity of the ions leaving the surface can be reduced. This is done by cooling the tip to liquid nitrogen or liquid hydrogen temperatures.

The field ion microscope has found application in the investigation of such phenomena as surface migration, adsorption, sputtering, field desorption, and surface structure, not to mention invaluable contributions made in the study of defects and related properties of the bulk crystal.[48,49] Despite the importance of these contributions, the field ion microscope is severely limited in its application to the examination of surfaces. The primary source of difficulty is, of course, the fact that the high electric field in which the studies must necessarily be made undoubtely causes rearrangement or desorption of the adsorbate. In extreme cases, field evaporation of the substrate atoms themselves may occur. The occurrence of field evaporation, restricts use of the field ion microscope to metals whose melting points exceed roughly 1700°K. Exceptions are possible if one is willing to sacrifice resolution by working at lower than optimum fields. Another problem

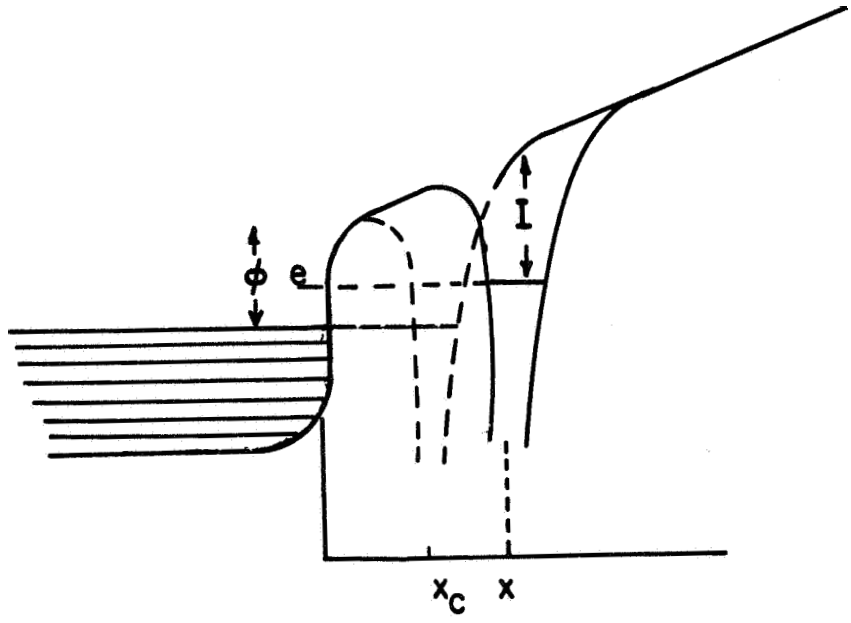

Figure 20. Potential energy diagram for field ionization.

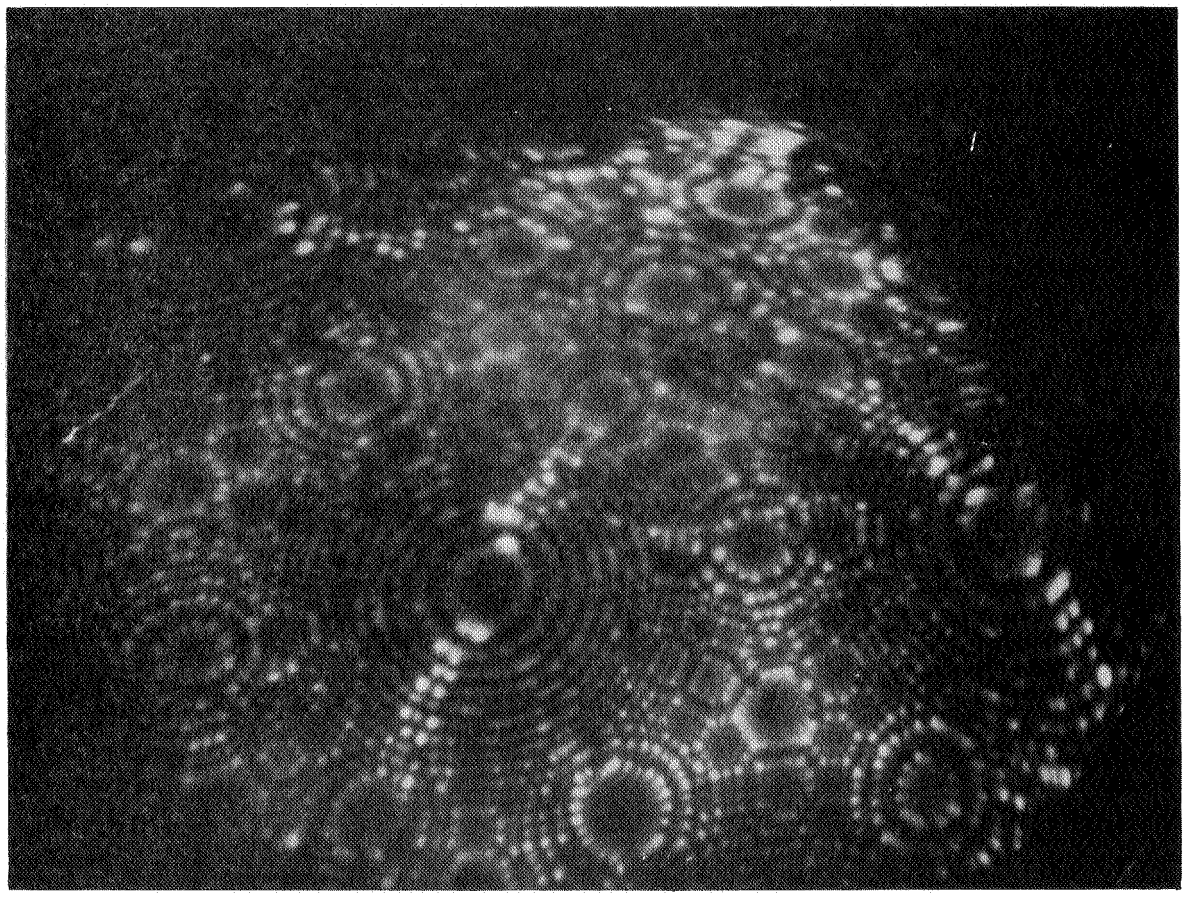

Figure 21. A field ion pattern of a tungsten surface illustrating the atomic resolution of the microscope.

that has been encountered is that of etching of the emitter tip by field enhanced chemical reactions of the adsorbate with the substrate.[50]

Field ion microscopy does lend itself very well to the inspection of clean surfaces since it is possible to actually clean the tip by field evaporation of the substrate by increasing the field slightly above that required for imaging of the surface.[48] Controlled removal of the surface layers allows one to investigate the depth of surface defects and other properties which lie a few atomic layers below the surface.

Theory of Field Ion Emission

The mechanism of field ionization is also a quantum mechanical phenomenon, and is essentially field emission in reverse in that electrons tunnel from the gas phase molecules into the tip. Since there are no empty electronic levels in the metal below the Fermi energy ϵ_F, the applied field must raise the valence level of the atom to ϵ_F, so that (neglecting polarization effects) the condition for field ionization is:

$$Fx_c \geq I - \phi - \frac{e^2}{4x_c} \tag{45}$$

where I is the ionization potential of the molecule, ϕ is the work function, and x_c is the minimum distance at which field ionization can occur; the last term of Equation (45) is due to the image potential.

As in the case of field emission, an expression for the field ion current is obtained by multiplying the rate of supply of molecules to the high field region near the tip by the probability of field ionization. The exact details of this calculation are complex and will not be reproduced here, except for the following approximate expression for the lifetime with respect to field ionization:

$$\tau_i = 10^{-16} \exp \frac{0.68\, I^{3/2}}{F} \tag{46}$$

where I is in electron volts and F in volts per angstrom.

In view of the above, the mechanism of image formation in the field ion microscope becomes quite clear. Atoms or molecules approaching the tip are ionized in the vicinity of x_c, either on the way in or on the rebound; the ions are accelerated along the Lines of force toward the negative screen so that a magnified image $\sim x/(k_t r_t)$ of the ionization zone is produced there, where x is the tip to screen distance in centimeters, r_t is the tip radius and $k_t \cong 1.5$ is an image compression factor.

According to Equation (46) the probability of ionization is a sensitive function of field, so that the ion image is a reproduction of the microscopic field distribution at the surface of the emitter. Since ionization occurs at x_c, any overlap of the equipotentials of the surface atoms will cause a certain amount of loss of structure. Also any distortion of the electronic structure at the surface due to the high fields required for image formation will also lead to image distortion.

The resolution of the field ion microscope depends on two factors; first, the transverse velocity of the image forming ions and second, the loss in detail in the field distribution at x_c. Diffraction effects, which must also be taken into account, are found to be negligible. As pointed out by Müller,[48] partial thermal accommodation on the tip reduces the incoming thermal and polarization velocity components of the image gas. Under these conditions the resolution limit due to transverse velocity components becomes

$$d = 4r_t k_t \left(\frac{kT}{eV}\right)^{1/2} \tag{47}$$

for $r = 10^{-5}$ cm, $k_t = 1.5$, and $V = 10^4$ Volts, Equation (47) gives a resolution of 10 Å at 300°K and 2.4 Å at 20°K.

The second factor which limits resolution is more difficult to assess, but an approximate calculation[30] shows the form of the functional dependence as

$$d \cong 53\,\epsilon \frac{(I - \phi)}{I^{3/2}} \tag{48}$$

where ϵ is a numerical constant of the order of 0.5 to 1.0, d is in angstroms, and I and ϕ are in electron volts. It can be readily shown that d, as given by Equation (48), goes through a maximum $20.4\,\epsilon\, I^{-1/2}$ at:

$$I = 3\phi \tag{49}$$

which suggests that Equation (48) places the most severe limitations on the resolution for imaging gases whose ionization potential is nearly three times the substrate work function.

It has also been postulated[48] that the impinging molecule, after partial thermal accommodation, undergoes a series of hopping motions because of the attraction of the inhomogeneous field acting upon the induced dipole. The average hopping height h turns out to be

$$h = \frac{3kTr_t}{4\alpha F^2} \tag{50}$$

where α is the polarizability of the impinging molecule. It is further suggested that most favorable resolution and highest image intensity are obtained when the hopping distance is slightly larger than x_c.

In order to realize best resolution and image intensity for the field ion image it will be necessary to optimize the conditions expressed in Equations (46) through (50) with respect to such variables at I, ϕ, T, r_t and F. Also, the above considerations, which are derived for a degenerate metal, may not apply exactly in the case of a nonmetallic adsorbate. For instance, the equipotentials above an adsorbed molecule may not reproduce its atomic structure unless the molecule behaves as a conductor (i.e., does not tolerate internal electric fields); in addition, the overlap of metal and adsorbate orbitals must be sufficient to allow fast electron exchange in order to maintain a uniform surface charge on the adsorbate during field ionization.

Summary

The field ion microscope is a unique tool for the investigation of surfaces because it permits single atom resolution of the surface. Consequently, field ion microscopy is a valuable tool for gaining information about the substrate. However, this technique is limited in its applications to the investigation of surface-adsorbate interactions because of the effects of the extremely high electric fields present at the surface which can cause rearrangement or even desorption of the adsorbed molecules.

REFERENCES

1. J.J. Lander, Recent Progress in Solid State Chemistry, (Pergemon Press, London, 1965) Vol. 2 p. 26

2. H.E. Farnsworth, Advan. in Catalysis 15, 31 (1964).

3. J.W. May, Industrial and Engineering Chem. 57, No. 7, 19 (1965).

4. L.H. Germer, Fundamental Phenomena in the Materials Sciences, (Plenum Press, 1966) 2, 23.

5. A.U. MacRae, Science 139, 379, No. 3553 (1963).

6. J.J. Lander and J. Morrison, J. Appl. Phys. 34, 3517 (1963).

7. E.A. Wood, J. Appl. Phys. 35, 1306 (1964).

8. G. Ehrlich, Advances in Catalysis 14, 255 (1963).

9. P.A. Redhead, J.P. Hobson, and E.V. Kornelson, Advances in Electronics and Electron Physics, (Academic Press, New York, 1962) Vol. 17, p.323.

10. L.J. Rigby, Can. J. Phys. 42, 1256 (1964).

11. T.E. Madey, J.T. Yates, and R.C. Stern, J. Chem. Phys. 42, 1372 (1965).

12. F. Ricca, A.G. Nasini and G. Saini, J. Catalysis 1, 458 (1962).

13. D.A. Degras, Paper presented at the Third International Congress of Vacuum, June 28 to July 2, 1965.

14. P. Kisliuk, J. Chem. Phys. 30, 174 (1959).
J.A. Becker, Solid State Physics (Academic Press, New York, 1958) Vol. 7 p.379.

15. P.A. Pasternak and B. Evans, Trans. Metallurgical Soc. of AIME 233, June 1965.

16. T.W. Hickmott and G. Ehrlich, J. Phys, Chem. Solids 5, 47 (1958).

17. R. Gibson, B. Bergsnov-Hansen, N. Endow and R.A. Pasternak, Tenth National Vacuum Symposium, (1963) p. 88.

18. G. Ehrlich, J. Appl. Phys. 32, 4 (1961).

19. P.A. Redhead, Vacuum 12, 203 (1962).

20. P. Marmet and J. D. Morrison, J. Chem, Phys, 36, 1238 (1953).

21. J.R. Young, J. Appl. Phys. 31, 921 (1959).

22. G.E. Moore, J. Appl, Phys. 32, 1241 (1961).

23. D.A. Degras, L.A. Peterman and A. Schram, Nat'l. Vac. Tech, Trans. 9, 497 (1962).

24. P.A. Redhead, Can. J. Phys. 42, 886 (1964).

25. G.E. Fischer and R.A. Mack, J. Vac. Sci. Tech. 2, 123 (1965).

26. S.O. Dean, Paper presented at the Annual Sherwood Vacuum Conference, U.S. Atomic Energy Commission, Jan. 30-31, 1964.

27. D. Menzel and R. Gomer, J. Chem. Phys. 41, 3311 (1964).

28. L.A. Peterman, Nuovo Cimento Suppl. 1, 601 (1963).

29. C.H. Hinrichs, Ph.D. Thesis, Washington State University, (1966).

30. R. Gomer, Field Emission and Field Ionization (Harvard Univ. Press, 1961).

31. R.H. Good, Jr., and E.W. Müller, Handbuch der Physik 21, 176 (1956).

32. A. Melmed and R. Gomer, J. Appl. Phys. 34, 1802 (1961).

33. W.P. Dyke and J.P. Barbour, J. Appl. Phys. 27, 356 (1956).

34, L.W. Swanson, R.W. Strayer and F.M. Charbonnier, Surface Science 2, 177 (1964).

35. L. Schmidt and R. Gomer, J. Chem. Phys. 42, 3573 (1965).

36. E. Wolf, 25th Annual Conf. on Physical Electronics, Mass. Inst. of Tech. (to be published).

37. L.W. Swanson, et al, Final Report for NASA Contract NAS3-2596 (Field Emission Corp., 1964).

38. L.W. Swanson, R. Strayer and F. Charbonnier, Surface Science 2, 177 (1964).

39, H. Utsugi and R. Gomer, J. Chem. Phys. 37, 1706 (1962).

40. L. SwansonandR. Gomer, J. Chem. Phys. 39, 2813 (1963).

41. E. Müller, Phys. Rev. 102, 618 (1956).

42, R. Gomer and L. Swanson, J. Chem. Phys. 38, 1613 (1963).

43. L. SwansonandR. Gomer, J. Chem. Phys. 39, 2813 (1963).

44. A. Melmed, J. Chem. Phys. 38, 1444 (1963).

45. R. Gretz, 24th Annual Conf. on Physical Electronics (MIT), p.80 (1964).

46. J.R. Oppenheimer, Phys. Rev. 31, 67 (1928).

47, E.W. Müller, *Z.* Physik 106, 541 (1937).

48. E.W. Müller, in Advances in Electronics and Electron Physics, ed. by L. Marton (Academic Press, New York, 1960) 13, 83..

49. G. Ehrlich, Advances in Catalysis 14, 255 (1963).

50, J.F. Mulson and E.W. Müller, J. Chem. Phys. 38, 2615 (1963).

SECTION B-COMPILATION OF EXPERIMENTAL DATA

Objectives

In this section, quantitative results are given on atom and ion desorption energies, activation energies for diffusion, work function changes due to adsorbed gas, adsorption site densities and vibration periods of adsorbate atoms. Some quantitative information has been given on dipole moments.

The quantitative data have been summarized and categorized alphabetically according to substrate. For each substrate, the adsorbates have been categorized into metals and electronegative gases for simplicity of presentation.

Reference to the experimental methods used is given in the text by the set of initials following the author's name and the date. A table following this introduction gives the techniques to which the initials apply. The list of techniques are variations on the general methods given in Section A of this report. A bibliography of authors referenced in Section B is presented at the end of the section.

Future Work

In the final report, we expect to cross-tabulate the data according to experimental parameters. Addition to the experimental results section will, in general, be in the form of graphs of the data which give information as to the coverage dependence of certain parameters.

Table of Techniques

CPD - Contact Potential Difference refers to any one of a variety of techniques in which the difference of potential between a reference electrode and an electrode of unknown work function is measured.

EID - Electron Impact Desorption is discussed in detail in Section A and refers to desorption of atoms from a surface by electron bombardment.

FD - Field Desorption refers to techniques involving desorption due to high fields at the surface of a field emitter tip.

FEM - Field Electron Microscopy refers to tunneling of electrons through a thin potential barrier surrounding a needle-shaped tip and subsequent radial expansion of the electron beam out to a screen. One studies the effects of adsorbates on the potential barrier.

FFD - Flash Filament Desorption refers to a variety of techniques discussed in Section A where experimental parameters are measured from the kinetics and thermodynamics of interaction of a gas with a macroscopic surface area.

FIM - Field Ion Microscopy is a technique where ions which come within a high field region close to a sharp tip are ionized and travel radially outward to a screen where they form a pattern which specifies positions of atoms of the tip.

LEED - Low Energy Electron Diffraction refers to the bombardment of a single crystal surface with low energy electrons. Owing to their wave nature, the electrons are diffracted as they interact with the lattice and produce a regular array of spots on a screen behind the source. The array is altered by the presence of adsorbates and gives information on the arrangement of adsorbates on single crystal planes.

LD - Langmuir Diode refers to a technique used for measuring alkali desorption rates by intercepting a fraction of desorbing species and ionizing them on a hot tungsten filament. The rate of neutral and ionic desorption can both be determined by application of appropriate potentials.

PB - Pulsed Beam is a method of determining adsorption lifetimes on a heated surface by use of a pulsed beam of adsorbate and observing the decay of adsorbate ion currents between pulses.

RT - Radiotracer Techniques refers to the use of radioactive isotopes of adsorbates to determine surface concentrations.

TEM - Thermionic Emission refers to a general body of techniques where experimental parameters are determined using work function variations as a heated substrate is continuously taking up and desorbing metallic adsorbates.

SP - Surface Potential refers to any one of a variety of techniques used for measuring the difference of potential between a reference surface and a surface of unknown work function.

TFC - Thin Film Calorimetry refers to a technique in which gas is adsorbed onto a thin film of metal and the actual temperature change of the film due to adsorbate-substrate interaction is measured.

TFSP - Thin Film Surface Potential refers to surface potential measurements applied to thin films.

EXPERIMENTAL RESULTS

Aluminum

Oxygen.- The integral heat of adsorption of oxygen on aluminum thin films was measured to be 9.2 eV. (Brennan, et al, 1960, TFC).

Chromium

Oxygen. - The maximum work function increase is 2.1 eV upon adsorbing oxygen at 78°K. (Quinn and Roberts, 1964 TFSP). The mean integral heat of adsorption has been measured as 7.05 eV. (Brennan et al, 1960, TFC). The initial sticking probability is 0.3. (Haque and Farnsworth, 1964, LEED).

Nitrogen. - The initial sticking probability was determined as 0.03 (Haque and Farnsworth, 1964, LEED).

Carbon Monoxide.- The initial sticking probability was determined to be 0.2 (Haque and Farnsworth, 1964, LEED).

Carbon Dioxide.-The average integral heat of adsorption was given as 3.5 eV. (Brennan and Hayward, 1965,TFC).

Cobalt

Carbon Monoxide. - The initial heat of adsorption is given as 2.0 eV. (Brennan and Hayward, 1965, TFC).

Carbon Dioxide. - The initial heat of adsorption is given as 1.6 eV. (Brennan and Hayward, 1965, TFC).

Oxygen.-The initial heat of adsorption is given as 4.3 eV. (Brennan et al, 1960, TFC).

Copper

Barium Oxide.- Adsorption of barium oxide onto a thin film of copper caused the work function to decrease from 4.3 to 2.1 eV. (Ptushinskii, 1960, TFSP).

Carbon Monoxide.-Carbon monoxide adsorbed on a thin film of copper deposited at 90°K produced a work function change of -0.315 eV. (Pritchard, 1962, TFSP).

Hydrogen. - Adsorption of hydrogen on films deposited and kept at 90°K resulted in a work function change of 0.35 eV. The activation energy for desorption at low coverage is 0.74 eV. (Pritchard, 1962, TFSP). Hydrogen has no effect on the work function of the (100) face of a copper single crystal. (Lee and Farnsworth, 1965, LEED).

Oxygen. - The addition of a large single dose of oxygen to a clean film at 298°K caused the work function to change by 0.55 eV. (Quinn and Roberts, 1964, TFSP).

Gold

Carbon Monoxide. - Carbon monoxide adsorbed on a gold film at 90°K caused the work function to decrease by 0.805 eV. (Pritchard, 1962, TFSP).

Hydrogen. -Hydrogen adsorbed onto a gold film deposited and kept at 90°K resulted in a work function increase of 0.193 eV. (Pritchard, 1962, TFSP).

Iridium

Acetylene, Ethane, Ethylene, and Hydrogen. - The qualitative character of field emission patterns indicated a rather uniform covering of the high index faces of iridium by all species studied in the temperature range 70-300°K. Hydrocarbon species, once chemisorbed, are substantially immobile at temperatures below 700°K; above 700°K an increase in electron emission, probably due to carbonization, occurs around the edges of the (111) planes. Iridium surfaces containing adsorbed species were flash heated for controlled periods of time to controlled temperatures; characteristic changes in work function resulted which were both time and temperature dependent. These experiments indicated that hydrogen is readily desorbed from iridium above 400°K, and that a large portion of the adsorbed ethane is readily desorbed at 100°K, but a residue from adsorbed ethane is not desorbed below 1000°K. For a given heating time, curves representing work function as a function of temperature for adsorbed ethylene and acetylene showed characteristic differences below 450°K. Results were interpreted as indicating chemisorption of ethylene, dehydrogenation of chemosorbed ethylene to form chemisorbed acetylene and chemisorbed hydrogen, desorption of chemisorbed hydrogen, dehydrogenation of chemisorbed acetylene and finally crystallization of carbon residue. (Arthur and Hansen, 1962, FEM).

Iron

Nitrogen. -Nitrogen adsorbed on an iron film caused the work function to diminish by 0.27 eV with increasing coverage up to 1×10^{15} molecules/cm2. (Suhrmann, et al, 1963, TESP).

Oxygen. -Successive oxygen doses resulted in a work function change of 1.55 eV for a film at 78°K. Subsequent warming of the film to 193°K decreased the work function change to +0.5 eV. (Quinn and Roberts, 1964, TFSP). The initial heat of adsorption of oxygen was measured to be 5.9 eV. (Brennan, et al, 1960, TFC).

Carbon Monoxide. - The initial heat of adsorption of carbon monoxide is 2.0 eV. (Brennan and Hayward, 1965, TFC).

Carbon Dioxide. - The initial heat of adsorption of carbon dioxide is 3.0 eV. (Brennan and Hayward, 1965, TFC).

Manganese

Carbon Monoxide. - The initial heat of adsorption of carbon monoxide was measured as 3.4 eV. (Brennan and Hayward, 1965, TFC).

Oxygen. - The initial heat of adsorption of oxygen is 6.5 eV. (Brennan and Hayward, 1965, TFC).

Molybdenum

Barium. -The electron work function was measured by Richardson method for three faces of molybdenum single crystal: ϕ_{110} = 5.10 ± 0.05 eV, ϕ_{100} = 4.40 ± 0.05 ev, ϕ_{111} = 4.15 ± 0.05 eV, using an arrangement employing spherical and plane electrodes. In the case of a spherical specimen a lower value of 4.8 to 4.9 eV was obtained for ϕ_{110}. Evaporation of barium on the (111) face lowered the work function to 2.3 ± 0.1 eV. The mean heat of adsorption of barium on the (111) face of the molybdenum crystal was determined from adsorption curves as E_{111} = 3.90 - 4.00 eV. (Azizov, et al, 1966, FEM TEM).

Cesium. - A minimum work function of 1.5 eV was found by field electron emission techniques. The work function-coverage curves agree closely with existing ones measured by thermionic methods. A study of the temperature effect on work function for cesium on molybdenum showed a negative temperature coefficient of approximately 1.3 x 10^{-4} eV/deg. (Swanson, et al, 1964a, FEM). Field effects were found to be the same as for tungsten, The heat of desorption of Cs^+ from molybdenum is given as 1.72 eV with a vibration time τ_o = 12.3 x 10^{-13} sec.(Husmann, 1965, PP).

Gold. -The heat of desorption was found to be 4.2 ± 0.2 eV and the vibration time 0.5 x 10^{-13} sec. (Von Goeler and Luscher, 1963, RT).

Nickel. - Nickel was found to adsorb coherently on molybdenum and preferentially on the (111) planes of the substrate. For coverages of about 1/5 of a

monolayer the activation energy of surface migration was 1.48 ± 0.06 eV. The desorption energy was 2.10 ± 0.05 eV and did not vary with—degree of coverage, Heavy adsorbed layers of nickel were investigated and the equilibrium position of heavy layers was found to be field dependent, (McIrvine and Bradley, 1957, FEM).

Silver.-The desorption energy of silver was measured as 1.9 ± 0.3 eV. (Von Goeler and Peacock, 1963, RT).

Carbon Monoxide. - The initial heat of adsorption on a thin film was measured as 3.2 eV. (Brennan and Hayward, 1965, TFC).

Hydrogen. - The initial heat of adsorption is given as 1.74 eV. (Cerny, et al, 1966, TFC). The sticking probability of hydrogen is 0.35 for filaments and a surface coverage of 8.2×10^{14} atoms/cm^2 was obtained at 295°K. Saturation surface coverages were independent of pressure for the range (10^{-8} - 10^{-5} torr) studied, but strongly temperature dependent in the range 225 to 500°K. Adsorbed hydrogen was readily replaced by other gases. (Pasternak and Wiesendanger , 1961, FFD).

Nitrogen. - In the adsorption of nitrogen on molybdenum filaments , the saturation surface coverage decreased about 30% as the temperature was raised from 222°K to 710°K, and the initial sticking probability decreased from 0.7 to 0.2 as the higher temperature was approached. At room temperature , the initial sticking probability is 0.7 and the surface coverage is 4.4×10^{14} at/cm^2. (Pasternak and Wiesendanger, 1961, FFD). The initial sticking probability for nitrogen on molybdenum films was found to be 0.6 at room temperature but the shape of the sticking probability vs coverage curve is different from that obtained using filaments. (Pasternak et al, 1966, TF).

Oxygen.-The maximum work function change for oxygen on molybdenum films is 1.65 eV. No distinction between values of the work function obtained at 77°K and 298°K could be made. Addition of hydrogen to an oxidized film at 25°K produced no change, but at about 423°K the work function decreased as hydrogen was slowly adsorbed.(Quinn and Roberts , 1964, TFSP).

Flash filament studies shaved two desorption peaks. These could be resolved by heating the filament to 1300°K in about 1 sec. The peaks occurred in the ranges 300 - 600°K and 800 - 1000°K. (Gasser and Schuftan, 1963, FFD). The initial heat of adsorption has been measured as 7.5 eV. (Brennan, et al, 1960, TFC).

Nickel

Barium. - Adsorption of barium caused a maximum work function decrease of 2.2 eV. Barium oxide caused a work function decrease of 2.9 eV. (Ptushinskii, 1961, TFSP).

Cesium. - A layer of cesium caused the work function to decrease by 2.9 eV. (Ptushinskii, 1961, TFSP).

Silver. - The heat of desorption of silver from nickel was determined to be 1.6 ± 0.3 eV. (Van Goeler and Peacock, 1963, RT).

Carbon Monoxide. -Carbon monoxide is present on nickel in three states whose desorption energies are given as 0.15, 0.28 and 2.28 eV. The differential activation entropies calculated from the experimental data for these states are -44.5 , -42.2 and 8.4 cal/mole-deg. (Degras, 1965, FFD). The initial heat of adsorption has been measured as 1.83 eV. (Brennan and Hayward, 1965, TFC).

Hydrogen. - It was found that boundary-free migration occurs at coverages up to $\theta \sim 1$ with an activation energy of 0.30 ± 0.04 eV by field electron emission studies. For $\theta > 1$ spreading occurs near 4°K, as with hydrogen on tungsten. The heat of desorption of H_2 from nickel was found to be 2.0 ± 0.13 eV for $\theta << 0.1$ from the temperature variation of the desorption rates. The failure to observe on nickel the intermediate coverage boundary spreading found on tungsten by field emission techniques is believed to result from the fact that nickel is much more closely packed, so that all portions of the nickel surface seem "smooth" to H atoms. Evidence in favor of this argument is found in the fact that the ratio of the diffusion heat to the adsorption heat is approximately 1 for nickel. This ratio corresponds to that found for radial boundary diffusion on tungsten. (Wortman, et al, 1957a, FEM). A field dependent transformation in the adsorbed film was found between 2° and 4°K and interpreted as a shift in the equilibrium between adsorbed H_2 molecules and the terminal fraction of adsorbed H atoms. The implications of this result for the mechanism of H_2 - D_2 exchange can be considered. (Wortman, et al, 1957b, FEM).

Hydrogen adsorbed on a (110) surface of a nickel single crystal has an isoteric heat of adsorption of 1.2 eV. (Germer and MacRae, 1962a, LEED). The average integral heat of adsorption is given as 0.95 eV. (Brennan and Hayes, 1964, TFC).

Oxygen. -The maximum work function change on a nickel thin film is 1.4 eV for a deposit formed and held at 78°K. (Quinn and Roberts, 1964, TFC). The initial heat of adsorption of oxygen on nickel is 4.6 eV. (Brennan et al, 1960, TFC).

Niobium

Nitrogen. -Nitrogen adsorbs onto niobium with an initial sticking probability of about 0.4 at 298°K and forms a surface coverage of 7×10^{14} atoms/cm^2. Above 400°K nitrogen diffuses into the bulk. (Pasternak, 1965, FFD).

Carbon Monoxide. -There are at least two chemisorbed binding states, the weaker one being desorbed above 150°K. The field electron emission

patterns resulting from heating to 600°K and above indicate a decomposition of the CO held on the surface in the more strongly bound state. Heating a CO covered surface in the region of 150°K leads to a characteristic mottling of the pattern ascribed to surface clustering. Evidence that adsorption and desorption are irreversible was given. (Klein and Little, 1964, FEM).

Oxygen. -The initial heat of adsorption is 9.0 eV. (Brennan et al, 1960, TFC).

Palladium

Carbon Monoxide. -The initial heat of adsorption of carbon monoxide is 1.9 eV. (Brennan and Hayward, 1965, TFC).

Oxygen. - The initial heat of adsorption is 3.0 eV. (Brennan et al, 1960, TFC).

Platinum

Carbon Monoxide, -The initial heat of adsorption is 2.1 eV. (Brennan and Hayward, 1965, TFC).

Hydrogen. -Hydrogen chemisorption at 300°K to a maximum coverage of about 0.2 monolayer was attained at a rate corresponding to a sticking probability of 0.001. (Wiesendanger, 1963, FFD).

Oxygen. - It was found that under certain circumstances of heavy oxygen contamination on platinum that it was nearly impossible to remove the contaminant, and there appeared to be a definite interaction with the platinum upon heating. This was established by controlled oxidation of platinum field emission tips. (Melmed, 1965a, FEM). The initial heat of adsorption is 3.0 eV. (Brennan et al, 1960, TFC).

Nitrogen. -No chemisorption of nitrogen occurs on platinum at 300°K and pressures below 10^{-7} torr. (Wiesendanger, 1963, FFD).

Rhenium

The heats of desorption of numerous alkali metal ions from rhenium have been studied and are given along with the respective vibration periods (τ_o) in the following table:

	τ_o (sec)	E_p (eV)	Worker
Ba^+	$(0.6 \pm 0.4) \times 10^{-13}$	4.74 ± 0.21	(Scheer and Fine, 1963a, PB)
Cs^+	1.93×10^{-13}	1.96	(Taylor, 1964a, LD)
Cs^+	11.4×10^{-13}	2.2	(Husman, 1965, PP)
Cs^+	$(1.9 \pm 0.9) \times 10^{-13}$	2.04 ± 0.04	(Scheer and Fine, 1963a, PB)
K^+	$(1.0 \pm 0.3) \times 10^{-13}$	2.33 ± 0.03	(Scheer and Fine, 1963b, PB)
Rb^+	$(0.8 \pm 0.3) \times 10^{-13}$	2.28 ± 0.03	(Scheer and Fine, 1963b, PB)
Na^+	$(0.2 \pm 0.1) \times 10^{-13}$	2.75 ± 0.03	(Scheer and Fine, 1963b, PB)

Thorium.- The Richardson constants for rhenium were found to be $\phi = 4.85$ eV, and $A = 66 A/cm^2 - deg^2$. The work function decreases as thorium is adsorbed to a minimum of 3.15 eV at a coverage of 4.2×10^{-14} atoms/cm^2 then rises to a constant value ϕ_o of 3.3 eV at $\sigma = 8 \times 10^{14}$ atoms/cm^2. A comparison with the tungsten system gives a ϕ_m and ϕ_o at the same respective coverages. The coverage at which ϕ becomes constant has the same density as the (100) plane of bulk thorium. The values of ϕ_o differ from that of bulk thorium by only 0.1 eV. For the temperature range 2203 - 2468°K, the activation energy for desorption is $E = 8.30 \pm 0.15$ eV for low coverages. (Anderson et al, 1963, FFD-TEM).

Rhodium

Carbon Monoxide.- The initial heat of adsorption of carbon monoxide is 2.0 eV. (Brennan and Hayward, 1965, TFC).

Oxygen.-The initial heat of adsorption of oxygen is 4.45 eV. (Brennan et al, 1960, TFC).

Tantalum

The heats of desorption of some of the alkali metal ions have been studied and are tabulated below along with their respective vibration periods (τ_o).

	τ_o (sec)	E_p (eV)	Worker
Cs^+	1.8×10^{-9}	1.65	(Husman, 1965, PP)
K^+	41.6×10^{-13}	2.05	(Husman, 1965, PP)
Rb^+	236×10^{-13}	1.81	(Husman, 1965, PP)

Cesium. - The minimum work function of cesium on tantalum was found to be 1.6 eV and the initial heat of adsorption 2.5 eV. (Gorbatyi and Ryabchenko, 1965, FEM).

Carbon. - Carbon, once deposited on tantalum, cannot be removed by high-temperature treatment, as in the case of tungsten. From field electron microscopy techniques low-carbon contamination causes (334) planes to appear as dark areas, just as for carbon on tungsten. At temperatures in the region of 950°K, platelets, presumably TaC, form and migrate to the (111) zones of the emitter single-crystal tip. The energy of activation of this surface migration process is 2.3 eV. (Klein and Leder, 1963, FEM).

Carbon Monoxide. -Adsorbed carbon monoxide shows three states of binding on tantalum. The weakest of these is desorbed at temperatures above 125°K with no observable surface migration; bonding with the surface is of the van der Waals type. This is in contrast with the second state, which is desorbed above 650°K. The third state is dissociated before desorption to give the oxygen-on-tantalum field electron emission pattern. Surface migration involving the second adsorbed state occurs with an activation energy of 1.7 eV. The work function of a carbon monoxide-covered tantalum surface, obtained by spreading the carbon monoxide on a shadowed tip at 40°K, is 0.8 eV greater than that of the corresponding clean tantalum, The first state of desorption yields a value of 0.17 eV for the desorption energy which is considerably higher than the heat of vaporization of carbon monoxide, 0.06 eV, so that some interaction with the tantalum occurs. (Klein and Leder, 1963, FEM). The initial heat of adsorption of carbon monoxide is 5.85 eV. (Brennan and Hayward, 1965, TFC).

Oxygen. - The initial heat of adsorption of oxygen is 9.2 eV. (Brennan et al, 1960, TFC). Adsorption of oxygen on a (110) face of a tantalum single crystal raised its work function by 0.1 eV. The work function of the clean (110) plane is 4.74 $\pm$ 0.02 eV. The activation energy for oxide growth was estimated to be 0.24 $\pm$ 0.04 eV. (Boggio and Farnsworth, 1964, LEED).

Tungsten

Barium. - The initial heat of adsorption was given as 3.6 eV (Moore and Allison, 1955, RT), 4.68 eV (Zingerman, et al, 1961, TEM), and 4.7 eV (Gavrilyuk and Medvedev, 1963, SP-FFD).

Upon adsorption of barium, the work function change at room temperature is -2 5 eV and then increases with further coverage to a final $\Delta\phi$ of -1.9 eV. (Zingerman, et al, 1961, TEM).

Field desorption of barium occurs at about 100 MV/cm. (Muller, 1956, FEM-FD).

It was found that adsorption seems to be polar but not ionic and that desorption of Ba^{++} occurs under the conditions of field desorption experiments. If this interpretation is correct, $\alpha \sim 60$ Å for the polarizability of adsorbed Ba which is close to the value for the free atom. It was found that positive fields have more effect on the activation energy and preexponential term of the diffusion coefficient than negative ones. While a $1/2\ \alpha F^2$ dependence of the activation energy is compatible with the limited data for negative fields, no simple behaviour was found for positive ones, the activation energy going through a minimum of 0, accompanied by a drastic reduction in preexponential term. Values for the zero heat of adsorption were obtained over a wide coverage interval and agree well with those of Moore and Allison, (above), where overlap occurs. (Utsugi and Gomer, 1962a, FEM-FD).

The electron desorption cross section for barium was found to be $< 2 \times 10^{-22}$ cm^2. (Menzel and Gomer, 1964, FEM-EID). The minimum work function of barium on tungsten was found to be 2.1 eV. (Zubenko and Sokol'skaya, 1961, FEM).

$BaAu_5$. - The minimum work function of several Payers was found to be 3.3 eV. (Zubenko and Sokol'skaya, 1961, FEM).

Barium Oxide. - The field desorption of BaO occurs as BaO^+ within the 80 - 400°K range and as BaO^{++} within the 500 -1000°K range. Barium is field-desorbed from W in the form of singly-charged ions over the 80 - 300°K and 1000 - 1200°K regions, and as doubly-charged ions at 300 - 1000°K. (Naumovets, 1963, FEM-FD).

Beryllium. - The adsorption of beryllium does not affect the work function of tungsten; presumably, because it has the same work function as tungsten. (Zingerman et al, 1961, TEM).

Calcium. - Adsorption of calcium lowers the work function by 1.9 eV at 5×10^{14} atoms/cm^2 and then raises it to $\Delta\phi$ = -1.7 at a full coverage of 8×10^{14} atoms/cm^2. (Zingerman, et al, 1961, TEM).

Cesium.- The initial heat of desorption and the respective vibration period for cesium ions from tungsten has been determined by several workers and the results are given as follows:

E_p(eV)	τ_o (secs^{-1})	Worker
1.91	----------	(Taylor and Langmuir, 1933 FFD)
2.04	1.1×10^{-12}	(Scheer and Fine, 1962b, PB)
2.73	2.4×10^{-15}	(Taylor, 1964a, LD)
1.95	1.77×10^{-12}	(Husman, 1965, PP)

A minimum work function of cesium on tungsten was found to be 1.70 eV (Taylor and Langmiur, 1933, FFD) and 1.5 eV (Swanson, et al, 1964a, FEM).

The field electron emission results for neutral desorption agree extremely well with the data of Taylor and Langmuir in the coverage range 0 to 1.4×10^{14} atoms/cm^2, but fall below the heats of these authors at higher coverages. The combination of neutral and ionic heats yields a value of $\phi = 5.3$ eV for the zero coverage work function of the regions from which ionic desorption occurs. The phenomenon of phase segregation observed by Taylor and Langmuir at very low coverages under steady-state conditions can be shown to be a kinetic rather than a thermodynamic effect. (Schmidt and Gomer, 1965c, FEM).

At low coverage the field desorption of Cs from tungsten can best be explained on the basis of a covalent ground state which suggests that an electronic transition is involved in the desorption process. On this basis the polarizability of adsorbed Cs is found to be close to that of the free atom. The results were much the same as those found for Ba. (Utsugi and Gomer, 1962b, FEM-FD). Field dependent variations of both the preexponential factor and activation energy of the surface diffusion coefficient written as $D = D_o \exp(-E_d^F/kT)$ were found. At temperatures sufficient to induce mobility, an increase or decrease in cesium coverage in the high field region of the emitter occurs with positive or negative fields; positive fields, on the other hand, produce large variations in desorption rates due to field desorption. Most of the field effects can be analyzed in terms of μF and $1/2\, \alpha F^2$ interactions. (Swanson, et al, 1964b, FEM-FD).

Copper.- The binding energy of copper on tungsten is 3.5 ± 0.5 eV. (Godwin and Lusher, 1965, FFD). Adsorption of one to ten atomic layers of Cu was followed through changes in the field electron emission pattern and average work function of the W field emitter. Surface diffusion was investigated for single-, double-, and triple-layer diffusion, and for successive diffusion of one layer of Cu on others up to four layers. The negative electric

field used in some of the measurements was found to decrease the apparent activation energy and the preexponential factor of the diffusion equation. The activation energy varied over the tungsten surface and increased with atomic roughness; it also varied with coverage, decreasing rapidly at first and then slowly with increasing coverage as shown in the following table:

Diffusion type	Region of Surface	E_d eV zero field	Temperature range, oK	D_o (cm^2/sec) (zero field)
Single layer	Average	0.74 ± 0.09	548-673	6×10^{-5}
Double layer	Average	0.56 ± 0.04	533-653	6×10^{-6}
Triple layer	Average	0.43 ± 0.04	488-653	6×10^{-7}
Second layer	Average	0.48 ± 0.04	553-673	2×10^{-8}
Third layer	Average	0.43 ± 0.04	553-673	2×10^{-6}
Fourth layer	Average	0.39 ± 0.04	553-673	1×10^{-6}
Single layer	(011)-(112)	0.48 ± 0.04	473-573	7×10^{-7}
Single layer	(001) - vicinal	0.95 ± 0.09	523-673	1×10^{-3}
Single layer	(011)	0.35	289-313	
Thermal desorption of 3 layers Cu/W:		3.82 ± .26	1513-1613	

(Melmed, 1965b, FEM).

The effect of adsorbed oxygen and nitrogen on the mobility of copper on tungsten depends on the relative amounts of gas and copper and on the local substrate crystallography,, Generally stated, they increase the activation energy for surface diffusion. The zero field activation energies for surface diffusion of Cu/W, Cu/O/W, and $Cu/N_2/W$ are as follows: 0.87 eV, 1.21 eV, and 1.17 eV respectively. (Melmed, 1966, FEM).

Gold. - The observed binding energy of gold on tungsten is 3.6 ± 0.5 eV. (Godwin and Lusher, 1965, FFD).

Magnesium. - Adsorption of magnesium lowers the work function by 0.9 eV at 7×10^{14} atoms/cm^2 and further adsorption to 12×10^{14} atoms/cm^2 causes $\Delta\phi$ to change to -0.75 eV. (Zingerman, et al, 1961, TEM).

Potassium. - The $\bar{\phi}$ vs $\bar{\theta}$ curve, representing average values of ϕ and θ over a field emission tip, has a minimum of 1.78 eV at $\bar{\theta} = 0.83$, $\bar{\sigma} = 3.2 \times 10^{14}$ atom/cm^2 which coincides with the minimum ϕ on the (1 10) planes and approaches the work function of potassium at $\bar{\theta} = 2.3$. Distinct minima also occur for other close-packed planes, like the (211). At $\bar{\theta} = 1$, $\bar{\sigma} = 3.9 \times 10^{14}$ atom/cm2,

$\bar{\phi}$ = 1.95 eV the emission pattern is indistinguishable from that of clean tungsten. The average charge per K atom varies from 0.27 at low θ to 0.2 electron charges at θ = 0.8. The value of the average charge per K atom on the close-packed W planes at low coverage may be considerably higher. The activation energy of neutral desorption varies from 2.67 to 2.4 eV over the interval $0 < \bar{\theta} < 0.4$ and falls rapidly at higher coverage, approaching the heat of sublimation of K, 1.0 eV, at θ 1.0. The activation energy of ionic desorption was measured over the interval $0 < \bar{\theta} \leq 0.07$, and indicates that ionic desorption occurs from regions of $\bar{\phi}$ = 5.3 eV. On these regions $d\bar{\phi}/d\bar{\theta}$ is very high, suggesting that the K-atom density exceeds the average by a factor of 3 or more, and that adsorption on these regions may be nearly ionic at low θ. The activation energy of surface diffusion was measured as a function of θ. E_d and the preexponential term of the diffusion coefficient increased with $\bar{\theta}$ in the range $0 < \bar{\theta} \leq 0.6\text{-}0.7$, E_d rising from 0.3 eV at $\bar{\theta}$ = 0 to 0.8 eV at $\bar{\theta}$ = 0.6. This was tentatively explained in terms of activated hopping into the almost empty second layer, followed by rapid diffusion, terminated by recombination of the excited atom with a hole in the first layer. At θ = 0.8 - 1.0, E_d falls sharply, corresponding to diffusion in the second layer. It was suggested that K adsorption sites are relatively weakly structure dependent, so that a displacement of atoms from the initially occupied, optimal sites occurs at $\theta > 0.4$ in order to accommodate more adsorbate in direct contact with the substrate. The experimental results were shown to be consistent with a model based on delocalized bonding, i.e., metallic adsorption. (Schmidt and Gomer, 1965a, FEM).

The binding energy of K^t on tungsten was found to be 2.22 eV and the vibration period 2.3×10^{-13} secs. (Husman, 1965, PP).

The results of experiments on field desorption of potassium from tungsten with no migration may be reasonably interpreted on the basis of the theory that the ions evaporate through a Schottky barrier, which at zero field yields E_p = 2.6 eV, $\nu \sim 10^{12}$ sec^{-1}. The linearity observed experimentally in the $\sqrt{F_d} = f(T)$ curve indicates that the forces binding the potassium ion with the (110) face of W may be regarded as electrostatic image forces up to a distance from the surface given by $x = 1/2\sqrt{e/F} \sim 3$ Å. The surface diffusion rate of K atoms over W is very strongly dependent on the magnitude and direction of the electric field. The dipole moment between adsorbed K atoms and tungsten, which shows up as a reduction in work function at constant coverage, is strongest at (110) faces. (Haumovets, 1964, FEM).

Potassium Chloride. - Thermal activation of potassium chloride on tungsten at approximately 500°K results in the desorption of potassium leaving a tungsten chloride (WCl_x) layer which is stable to about 1100°K. Data were interpreted as showing that potassium chloride in the presence of tungsten at room temperature forms a WClK with the K-Cl bond being the weakest. It was shown by field electron emission techniques that potassium chloride on tungsten and chlorine on tungsten demonstrate identical properties in the

temperature range 1100°-1900°K. Limiting processes above 1100°K were believed to be the formation and subsequent desorption of tungsten chloride and atomic chlorine. The heats of desorption and work function were found as follows: In the range of 475-600°K, E = 0.43 to 3.09 eV and ϕ = 2.3 to 5.3 eV; in the range 1100°-1400°K, E = 3.22 $\pm$ 0.65 eV and ϕ = 5.3 to 4.6 eV; in the range 1700°-1884°K, E = 3.56 $\pm$ 0.70 eV and ϕ = 4.6 to 4.5 eV. The behavior of chlorine on tungsten was shown to be similar to that of oxygen on tungsten in the temperature range studied. (Silver and Witte, 1963, FEM).

Potassium and Hydrogen.-Molecular hydrogen does not appear to be chemisorbed on potassium at low temperatures. Atomic hydrogen interacts, probably by the formation of a hydride structure with K atoms outermost from the surface. The coadsorption of H and K on tungsten causes a decrease in work function over that caused by potassium alone, and increases the temperature range required for potassium surface diffusion on tungsten. These facts are explained in terms of a surface complex WHK in which H is negatively charged relative to K. (Schmidt and Gomer, 1965, FEM).

Rubidium.- The binding energy and vibrational period of rubidium atoms was found to be 2.60 $\pm$ 0.1 eV and 2.5 x 10^{-13} sec. (Hughes, 1959, PB) and 2.07 eV and 3.4 x 10^{-12} sec (Husman, 1965, PP) respectively. The binding energy of Rb^+ is 1.90 $\pm$ 0.05 eV and the vibration period is 3.5 x 10^{-12} sec (Hughes and Levinstein, 1959, PB).

Sodium.- It was shown that for small coverages adsorption of sodium lowers the work function, ϕ, of all planes of tungsten, The most abrupt and greatest lowering of ϕ by sodium was observed on the (110) faces. which is related to the higher concentration of sodium on this face, and to the initially high work function of the face. (Shrednick and Snezhke, 1964, FEM).

Measurements were made of the work function as a function of coverage and temperature. A curve was calculated for the mean heat of evaporation. Field desorption measurements made it possible to obtain an independent value for the heat of adsorption in this stage. The zero coverage heat of adsorption was found to be 2.4 eV and the minimum work function was $\sim$1.9 eV. (Shrednik and Snezekho, 1964, FEM). The binding energy for ionic desorption is 2.33 eV and the vibration period is 6.3 x 10^{-13} sec. (Husman, 1965, PP).

Strontium,-A study of the migration of Sr on W by field electron emission techniques revealed two modes. In the first mode, for $\theta > 1$, no boundary is observed. The activation energy for the first mode was found to be 0.79 $\pm$ 0.06 eV and the activation energy for the second mode was found to be 1.44 $\pm$ 0.08 eV. (Barnaby, et al, 1964, FEM).

The activation energy for the thermal desorption of Sr from W falls from 4.21 $\pm$ 0.22 eV at zero Sr coverage to 1.78 $\pm$ 0.13 eV at "monolayer" coverage. The latter value approaches the heat of sublimation of bulk Sr (1.69 eV). The desorption energies found using field electron emission techniques deviate

markedly from the extrapolated thermionic results of Moore and Allison (near) $\theta = 0$ and for $\theta > 0.5$. A linear relationship was found to exist between the activation energy for desorption and the logarithm of the preexponential factor in the rate equation. (Madey, et al, 1965a, FEM).

The energy of desorption is 3.56 eV. The monolayer surface coverage is 4.89 x 10^{14} atom/cm^2 and the monolayer work function is 2.2 eV. (Moore and Allison, 1955, RT). A study of work function vs coverage gives $\Delta\phi_m$ as -2.1 eV at 4 x 10^{14} atom/cm^2 with a final $\Delta\phi$ of -1.8 eV at 8 x 10^{14} atom/cm^2. (Zingerman, et al, 1961, TEM).

Strontium Oxide.- Reactions take place on the (111) and (100) which have high concentrations of four nearest neighbor surface atoms. Below 1150°K evidence was given for the dissociation of SrO and migration of Sr to the (110) edges where clusters of crystallites are formed. Two modifications of field emission patterns associated with the (Sr-O-W) complex within 1150-1550°K were tentatively identified with the basic and normal tungstate; apparently the first goes over to the second with an activation energy of 2.6 eV as determined from desorption data, An unusually sharp decrease in Fowler-Nordheim work function to (2.6 eV) occurs during this reaction. In the later stages of desorption above 1550°K patterns identifiable with an oxygen-tungsten surface were obtained. Desorption at this stage takes place with an activation energy of ~ 6.1 eV. (Gape and Coomes, 1960, FEM).

Thorium.-Field desorption of thorium occurs in the 200 MV/cm range, (Muller, 1956, FEM-FD). The (111) planes have the strongest adsorbing force for thorium atoms and more than a monoatomic layer is formed on the plane. The (211) planes have the weakest adsorbing force. The field emission current from a (111) plane has a maximum value (goes through a minimum work function), while the current from a (211) plane changes monotonically (no minimum in work function)., This phenomena was explained by a balance between the diffusion of thorium atoms from the interior of tungsten and the evaporation of thorium from the surface. The lowest work function of the (111) planes is about 2.7 eV, but the lowest value of the average work function is 2.9 eV. The surface diffusion energy of Th-atoms along the tungsten surface and the desorption energy were measured and found to be 2.8 and 7.4 eV respectively. (Sugata and Kim, 1961, FEM).

The minimum work function of thorium on tungsten was found to be 3.0 eV by field emission techniques and 3.31 ± 0.02 eV by the Richardson method. (Zubenko and Sokol'skaya, 1961, FEM).

A study of the (110) and (411) planes showed that the work function goes through a minimum for both planes at a coverage of 4.2 x 10^{14} atom/cm^2. The monolayer coverage is 9 x 10^{14} atoms/cm^2. The (100) plane has an initial work function of 4. 52 eV, a minimum of 3.35 eV. The (411) plane has

an initial work function of 4.41 eV, a minimum of 3.05 eV and a final value of 3.35 eV. (Estrup, et al, 1966, LEED).

Titanium.-It was shown that upon adsorption of titanium the work function varies monotonically. The rate of vaporization of titanium from tungsten carbide is lower than from tungsten, while the heat of vaporization is approximately the same. (Zubenko, 1963, FEM),

Zirconium. - Both electron and ion (deuteron and proton) field emission patterns were observed. It was found that zirconium lowers the work function markedly on the (100) plane. It was shown by best image ion voltage measurements that Zr on W roughens the surface around the (100) plane thereby changing the field factor, especially for high concentrations of Zr (>monolayer). The work function for a monolayer of Zr on W was found to be 2.62 eV which falls to 2.2 eV as more Zr is added. The latter lowering is attributed to a field factor change. A (100) plane adherence is postulated by means of a hard sphere fit of Zr atoms (3.16 Å diameter) on the (100) planes of W (3.16 Å lattice const.). (Shrednik, 1961, FEM-FIM).

Argon.-It was found that a work function decrease of 0.80 eV occurs for a saturated monolayer when measured at 4.2°K. The work function change is most pronounced near the (100)face. Multilayer adsorption also occurs. It appears that dipole-dipole repulsions suffice to make the first layers gas-like. (Gomer, 1958b, FEM).

Adsorption lowers the work function by 0.87 eV for A at 20°K. Binding to the surface is structure sensitive--it is strongest around the (100) poles, in the vicinity of the (116) and (130) planes, and weakest at the (111), as observed in field electron emission patterns. This sequence of binding energies corresponds to that calculated for different lattice sites on the assumption of dispersion forces. The lowering of the work function caused by adsorption was interpreted as a polarization of the gas atoms by the dipole layer of the metal surface; formally, the interactions at a metal resemble those of the rare gases adsorbed on ionic crystals. Interaction of polarized adatoms and the antiparallel field applied for electron emission increases the free energy of the adlayer, bringing about rearrangements particularly important for adsorbed argon. Observations of changes in field electron emission with temperature yield a value of 0.04 eV for the diffusion of argon over the (310) toward the (100). (Ehrlich and Hudda, 1959, FEM).

Bromine. - At low bromine coverages, ϕ decreases to a minimum of 4.1 $\pm$ 0.1 eV corresponding to a $\Delta\phi$ change of -0.4 eV, accompanied by a 60 times reduction in emitting area, ascribed to the penetration of bromine atoms below the effective surface plane. Extended exposure to bromine (5×10^{-9} torr) vapor produces a constant $\Delta\phi$ of 1.0 eV with respect to clean tungsten. (Duell and Moss, 1965, FEM).

Carbon Monoxide. -Adsorption of carbon monoxide has been studied using various techniques. The more recent data has employed ultrahigh vacuum techniques and a summary of the data is given in the following table:

$\Delta\phi$ eV	$s_{300^\circ K}$	$\sigma_{300^\circ K}$	Desorption Energies eV a	β_1	β_2	β_3	Worker
				2.3			(Klein, 1959, FEM)
0.85	0.2	7.4×10^{14}	1.26	2.56	3.02	3.28	.(Redhead, 1961, FFD)
	0.49	9.5×10^{14}	0.87		3.26	4.35	(Ehrlich, 1961b, FFD)
				2.3	3.3	4.3	(Ehrlich, 1962, FEM)
			0.87	2.26	3.04	4.35	(Rootsaert, et al, 1962, FEM)
0.85	0.50	4.5×10^{14}	0.91	2.70		4.00	(Gavrilyuk and Medvedev, 1963, FFD)
	0.48	5.8×10^{14}	1.0	2.74	3.35	3.9	(Rigby, 1964, FFD)
			1.0	2.6			(May and Germer, 1966, LEED)

The desorption kinetics indicate that adsorption is nondissociative and can be quite complex. At room temperature, transfer takes place between the a phase and the gas phase and also between the a phase and the β phase. (Rigby, 1964, FFD). Further complexities involve the β state which is a composite of at least three substates each with different desorption energies, The β_1 state occurs on (411), (310) and (210) faces, the β_2 state occurs on (111) and other faces and the β_3 occurs on the (111) zones. (Rootsaert, et al, 1962, FEM). The complexities of the system are even more pronounced at low temperatures, with the appearance of a nonreversible state called the "virgin layer". This layer appears upon adsorption at low temperature (20°K) and increases the work function to 5.6 eV, indicating a negative dipole moment. This layer appeared to desorb, and convert to the recognized *a* and β states upon heating above 170°K, but further readsorption does not restore the previously obtained high work function. This characteristic was interpreted by recognizing the fact that the a state demonstrates a positive dipole moment and the β state is characterized by a negative dipole moment, so that after heating the "virgin layer" to 170°K, redosing cannot restore the initial conditions represented by the negative dipole but instead is the result of depositing more of the a CO on top of the β. (Swanson and Gomer, 1963, FEM-FD). The relative abundance, relative dipole moments, and absolute sticking coefficients of virgin, *a* and β CO adsorbed on tungsten have been determined by a combination of work function vs coverage measurements with step-desorption spectra and sticking coefficient measurements. The dipole ratios were $\mu_a/\mu_{virgin} = 0.68$; $\mu_\beta/\mu_{virgin} = 0.68$ for the initial, and $\mu_\beta/\mu_{virgin} = 1.0$ for the terminal portion of the β layer. The relative abundances were total β/total virgin = 0.55; (virgin converted to β)/(β from virgin conversion) = 2.1; *a*/total β = 1.2.

Initial sticking coefficients are close to unity up to 700°K and decrease rapidly at coverages {relative to the maximum amount of adsorbate retained at that temperature) of 0.6 - 0.4. (Bell and Gomer, 1966, FEM-FFD). It was found that the binding modes of CO could be distinguished and confirmed by their differing electron desorption cross sections which are $Q_{virgin} = 3 \times 10^{-19}$ cm^2, Q_{virgin} to $\beta = 10^{-19}$ cm^2, $Q_{\alpha} = 3 \times 10^{-18}$ cm^2 for 80 volt electrons. Evidence for thermal conversion of virgin states to both β and *a* states was obtained. Electrons also seemed to convert virgin to β states. In addition to desorption, dissociation with carbon formation occurred. The ratio of dissociation to desorption was estimated to be between 0.5 and 0.1 , and seems to be least for *a* and greatest for β desorption. The results on carbon formation showed that a large fraction of CO in the *a* and virgin modes is adsorbed with the C end of the molecule bonded to the substrate. (Menzel and Gomer, 1964b, FEM-EID).

General agreement with the theory of field desorption seems to hold for the GO-W system and could be confirmed, in particular, for the energetics of desorption and for adsorbate tunneling. The general reasonableness of the potential curves and that of the GO-W spacings obtained indicates that the ion-metal interaction can be expressed by an image potential to distances of the order of 2 Å. (Swanson and Gomer, 1963, FEM-FD).

Carbon Dioxide. -Heating of a field emission tip partly covered with CO_2 to 400-600°K resulted in the surface diffusion of oxygen onto the initially clean portions of the emitter. Further heating to 750°K resulted in the diffusion of another substance with an activation energy of 2.18 ± .22 eV. The temperature change and pattern appearance made it very probable that this was CO. These results suggested that CO_2 is dissociated into CO and O on a tungsten surface. The oxygen coverage before diffusion could be estimated as 0.15 from the change in work function of the initially clean portion of the emitter after oxygen diffusion. Since the maximum CO_2 uptake on evaporated W films at 300°K corresponds to a coverage of 0.19, this indicates that dissociation is almost complete at , or possibly below , 600°K. There was an indication that a small fraction of undissociated, loosely chemisorbed CO_2 exists at high coverage and low temperature, (below 600°K). Some desorption of the dissociation products , presumably CO, occurs near 1000°K. Heating above 1000°K leads to the formation of the typical oxide patterns which result from the heating of W emitters with small initial oxygen deposits. When large doses of CO_2 were deposited on a cold emitter, migration occured with a sharp moving boundary, at 60-70°K. This corresponds to the diffusion of physically adsorbed gas on top of the first layer with precipitation at its edge. The activation energy of diffusion of physically adsorbed CO_2 was estimated as 0.10 eV from the rate of this process. The heat of binding in this layer was found to be 0.24 eV from the maximum diffusion distance of constant CO_2 doses at various temperatures. The work function increase at maximum chemisorption coverage is 1.0 eV. The presence of a second, physically adsorbed layer decreases this by 0.4-0.5 eV. (Hayward and Gomer, 1959, FEM).

Germanium. -At least two types of migration have been observed. Low-temperature migration which occurs, starting at room temperature, with an activation energy of 0.2 eV is related to a mechanism in which the only mobile atoms are those in the second, physically adsorbed layer. Migration of the second type which occurs starting at T= 800°K, with energies of 1.24 and 1.7 eV is participated in by the atoms in the chemisorbed layer, An analysis of the volt-ampere characteristics of the field-emission current, the emission patterns, and the nature of the migration, led to the conclusion that the result of the low-temperature migration is to produce germanium layers having semi-conducting properties, while the layers resulting from high-temperature migration are not continuous, and the electron-emitting parts of the layers are spots of pure tungsten. (Sokol'skaya and Mileshkina, 1964, FEM).

Hydrogen.-Hydrogen adsorbs with an initial sticking probability of approximately 0.2 and the work function rises to 5.0 eV as the surface concentration reaches its room temperature maximum of 7.5 t 1.0 x 10^{14} mole/cm^2. Two adsorption peaks were found at 1100°K and 1800°K with an energy difference of 0.5 eV. (Einsinger, 1958, **FFD).**

A sticking probability of 0.1 is given by Hickmott and two distinct states are isolated. At a coverage of less than 3 x 10^{13} mole/cm^2 a β state was observed which obeys second order kinetics and has an activation energy for desorption of 1.35 eV. At higher coverages the energy lowers, probably due to the formation of a molecular *a* state. The concentration in the *a* state is proportional to pressure, Above 1100°K, atoms evaporate with an activation energy of 2.9 eV. (Hickmott, 1960, **FFD).**

Russion workers found two β states which obey second order kinetics with activation energies of 0.61 eV ± 0.06 and 1.48 eV t 0.07. (Ageev, et al, 1964, **FFD).**

Ricca, et al, reported three pairs of states from desorption spectra, Of the six observed peaks, two (γ t γ_2) occur in the temperature range 77-90°K. The *a* states (a_1 and a_2) occur between 190 and 300°K, and the β states (β_1 and β_2) occur in the region 300 to 600°K. The β_2 state appears to be practically filled before the β_1 state is significantly populated. (Ricca et al, 1965, **FFD).**

Rigby reported two β states with first order kinetics at 1.10 eV and 1.26 eV and a third β state with second order kinetics at 1.22 eV. (Rigby, 1965b, FFD).

Four chemisorbed complexes were identified for hydrogen by Rootsaert, et al. The bond strengths on individual sites correlate with the number of surface atoms contacted simultaneously and with their degree of unsaturation. At low over-all coverage the adsorbate is concentrated on the faces with highest heat of adsorption, these faces becoming populated mainly by surface migration from less attractive faces. Only at very low temperature, where surface migration is severely restricted, does a uniform distribution of the adsorbate over the crystal faces result. The heat of adsorption on the (211)

faces was found to be 2.0 eV. On the overall tip, four states of adsorption were found with the following temperature dependence:

T °K	E.	
> 280	0.87-2.0 eV	increase in work function,
220-280	0.65-0.87 eV	decrease in work function,
120-200	0.35-0.61 eV	increase in work function,
< 120	0.26-0.43 eV	physisorbed state.

(Rootsaert, et al, 1962, FEM)

It was found by Gomer, et al, that spreading of hydrogen on tungsten occurs in three distinct phases, At very high initial coverages a moving boundary migration occurs below 20°K, corresponding to migration of physically adsorbed H_2 on top of the chemisorbed layer. Precipitation at its edge, and further migration over the newly-covered region. For initial deposits corresponding to, 1 monolayer, spreading sets in at ~180°K with a boundary moving radially outward from the close-packed (110) faces. The 'activation energy of this process is — 0.26 eV and corresponds to migration over the smooth (close packed) regions of the tip followed by precipitation of chemisorbate at trap sites on the rough regions, At coverages too low to permit saturation of traps, diffusion out of the latter becomes rate controlling so that boundary-free diffusion with $E_d \sim 0.41$ eV and at even lower coverages with $E_d \sim 0.69$ eV is observed. The heat of adsorption of H_2 at extremely low coverage was found to be 2.78 eV but drops rapidly with increasing coverage. These results lead to the conclusion that surface heterogeneity is largely the result of surface topography and is inherent on all but the close-packed faces of W. The activation energies for diffusion were found to be 10 to 20% of the binding energy, depending on the nature of the sites. It was also seen from the low-temperature spreading that ~75% of the chemisorbed layer can be formed below 20°K with effectively zero activation energy. (Gomer, et al, 1957, FEM).

Electron induced desorption cross sections Q were determined from work function and Fowler-Nordheim preexponential changes and are significantly smaller than would be expected for comparable molecular processes. $Q_h = 3.5 \times 10^{-20}$ cm^2 and 5×10^{-21} cm^2 for processes tentatively interpreted as the splitting of molecularly adsorbed H_2 and desorption of H, respectively. These results were interpreted in terms of transitions from the adsorbed ground state to repulsive portion of excited states, followed by de-exciting transitions which prevent desorption. It was argued that the excitation cross sections should be essentially "normal" i.e. 10^{-16} to 10^{-17} cm^2, and that the much smaller over-all cross sections observed are due to high transition probabilities to the ground state, estimated as 10^{14} to 10^{15} sec^{-1}. (Menzel and Gomer, 1964a, FEM-EID).

In conclusion, the energetics of the tungsten hydrogen system do not appear to be well resolved.

Single crystal studies of sticking probabilities and work function as hydrogen adsorbs on tungsten have been studied(Armstrong, 1966, LEED) and are given in the following table:

Plane	W(100)	W(211)	W(111)	W(110)
$\Delta\phi_m$	0.88	0.65	0.15	---
S_o	0.1	0.3	~ 0.01	$< 10^{-3}$

Iodine. - It is believed that the "triangular" sites which occur on the (111) planes are favorable for iodine adsorption. (Moss and Kimball, 1960, FEM).

Extended exposure to Iodine (5×10^{-9} torr) vapour produces *a* constant **A0** increase of 0.4 eV with respect to clean tungsten. Iodine adsorption/ desorption is sensitive to surface topography adsorbing on the (133), (122), (233) planes and in the region of the (124) planes on heating. (Duell and Moss, 1965, FEM).

Krypton. - Adsorption lowers the work function by 1.18 eV for Kr at 20°K. Binding to the surface is structure sensitive and resembles argon. Observations of changes in field electron emission with temperature yield an activation energy for surface diffusion of Kr over the (310) toward the (100) of > 0.048 eV. (Ehrlich and Hudda, 1959, FEM).

Neon. -It was found that a work function decrease of 0.15 eV occurs for saturated monolayers when measured at 4.2°K. It is believed that dipole-dipole repulsions are very small and do not necessarily make the first layers gas-like. (Gomer, 195813, FEM).

Nitrogen. - Three states of adsorption were observed by 1961, a γ state with an energy of ~ 0.39 eV, an *a* state with an energy of -0.87 eV and a β state with an energy of ~ 3.5 eV. (Ehrlich, 1961a, FFD), (Ehrlich and Hudda, 1961, FEM), (Ehrlich, et al, 1958a, FEM-FFD).

The β state obeys second order kinetics at low coverages. At higher coverages, the β_2 peak splits and a second peak, β_1 was found which obeys first order kinetics and has an activation energy for desorption slightly lower than the β_2 peak. The β state is believed to be atomically bound, but at higher coverages, it may be difficult to distinguish the desorption of two adjacent atomically bound atoms from molecular desorption using the kinetic behavior alone. Mass spectrometric evidence using isotopes showed

that the small *a* phase was molecular and the β phase atomic. (Rigby, 1965a, FFD).

The results of Rigby were simultaneously confirmed and the γ state was shown to be molecular from isotopic exchange studies. (Yates and Madey, 1965, FFD). Nitrogen raises the work function in all states except the γ state in which the work function is lowered. (Ehrlich and Hudda, 1961, FEM). This effect was substantiated by Hill and Pethica using flash filament techniques. (Hill and Pethica, 1962, FFD-FEM).

A study by Delchar and Ehrlich combining flash filament techniques with contact potential measurements on macroscopic planes cut from single crystal tungsten provided information on the relationship between binding states and crystal face. An atomically bound β state forms on the (100) plane which lowers ϕ_{100} by 0.4 eV. Two states, a molecular *a* state and a β state, form on the (111) plane and raise ϕ by a total of 0.15 eV. At high concentrations, a second β state was observed on the (111) plane. The (110) is inactive except at low temperatures, where it forms a γ state which is atomic and lowers ϕ. (Delchar and Ehrlich, 1965, FFD), (Ehrlich, 1962, FEM-FIM). This work provides evidence of the sensitivity of adsorption to structure and the multiplicity of states on single crystal planes.

The sticking probability is about 0.3 to 0.4 and the room temperature coverage reported is usually from 3 to 10×10^{14} mole/cm^2. The variation in these parameters could be due in part to experimental uncertainty and the variations in the specific nature of the surface used.

Oxygen. - Becker and Brandes observed oxygen adsorption on tungsten in the field electron microscope and detected three stages of adsorption. The heats of adsorption were found to be about 5 eV and 2.5 for two of the stages and the third stage consisted of molecular complexes with the substrate. (Becker and Brandes, 1956, FEM). Gomer and Hulm examined low temperature desorption of oxygen on tungsten and found three types of migration. At 27°K diffusion occurs with a sharp boundary and an activation energy ~0.04 eV, which was believed to be migration of physically adsorbed O_2 over the chemisorbed layer, with precipitation on the clean tungsten surfaces. A study yielded an estimate of 0.1 eV for the heat of adsorption in the physisorbed layer. At 400-500°K and high coverages activation energies of 1.0-1.08 eV were determined. It was found that 80% of the chemisorbed layer can be formed without appreciable activation at 27°K. (Gomer and Hulm, 1957, FEM). An initial heat of adsorption of 8.4 eV has been given for oxygen on tungsten thin films., (Brennan, et al, 1960, TFC). Evidence has been presented for the chemisorption of a monolayer of gas with a sticking coefficient of unity and the adsorption of a second, initially mobile layer of oxygen, also with a sticking coefficient of unity when the substrate temperature is 20°K. The results are independent of the degree of surface order over the range considered. The second adsorbed layer is not observed at

substrate temperatures of 300°K, and the use of the Langmuir postulate that only the clean surface contributes to the adsorption allows the definition of a constant sticking coefficient of 0.8 for oxygen on tungsten at 300°K. (George and Stier, 1962, FEM-FIM). Kinetic rate studies of desorbed species using an in-line mass spectrometer indicate that oxygen adsorbs on tungsten in two states whose energies are 6.25 and 4.95 eV. Occupation of the lower state begins after the upperstate is filled. (Schissel and Trulson, 1965, FFD). Desorption cross sections were found to be 4.5 x 10^{-19} cm^2 for the loosely bound state and 2 x 10^{-21} cm^2 for all other states. (Menzel and Gomer, 1964a, FEM-EID).

Xenon. -Adsorption lowers the work function by 1.38 eV for Xe. The work function diminishes monotonically with Xe coverage even after more than a single layer is formed. Binding is believed similar to argon on tungsten. Observations of changes in emission with temperature yield a heat of desorption of .35 eV for Xe, as well as the following values for the activation energy for surface diffusion: Over the (310) toward the (100) = 0.16 eV and over the (111) = $0.07 \leq E \leq 0.15$ eV. (Ehrlich and Hudda, 1959, FEM).

It was found that work function decreased 1.4 eV for saturated monolayers when measured at 4.2°K. Work function changes are most pronounced near the (100) faces. Multilayer adsorption also occurs. It appears that dipole-dipole repulsions suffice to make the first layers gas-like. (Gomer, 1958b, FEM)

The adsorption of xenon shows a distinct topographic dependence. Heats of adsorption for the (400) plane were found to be 0.33 eV and 5.22 eV for the (111) plane. (Rootsaert, et al, 1962, FEM).

BIBLIOGRAPHY OF AUTHORS
REFERENCED IN EXPERIMENTAL RESULTS

Ageev, V.N. and N.I. Ionov, and Yu. K. Ustinov, ZhTF 34, 2056 (1964). Trans: Soviet Physics-Tech. Phys. 9, 1581 (1965).

Anderson, J., W.E. Danforth and A.J. Williams, J. Appl. Phys. 2260 (1963).

Armstrong, R.A., Can. J. Phys. 44, 1753 (1966).

Arthur, J.R., Jr., and R.S. Hanson, J. Chem. Phys. 36, No. 8, 2062 (1962).

Azizov, U.V., V.M. Vaknidov, V.M. Sulmanov, B.M. Sheinberg, and G.N. Shuppe, Soviet Physics-Solid State 7, No. 9, 2232 (1966).

Barnaby, B.E., T.E. Madey, A.A. Petrauskas and E.A. Coomes, J. Appl. Phys. 35, No. 6, 1759 (1964).

Becker, J.A., and R.G. Brandes, J. Chem. Phys. 23, 1323 (1956).

Bell, A.E. and R. Gomer, J. Chem. Phys. 44, No. 3, 1065-1080 (1966).

Boggio, J.E., and H.E. Farnsworth, Surface Science 1, 399 (1964).

Brennan, D., F.H. Hayes, Trans, Faraday Soc. 60, 589-596 (1964).

Brennan, D., D.O. Hayward, Phil. Trans. A(GB) 258, 375-386 (1965).

Brennan, D., D.O. Hayward and B.M.W. Trapnell, Proc. Roy. Soc. A256 81 (1960).

Cape, J.A. and E.A. Coomes, J. Chem. Phys. 32,210 (1960).

Cerny, S., V. Ponec, and L. Hlodek, J. Catalysis 5, 27-38 (1966).

Degras, D.A., 3 eme Congres International du Vide, Stuttgart, (28 June-2 July 1965).

Delchar, T. T.A. and G. Ehrlich, J. Chem. Phys. 42, 2686 (1965).

Duell, M.J. and R.L. Moss, Trans. Faraday Soc. 61, Pt. 10, 2262 (1965).

Ehrlich, G., J. Chem. Phys. 34, 29 (1961a).

Ehrlich, G., J. Chem. Phys. 34, 39 (1961b).

Ehrlich, G., T.W. Hickmott and F.G. Hudda, J. Chem. Phys. 28, 506 (1958a).

Ehrlich, G., T.W. Hickmott and F.G. Hudda, J. Chem. Phys. 28, 977 (1958b).

Ehrlich, G. and F.G. Hudda, J. Chem. Phys. 30, 493 (1959).

Ehrlich, G. and F.G. Hudda, J. Chem. Phys. 35, 1421 (1961).

Ehrlich, G., J. Chem. Phys. 36, 1171 (1962).

Eisinger, J., J. Chem. Phys. 28, 165 (1958a).

Eisinger, J., J. Chem. Phys. 29, 1154 (1958b).

Estrup, P.J., J. Anderson and W.E. Danforth, Surface Science 4, 286 (1966).

Gasser, R.P.H., and D.E.A. Schuftan, Vacuum 13, 146 (1963).

Gavrilyuk, V.M. and V.K. Medvedev, Soviet Physics-Solid State 4, 1737 (1963).

George, T.H. and P.M. Stier, J. Chem. Phys. 37, No. 9, 1935 (1962).

Germer, L.H. and A.U. MacRae, J. Chem. Phys. 37, 1382 (1962a).

Germer, L.H. and A.U. MacRae, J. Appl. Phys. 33, 2923 (1962b).

Godwin, R.P. and E. Luscher, Surface Science 3, 42 (1965).

Gamer, R. and J.K. Hulm, J. Chem. Phys. 27, No. 6, 1363 (1957).

Garner, R., R. Wortman and R. Lundy, J. Chem. Phys. 26, 1147 (1957).

Gomer, R., J. Chem. Phys. 28, 168 (1958a).

Gomer, R., J. Chem. Phys. 29, 441 (1958b).

Gorbatyi, N.A. and E.M. Tyabchenke, Soviet Physics-Solid State 7, No. 4, 921-926 (1965).

Haque, C.A. and H.E. Farnsworth, Surface Science 1, 378 (1964).

Haumovets, A.G., Soviet Physics-Solid State 5, No. 8, 1668 (1964).

Hayward, D.O., and R. Gomer, J. Chem. Phys. 30, 1617 (1959).

Hickmott, T.W., J. Chem. Phys. 32, 810 (1960).

Hill, M.P. and B.A. Pethica, J. Chem. Phys. 36, No. 11, 3095 (1962).

Hughes, F.L., Phys. Rev. 113, 1036 (1959).

Hughes, F.L. and H. Levinstein, Phys. Rev. 113, 1029 (1959).

Husmann, O.K., Phys. Rev. 140, A546 (1965).

Klein, R., J. Chem. Phys. 31, 1306 (1959).

Klein, R. and L.B. Leder, J. Chem. Phys. 38, No. 8, 1866 (1963).

Klein, R. and J.W. Little, Surface Science 2, 167 (1964).

Lee, R.N. and H.E. Farnsworth, Surface Science 3, 461 (1965).

Madey, T.E., A.A. Petrauskas, and E.A. Coomes, J. Chem. Phys. 42, 479 (1965z).

Madey, T.E., J.T. Yates and R.C. Stern, J. Chem. Phys. 42, 1372 (1965b).

May, J.W. and L.H. Germer, J. Chem. Phys. 44, 2895 (1966).

McIrvine, E.C. and R.C. Bradley, J. Chem. Phys. 27, No. 3, 646 (1957).

Melmed, A.J., J. Appl, Phys. 36, No. 11, 3691 (1965a).

Melmed, A.J., J. Chem. Phys. 43, No. 9, 3057 (1965b).

Melmed, A.J., J. Appl, Phys. 37, No. 1, 275 (1966).

Menzel, D. and R. Gomer, J. Chem. Phys. 41, No. 11, 3311 (1964a).

Menzel, D. and R. Gomer, J. Chem. Phys. 41, No. 11, 3329 (1964b).

Moore, G.E. and H.W. Allison, J. Chem. Phys. 23, 1609 (1955).

Moss, R.L. and C. Kemball, Trans. Faraday Soc. 56, No. 454, Part 10, 1487 (1960).

Muller, E.W., Phys. Rev. 102, No. 3, 618 (1956).

Naumovets', A.G., Ukrainiskii Fizichnii Zuhurnal 8, No. 1, 65 (1963).

Pasternak, R.A., Transactions, Eighth Annual Conference on Vacuum Metallurgy, (June 1965).

Pasternak, R.A., N. Endow, and Bergsnov-Hansen, J. Phys. Chem. 70, 1304-1310 (1966).

Pasternak, R.A., and H.U.D. Wiesendanger, J. Chem. Phys. 34, 2062 (1961).

Pritchard, J. Nature 194, 38 (1962).

Ptushinskii, Yu. G., Radiotekhn i Elektron 5, 1663 (1960).

Ptushinskii, Yu. G., Radiotekhn i Elektron 6, 382 (1961).

Quinn, C.M. and M.W. Roberts, Trans. Faraday Soc. 60, 899-912 (1964).

Redhead, P.A., Trans. Faraday Soc. 57,641 (1961).

Ricca, F., R. Medana and G. Saini, Trans. Faraday Soc. 61, 1492 (1965).

Rigby, L.J., Can. J. Phys. 42, 1256 (1964).

Rigby, L.J., Can. J. Phys. 43, 532 (1965a).

Rigby, L.J., Can. J. Phys. 43, 1020 (1965b).

Rootsaert, W.J. M., L.L. van Reijen, W.M.H. Sachtler, J. Catalysis 1, 416 (1962).

Scheer, M.D., and J. Fine, J. Chem. Phys. 37, 107 (1962a).

Scheer, M.D. and J. Fine, J. Chem. Phys. 36,1647 (1962b).

Scheer, M.D., and J. Fine, J. Chem. Phys. 38, 307 (1963a).

Scheer, M.D. and J. Fine, J. Chem. Phys. 39, 1752 (1963b).

Schissel, P.O., and O.C. Trulson, J. Chem. Phys. 43, 737 (1965).

Schmidt, L.D. and R. Gomer, J. Chem. Phys. 42, 3573 (1965a).

Schmidt, L.D. and R. Gomer, J. Chem. Phys. 43, No. 1, 95 (1965b).

Schmidt, L.D. and R. Gomer, J. Chem. Phys. 43, No. 6, 2055 (1965c).

Shrednik, V.N., Soviet Physics-Solid State 3, No. 6 (1961).

Shrednik, V.N. and E.V. Snezhke, Soviet Physics-Solid State 6, No. 5 1173 (1964).

Shrednik, V.N. and E.V. Snezhke, Soviet Physics-Solid State 6, No. 11 (1965).

Silver, M. and R.S. Witte, J. Chem. Phys. 38, 872 (1963).

Sokolo'skaya, I.L. and N.V. Mileshkina, Soviet Physics-Solid State 6, No. 6 1401 (1964).

Suhrmann, R., U. Richter, G. Wedler, Naturwissenschaften, 50,641-642 (1963).

Swanson, L.W. and R. Gomer, J. Chem. Phys. 39, No. 11, 2813 (1963).

Swanson, L.W., R.W. Strayer, and F.M. Charbonnier, Proceedings of the Twenty-Fourth Annual Conference on Physical Electronics, 120 (1964a).

Swanson L.W., R.W. Strayer, and F.M. Charbonnier, Surface Science 2, 177 (1964b).

Taylor, J.B. and I. Langmuir, Phys. Rev. 44, 423 (1933).

Taylor, L.H., Surface Science 2, 188 (1964a).

Utsugi, H. and R. Gomer, J. Chem. Phys. 37, No. 8, 1706-1719 (1962a).

Utsugi, H. and R. Gomer, J. Chem. Phys. 37, No. 8, 1720-1722 (1962b).

Von Goeler, E,, and E. Lusher, J. Phys. Chem. Solids 24, 1217 (1963).

Von Goeler, E. and R.N. Peacock, J. Chem. Phys. 39, 169 (1963).

Wiesendanger, H.U.D., J. Catalysis 2, 538-541 (1963).

Wortman, R., R. Gomer, and R. Lundy, J. Chem. Phys. 26, 1334 (1957a).

Wortman, R., R. Gomer, and R. Lundy, J. Chem. Phys. 27, 1099 (1957b).

Yates, J.T., Jr., and T.E. Madey, J. Chem. Phys. 43, 1055 (1965).

Zingerman, Ya. P., V.Z. Ishchuk, and V.A. Morozovshii, Soviet Physics-Solid State 2, 2030 (1961).

Zubenko, Yu. V. and I. L. Sokol'skaya, Soviet Physics-Solid State 3, No. 5 1133 (1961).

Zubenko, Yu.V., Radio Engng. and Elect. Phys. 8, No. 7, 1208-1213 (1963).

TASK 11-LITERATURE SEARCH OF COMPOSITE SURFACE WORK FUNCTION AND ION AND ATOM DESORPTION MODELS

OBJECTIVE

The objective of this section of the literature search work is to provide a review of existing theoretical models which attempt to describe work functions or ion-neutral desorption energies as a function of surface coverage.

INTRODUCTION

This aspect of the literature search is divided into four parts which deal with atom desorption energies, ion desorption energies, work function calculations and calculations of potential energies anywhere in front of either a complete array of discrete ions or along a line perpendicular to a single substrate vacancy. The complete array results are useful for calculations of work functions, especially in the high field situation which occurs in field emission. In this case, the applied field cuts the potential barrier to electron emission from the metal so close to the metal that the barrier is diminished by an amount which is related to the coverage of adsorbate and to the value of the applied field. The incomplete array results on the other hand enable ion desorption energies to be computed as a function of coverage. These energies are usually related to the work function change ($\Delta\phi$) due to adsorption by means of the equation $f = (-AE_P) / (\Delta\phi)$ where f is the ion array penetration coefficient.

It is felt that none of the work function theories outlined below is satisfactory for the complete range of coverage from 0 to 1. Langmuir's theory accounts for the work function change up to $\theta = 0.5$, but beyond this poor agreement of experiment with theory is obtained. In spite of its semiempirical nature, Langmuir's theory is not surpassed in credibility or accuracy by any of the other theories presented here.

Gyftopoulos and Levine's theory of atomic desorption energies agrees quite well with the experimental results and appears to justify use of the analogy between adsorption bonds on the one hand and molecular bonds on the other which Gyftopoulos and Levine use to calculate energies in terms of the properties of the substrate and adsorbate.

The classical discrete element model employed by Barlow and Macdonald, is probably the most rigorously constructed model of this type for the calculation of ion desorption energies but it suffers from the fact that it offers no clue as to how Z, the average charge on the adsorbate elements, varies with coverage so that the coverage range of its applicability is likely to be small.

For the sake of consistency, we have altered some of the symbols appearing in the papers reviewed here; however, the symbol Ψ instead of V has been retained in one of Barlow and Macdonald's papers for purposes of clarity.

The first part of each discussion below contains a summary of the paper reviewed while the second contains a critique of it.

FUTURE WORK

The papers reviewed here represent a cross section of the theoretical papers which permit a comparison between theory and experiment. Further theories of this type will be reviewed in the next six months. Also, papers offering a more rigorous, but more qualitative description of work function changes and desorption energies will be reviewed.

The Wave Mechanics of the Surface Bond in Chemisorption

By T.B. Grimley

Review .- Grimley has elucidated certain qualitative features of chemical adsorption by performing simplified wave-mechanical calculations on one-dimensional chains of atoms, each of which is associated with a single orbital $\phi(r,m)$.

The first part of the calculations was concerned with the properties of a free surface which in a one-dimensional model is represented by the end atom in a finite chain containing N atoms. Only if the coulomb integral α' of the end atom differs significantly from that of other atoms (α) in the chain will any new electronic properties be introduced. In this case if $|Z| > 1$, where Z is given by $(\alpha-\alpha')/2\beta$, then a single localized state of energy, outside the normal band of levels associated with the one-dimensional crystal, will result. The symbol β is the resonance integral between nearest neighbors in the chain. A state $\mathcal{H}$ corresponding to $Z > 1$ will lie above the band in energy while that corresponding to $Z < -1$, a P state will lie below. As $Z \to \infty$ both of these states will revert to that of a single orbital $\phi(r,m)$.

If, in the three-dimensional model of a finite crystal, containing N^3 atoms, Z is large, the single end state of the linear model becomes a band of states, 8β wide, containing N^2 levels: the main crystal band being depleted by the same amount.

Addition of a foreign atom of Coulomb integral α'' to the finite linear chain may result in separation from the main band of a new localized state. Defining Z, Z' and η as follows:

$$Z = \frac{\alpha - \alpha'}{\beta} \quad , \quad Z' = \frac{\alpha - \alpha''}{\beta} \quad , \eta = \frac{P'}{\beta}$$

then the two localized states may exist in certainregions of the ZZ' - plane obtained from the two hyperbolas

$$(Z \pm 1)(Z' \pm 2) = \eta^2$$

$$(Z - 1)(Z' - 2) = \eta^2$$

In some regions two localized states may exist; these may be two P, two or one each of P and $\mathcal{H}$ states. In other regions one state only may exist and this can be either P or $\mathcal{H}$; finally, if $\eta^2 < 2$ a forbidden region occurs in which only nonlocalized states exist Extension of the perturbing influence

of the foreign chemisorbed atom to substrate atoms beyond the terminal one leads to the introduction of additional localized states.

Consideration of a three-dimensional model in which perturbation of the crystal by the foreign atom extends only over a group — of crystal atoms indicates that a set of localized states associated with the foreign atom and the group may be formed which have energies outside the normal crystal and surface bands. The three-dimensional analogue of the one-dimensional chain with single chemisorbed atom is a crystal lattice completely covered by adsorbate. If $\eta = \beta'/\beta'' = 1$ where β'' is the resonance integral between nearest neighbors in the adsorbed layer, then the discrete localized levels (P and $\mathcal{H}$) of the one-dimensional model now appear as bands of surface states and each band may contain N^2 levels. Depending on the values of Z and Z' these bands may or may not overlap the normal band of crystal states, When $\eta' \neq 1$, one or both bands P and $\mathcal{H}$ may be incomplete. Complete surface coverage requires at least a complete band of those states which lie below the main crystal band in energy so that if some of these are missing, less than a complete monolayer will be adsorbed on the crystal surface. It is suggested by Grimley that this may provide the mechanism for falling heats of chemisorption with surface coverage.

By considering a linear chain to which two foreign atoms were attached, Grimley was able to investigate the manner in which chemisorbed atoms interact with one another in chemisorbed layers. If the localized level formed by interaction of a single atom with a crystal does not lie too far below the normal crystal band, the wave function for the localized level is attenuated only slowly in the crystal so that two chemisorbed atoms can interact at distances where the interaction between isolated atoms would be negligible. For two identical foreign atoms attached to the chain at points equidistant from the end, four wave functions for localized states may arise. These are due to P and $\mathcal{H}$ states and may be even or odd in the center of symmetry of the chain. Provided that a single foreign atom on the chain gives rise to at least one P state, then two atoms give rise to an even state. Two P states for the single atom give rise to two even states and their energies fall lower as the distance between the adsorbed atoms decreases: the reverse is true for the odd P states. In certain circumstances the odd P state is missing, its place being taken by an extra level in the nonlocalized crystal band.

Falling heats of chemisorption with coverage can be accounted for in terms of the above concepts: as two atoms adsorbed on the linear chain are brought together the individual localized states belonging to each atom are split into double occupied even and odd states, the latter of which is forced higher and higher in energy until it joins the normal crystal band.

If the foreign atom is chemisorbed by a one-electron bond only, two such chemisorbed atoms should attract each other because the even P state

which is now the only state filled, lies below the state for an isolated chemisorbed atom. Separation of these chemisorbed atoms would raise the energy of the doubly filled even state. This may explain how an activation energy may be involved in the mutual separation of the atoms formed in dissociative chemisorption.

Even though no localized states result when a foreign atom is chemisorbed, binding is still of course possible. The total electronic energy of a chain of identical atoms is :

$$\epsilon_n = N\left(\alpha + \frac{4\beta}{\pi}\right) + \beta\left[\frac{2}{\pi}(Z + 1/Z)\tan^{-1}Z - (1 + Z)\right]$$

It is assumed that there is one electron per atom in the chain, so that the band is half-filled, $\beta < 0$ and no surface states are occupied, On bringing up a foreign atom to the free end of the chain and assuming for simplicity that $\beta' = \beta$ and $\alpha = \alpha'$ we have a new total system energy:

$$\epsilon_{n+1} = (N + 1)\left(\alpha + \frac{4\beta}{\pi}\right) + \beta\left[\frac{2}{\pi}(Z' + 1/Z')\tan^{-1}Z' - (1 + Z')\right]$$

The change in total electronic energy when the foreign atom is chemisorbed is given by $\Delta\epsilon = \epsilon_{n+1} - \epsilon_n - E$ where E is the energy of the valence level electron of the isolated foreign atom.

$$A_E = \left[\alpha + \left(\frac{4\beta}{\pi}\right) - \epsilon\right] + \Delta\epsilon_S$$

$\Delta\epsilon_S$ is the difference in the surface terms in the above equations. The first term is the energy associated with the delocalization of the valence electron on the foreign atom while the second is the change in surface energy caused by the presence of the foreign atom. The delocalization energy is positive or negative according as E lies below or above the mean energy of electrons in the normal band, while $\Delta\epsilon_S$ is positive according to whether Z' is greater or smaller than Z. Because of this the two terms tend to cancel. No further information can be gained unless Z or Z' can be calculated.

Critique, -The ultimate aim of theoretical work dealing with adsorbate-adsorbent interactions is to predict heats of adsorption and work function changes as a function of surface coverage from known physical properties of the solid adsorbate, Grimley's paper contains an outline of an approach which may eventually meet these objectives. It accounts for some of the main features of chemisorption: heats of adsorption which fall as adsorption proceeds, the fact that for some systems saturation occurs when only a

fraction of the surface is covered by adsorbate; it also predicts that an activation energy should be required to separate atoms formed in dissociative chemisorption. However, no quantitative estimates of heats are available so that no experimental check can be made.

Correlation of Emission Processes For Adsorbed Alkali Films on Metal Surfaces

By N.D. Rasor and C. Warner

Review. - Rasor and Warner used an analytic model similar to that of Langmuir' insofar as the ion cores of the adsorbed particles, to a first approximation, can be considered as classical spheres resting on a conducting plane and occupying sites in an array determined by the substrate surface structure. Gurney2 pointed out that as an adsorbate atom approaches a metal the valence level of the atom (if $I \sim \emptyset$) will broaden into a band of states common to both metal and atom. The extent of this broadening, ΔU, depends on the distance of the adsorbate atom ion core from the surface. If this is small enough so that $\Delta U \ll kT$, the valence energy band of the atom is sharp and ions and neutrals exist as separate states on the surface. The relative probability of atomic and ionic states is given by:

$$\frac{\theta_a}{\theta_i} = q \exp\left[\frac{-\Delta E}{kT}\right] \qquad (1)$$

where ΔE is the mean energy difference between these states on the surface, and $q = 2j$ for j highly localized energy levels in the valence band; j is the number of highly localized energy levels in the valence band. The work function change due to adsorption was expressed as:

$$\Delta\emptyset = 2\pi\sigma\,(M_i\,\theta_i + M_a\,\theta_a) \qquad (2)$$

where σ is the surface site density and M the dipole moment associated with a surface ion or atom. Owing to depolarization M is related to the moment at zero coverage by:

$$M_i = M_{io} - \alpha_i F \;,\; M_a = M_{ao} - \alpha_a F \qquad (3)$$

Consideration of a simple thermodynamic cycle yielded:

$$\Delta E + E_a + I - E_P - \emptyset = 0 \qquad (4)$$

$$AE_o + E_{ao} + I - E_{po} - \emptyset_o = 0 \qquad (5)$$

where AE is the difference in bonding energy between the adsorbed ion and adsorbed atom, E_a is the atom adsorption energy, I, its ionization potential,

E_p, the ion desorption energy and ϕ the substrate work function. Equation (5) contains the same quantities at zero surface coverage. The ion array penetration coefficient, f, is defined as:

$$f = \frac{E_p - E_{po}}{\Delta\phi} \tag{6}$$

Rasor and Warner expressed the depolarization field F as:

$$F = (1 - f)\frac{\Delta\phi}{e r_i} \tag{7}$$

where r_i is the ionic radius. By combining the above equations, using $\theta = \phi_i + \theta_a$ and noting that $AE = \Delta E_o - (1 - f)\Delta\phi + \Delta E_a$ where $\Delta E_a = E_a - E_{ao}$, the final implicit expression obtained for $\Delta\phi$ was

$$\Delta\phi = \frac{4\pi e^2 \sigma \left[1 - \left[a_i (1 - f)/2 e^2 r_i\right] \Delta\phi\right] \theta}{1 + q \exp(-\Delta E/dT)} \left(1 + \frac{M_a \theta_a}{M_i \theta_i}\right) \tag{8}$$

f may be calculated from geometric considerations and ΔE_o depends on E_{ao} and E_{po} both of which are estimated below. Calculation of $\Delta\phi$ requires some assumptions to be made about M_a and ΔE_a. Comparison of the experimental with theoretically predicted values indicates that ΔE_a and $(M_a/M_i)(\theta_a/\theta_i)$ may be neglected. M_{io} was assumed to be given by $M_{io} = 2 e r_i$. E_{ao} was estimated from a semiempirical formula:

$$E_{ao} = b (h_a h_o)^{1/2} \tag{9}$$

where $0.5 < b < 1$, h_a is the heat of vaporization of the bulk adsorbate and h_o that of the substrate. An attempt to express E_{ao} in terms of ϕ_o was also made and the semiempirical relation:

$$E_{ao} \sim 0.34 + 0.3\,\phi_o \tag{10}$$

was obtained. For the noble metals, the term $0.7\,\phi_o$ was found to be more appropriate than $0.30\,\phi_o$. By noting that experimentally, h_o is approximately proportional to substrate work function ϕ_o, Equation (9) may be used to predict E_{ao}. A calculation based on the classical image forces on the valence electron, the ion core, and a free electron gave the following relation between ϕ_o and E_{ao}:

$$E_{ao} = \frac{e^2}{8R} \ln \left[1 + \frac{8R}{e^2} \phi_o \right] \qquad (11)$$

Critique. - The authors of this review are surprised at Rasor and Warner's conclusion from Gurney's work that ions and neutrals may exist as distinct states on the adsorbent surface especially for the case of cesium adsorbed on tungsten. On the one hand, Rasor and Warner conclude that tunneling should be extremely rapid between adsorbate and adsorbent ($\Delta t << 10^{-13}$ sec where At is the lifetime of an atomic state) and that "the forces of interaction between the particle and the surface and with other particles should be equivalent to that from a single species of charge having a time average charge intermediate between 0 and +e"; on the other hand, in apparent contradiction to this, they derive an expression for the work function change (Equation 8) which is based on the assumption of the existence of separate ions and neutrals on the surface.

Equation (1) which expresses θ_i in terms of θ_a, AE and T is crucial to the devebpment of Equation (8) because the latter equation by comparison with experiment indicates that only ions make a significant contribution to $\Delta\phi$. The applicability of Equation (1) rests on the validity of the inequality $\Delta U << 0.2$ eV where 0.2 eV is the value of kT at thermionic temperatures. If the inequality holds, then the valence level of the adsorbate level of the adatom may be considered sharp. A U was estimated from the uncertainty relation $\Delta U \sim h/(2\pi\Delta t)$. If At — 10^{-13} sec, then $\Delta U \sim 0.01$ eV and of course $A << 0.2$ eV. However, for a potential barrier 1 volt high and 1 Å wide, Rasor and Warner conclude that $\Delta t << 10^{-13}$ sec, which leads to $\Delta U >> 0.01$ eV. Moreover, Gomer and Schmidt conclude that for potassium adsorbed on tungsten, "the adsorbate level of the adsorbate atom lies below the 4s level of the isolated K atom for all surface-atom distances < 3.5 Å", so that the inequality $\Delta t << 10^{-13}$ certainly holds for this system. This implies that $\Delta U > 0.2$ eV; indeed Gomer[1] estimates a value of several eV for potassium on tungsten. Similar considerations should hold for cesium because the atomic radius of cesium is only slightly larger than that of potassium (2.60 Å compared to 2.20 Å). Consequently, Equation (1) may not be used to estimate θ_i.

---

[1] Gomer and Schmidt, J. Chem. Phys. 42, 3573, (1965)

Adsorption Physics of Metallic Surfaces Partially Covered By Metallic Particles I Atom and Ion Desorption Energies

By J.D. Levine and E.P. Gyftopoulos

Review.-In their paper I of 1964, Gyftopoulos and Levine continued their phenomenological approach which makes use of certain concepts developed in molecular physics. Thus, they draw the analogy between the energy of dissociation of diatomic molecules on the one hand and the energy of desorption or sublimation of adsorbed atoms from solids on the other.

It is assumed that metal-adsorbate bonds may be partly ionic and partly covalent so that desorption energy E_a can be represented by:

$$E_a = H_{ii} + H_{cc} \tag{1}$$

where H_{ii} is the ionic contribution to the bond and H_{cc} is the covalent contribution. E_a was calculated subject to the following conditions:

1. H_{ii} vanishes for a purely covalent bond.
2. H_{cc} vanishes for a purely ionic bond.
3. H_{cc} reduces to heat of sublimation of material from its own lattice when we consider heat of desorption of material from surface of the same bulk material.

H_{ii} is assumed to arise from a fraction of charge F of the adsorbate which is transferred to the substrate. F determines the partial ionic character of the bond and is associated with surface dipole moment. By means of a Born Haber type of thermodynamic cycle calculation the following expression for H_{ii} was derived

$$H_{ii} = F\phi \left[1 \mp \delta\right] \tag{2}$$

where

$$\delta = \frac{F}{\phi}\left(\frac{e^2}{R} - I\right) \tag{3}$$

and where R is the internuclear distance between substrate and adsorbate. I is the ionizing potential of the adsorbate. ϕ has been calculated in a previous paper of Gyftopoulos and Levine and is the work function of the composite surface.

H_{cc} was assumed to be a function of E'_f, the heat of sublimation of the adsorbate, S_f the angular strength of the adsorbate valence orbital, q_f the valence charge of the adsorbate and a function of corresponding quantities of the metal. The adsorbate contribution to H_{cc} as assumed to be proportional to $\emptyset'_f S2_f q_f$. Inclusion of E'_f ensures that H_{cc} is equal to E'_f when the adsorbate is adsorbed on its own bulk material while the S^2_f concept has been used successfully by Pauling. S_f depends on what valence orbital participates in the bond. Thus, $S_f = \sqrt{1}$ for σ-orbitals, $\sqrt{3}$ for p orbitals etc. q_f was included so that H_{cc} vanished when a purely ionic bond is formed, in which case, $q_f = 0$. The simplest expression for H_{cc} consistent with the following assumptions:

$$H_{cc} \propto E'_f S^2_f q_f$$

$$H_{cc} \propto E'_m S^2_m q_f$$

$$-H_{cc} = E'_f \text{ form} = f$$

and

$$H_{cc} = 0 \text{ for } qf = 0$$

is the geometric mean

$$H_{cc} = \left| E'_f E'_m \left(\frac{4 S^2_f S^2_m}{\left(S^2_f - S^2_m \right)^2} \right) \left(\frac{4 q_f q_m}{\left(q_f - q_m \right)^2} \right) \right|^{1/2} \qquad (4)$$

note:

$$q_f = \nu - F$$

$$q_m = \nu + F \qquad (5)$$

where ν is he largest number of valence electrons that can par icipate in the covalent bond e.g., $\nu = 1$ for alkali metals, 2 for alkaline earths. The above expressions for H_{cc} and $H_{..}$ together yield for E_a:

$$Ea = F\emptyset \, (1 \pm \delta) \pm (E'_f E'_m)^{1/2} \, Sfm \, Qfm \qquad (6)$$

where:

$$S_{fm} = \frac{2}{\frac{S_f}{Sm} + \frac{Sm}{S_f}} \quad \text{and} \quad Q_{fm} = \left(1 - \frac{F^2}{\nu^2} \right)^{1/2} \qquad (7)$$

The ion desorption energy E_p is related to the atom desorption energy and the composite surface work Function E_a by:

$$E_p = E_a + I - \phi_e \qquad (8)$$

where I is the ionization potential.

Critique. -The phenomenological approach used by these authors to calculate atom and ion desorption energies yields values of E_a and E_{ao} which are in good agreement with experiment. Thus, their values of E_a follow closely the experimental values determined by Langmuir and Taylor: [1] moreover, good agreement between theory and experiment was found for a range of E_{ao} values between 2.5 eV and 8.0 eV.

The theoretical expression for the electron work function ϕ_e which was obtained by Gyftopoulos and Levine has been criticized in an earlier part of this report, However, since the functional dependence of ϕ_e on θ was severely constrained by the imposed boundary conditions (i.e., $\phi_e = \phi_f$ when $\theta = 1$ and $\phi_e = \phi_m$ when $\theta = 0$ etc.) an error in ϕ_e does not seriously affect the final calculated value of E_a. In the case of E_{ao}, ϕ_e devolves to ϕ_m the work function of the clean substrate so that no error is introduced in the calculation of E_{ao} by an incorrect formulation of ϕ_e.

In the absence of any detailed quantum mechanical models of adsorption which yield predicted values of ϕ_a, the model of Gyftopoulos and Levine fulfills an important need.

---

[1] I. Langmuir and J.B. Taylor, Phys. Rev., 44, 423 (1933).

ION DESORPTION ENERGIES

Penetration of an Ion Through a Monolayer of Similar Ions Adsorbed on a Metal

By J.W. Gadzuk and E.N. Carabateas

Review. - In their paper of 1965, Gadzuk and Carabateas derived ion penetration coefficients for the limiting cases of mobile and immobile adsorption of ions on a metal substrate and also for the case of a partially mobile adsorbate film. f is defined as follows:

$$f = \frac{\Delta E_p}{\Delta \phi} \tag{1}$$

where $\Delta\phi$ is the change in electron work function at any coverage θ, and ΔE_p is the change in ionic work function--this is not equal to the electron work function because the ion does not enter the metal when adsorbed. Consequently, adsorption leads to penetration by the ion of only part of the potential of the dipole layer.

The potential on an ion at any distance from the surface as a result of the field of the other ions and their images is

$$V(r) = e \sum_i \sum_j P_{ij}(\theta) \left(\frac{1}{r_{ij}^+} - \frac{1}{r_{ij}^-} \right) \tag{2}$$

where P_{ij} is the probability that an adsorbate exists at a lattice site, ij, in a square array. λ is the distance between the center of charge of an adsorbed ion and the image plane.

$$r_{ij}^+ = (r - \lambda)^2 + r_{ij}^2$$
$$r_{ij}^- = (r + \lambda)^2 + r_{ij}^2 \tag{3}$$

For the immobile case, $P_{ij}(\theta)$ vanishes except for the most probable sites, $2d/\theta_i^{1/2}$ apart, at which it is 1. In this case,

$$V(r) = V_{im} = \frac{2.25 e \lambda^2 \theta_i^{3/2}}{d^3} \tag{4}$$

For mobile films: $P_{ij}(\theta) = \theta_i$ and $V(r) = V_m$ is given by

$$V_m = \frac{2.25e\lambda^2 \theta_i}{d^3} \tag{5}$$

Because $f = \left[V_\infty - V(r = h)\right] / V_\infty$ we have for f:

$$f_{im} = \frac{1 - 2.25\lambda\theta_i}{\pi d}^{1/2} \tag{6}$$

and

$$f_m = 1 - \frac{2.25\lambda}{\pi d} \tag{7}$$

An expression for the intermediate case of partially mobile films can also be derived by noting that thermal energy will displace some of the ions from a well ordered array of the immobile film. This displacement results in an increase in potential AV in Equation **(4)** given by:

$$\Delta V = \frac{1}{N}\int_{V_{im}}^{\infty} V \exp\left(-\frac{V}{kt}\right)\left(\frac{\theta_i \pi}{6d^2}\right)\left(2e\lambda^2\right)^{2/3} V^{-5/3}\, dV \tag{8}$$

f_{im} is then modified to give for the case of partially mobile films

$$f = f_{im} - \frac{AV}{V_\infty} \tag{9}$$

Equation (8) can only be integrated numerically.

Critique.-Barlow and Macdonald[1] have pointed out that the immobile array of Gadzuk and Carabateas is equivalent to what is usually considered to be a mobile array; whereas their mobile array is equivalent to the usual definition of localized films.

The values of f given in this paper neglect:

(1) The potential due to the image of the dipole induced in the ion which is being adsorbed at an empty site,

(2) All effects due to polarization of the adsorbed ions,

(3) Possible redistribution effects of the existing lattice which may deform to accommodate the incoming ion.

Barlow and MacDonald have demonstrated in their recent paper that these effects are significant and deduce as a limiting case the formula of Gadzuk and Carabateas for an immobile and mobile array.

Ref. 1 Barlow and MacDonald, J. Appl. Phys. 37, 3471 (1966) Paper 5 this series.

Penetration Parameter for an Adsorbed Layer of Polarizable Ions

By J. Ross MacDonald and C.A. Barlow, Jr.

Review.- This paper contains calculations and discussion of the distinctions to be made between several different definitions of f which were shown not to be equivalent when the ion polarizability *a* was not zero and when redistribution effects and interaction with self images could not be neglected. **f** the ion array penetration parameter is defined as follows:

$$f = \frac{-\Delta W_i}{Z \Delta W_e} \tag{1}$$

where ΔW_e is the change in electron work function on adsorption and ΔW_i is the energy required to remove an adion from its equilibrium position in the array to infinity minus that required when the surface coverage of adions approaches zero. Covalent contribution to ΔW_i are ignored and the array is assumed to be hexagonal and mobile. The simplest definition of f (let this be f_1) ignores possible redistribution effects in the adlayer when ions are removed or added and also does not consider the influence of the removed adions own image. Then:

$$f_1 = 1 - \frac{\Psi_a}{\Psi_\infty} \tag{2}$$

where Ψ_a is the potential at the site of the missing adion and Ψ_∞ is the potential arising from the adion-image array at an infinite distance from the adsorbing plane.

A more accurate definition of f includes the effect of the image of the induced dipole:

$$f_2 = 1 - \frac{\Delta \Psi_e}{\Psi_\infty} \tag{3}$$

where

$$\Delta \Psi_e = \Psi_a + 1/2 \left[\phi_d - \phi_{do}\right] \tag{4}$$

ϕ_H is the potential at the missing adion site arising from the image of the induced dipole of an ion. $\phi_d = \phi_{do}$ when $\theta = 0$. Hence:

$$f_2 = f_1 \, t \, T \tag{5}$$

where

$$T = - \frac{\phi_d - \phi_{do}}{2\psi_\infty} \tag{6}$$

Both f_1 and f_2 neglect possible rearrangement effects and these are calculated as follows:[1]

$$U = \frac{Ze}{2} \; N\psi_i \tag{7}$$

where U is the total system energy for an adsorbed array of polarizable ions and ψ_i is the potential at the site of an ion which includes induced polarization effects. On removing an ion, N changes to N' and ψ_i to ψ_i'.

$$\psi_i' = \psi_i + \delta\psi_i$$

$$N' = N \; t \; \delta N \qquad \delta N = -1$$

After removing an ion to infinity the new total system energy is

$$U' = Ze\psi_\infty + \frac{Ze}{2} \; N' \; \psi_i'$$

from which:

$$\delta U = \Delta W_i = Ze\left\{\psi_\infty - 1/2\left[\psi_i + N \; \frac{d\Delta\psi_i}{dN}\right]\right\} \tag{8}$$

Using Equation (1) we have for f_3:

$$f_3 = 1/2 \left[1 + f_2 + T - \left(\frac{N}{\psi_\infty}\right)\left(\frac{d\Delta\psi_i}{dN}\right)\right] \tag{9}$$

The next section of the paper is concerned with the evaluation of f_1, f_2 and f3. f_1^o which is the value of f_1 when $a = 0$, appears in the final expressions for these quantities and is defined as:

$$f_1^{\circ} = 1 - \frac{\Psi_a^{\circ}}{\Psi_{\infty}^{\circ}}$$

where $\Psi_{\infty}^{\circ} = 4\pi NZe\beta$ and Ψ_a°, the value of Ψ_a for $\alpha = 0$, is calculated[1] from Graham's "cut-off" model in which the discrete adion-image charges are smeared out into uniform sheets of charge (having the same charge density as the discrete layers) with colinear circular vacancies of radius $r_o = 4\pi r_1 / \sqrt{3}\sigma$. f_1° is then given by:

$$f_1^{\circ} = 1 + \left(\frac{2\pi R_1}{\sqrt{3\sigma}}\right) - \left[\left(\frac{2\pi R_1}{\sqrt{3\sigma}}\right)^2 + 1\right]^{1/2} \qquad (10)$$

f_1 is obtained from Equation (2). Ψ_{∞} has been calculated in an earlier paper in this series' and Ψ_a is calculated by resolving Ψ_a into Ψ_a° and Ψ_{ap} which is due to the induced dipole array. Ψ_a° was introduced in the calculation above of f_1° while Ψ_{ap} is calculated by a similar procedure to that employed for the calculation of Ψ_{∞} and is given by:

$$\Psi_{ap} = -\left(\frac{\Psi_{\infty}^{\circ}}{2}\right)\left[1 + \left(\frac{2\pi R_1}{\sqrt{3\sigma}}\right)^2\right]^{-1/2} g(R_1) \qquad (11)$$

The expression for $g(R_1)$ is given in Equations (3) and (4) of reference 2. We then have for f_1:

$$f_1 = \frac{f_1^{\circ} - g(R_1)\left\{1 + 1/2\left[1 + (2\pi R_1/\sqrt{3\sigma})^2\right]^{1/2}\right\}}{1 - g(R_1)} \qquad (12)$$

The more accurate ion array penetration parameter f_2 may be calculated by using Equation (5) and noting that $\phi_d = -Zeg(R_1)/4\beta$. From Equation (5) $f_2 = f_1 \cdot T$ where T is given by:

$$T = (\sqrt{3}/64\pi)R_1^2\left[g(R_1) - g(\infty)\right] / \left[1 - g(R_1)\right] \qquad (13)$$

and

$$g(\infty) = 2J(1/2 - S)/(4 - J) \qquad (14)$$

where $J = \alpha/\beta^3$ and $S = 2(\beta/Ze)(\beta E_{ni})$.

Equation (9) indicates that f_3 may be calculated from f_2 and T, provided that $Nd\Delta\Psi_i/dN$ can be calculated. $\Delta\Psi_i$ may be written as:

$$\Delta\Psi_i = \Psi_a^{\circ} + \Psi_{ap} + \phi_d - \phi_{do} \qquad (15)$$

while from reference 1, η may be expressed as:

$$\eta = \left(\frac{N}{\Psi_a^o}\right)\left(\frac{d\Psi_a^o}{dN}\right) \tag{16}$$

$$\text{Let } \zeta = -\left(\frac{N}{\Psi_\infty}\right)\left(\frac{d\Delta\Psi_i}{dN}\right) = \left(\frac{R_1}{2\Psi_\infty}\right)\left(\frac{d\Delta\Psi_i}{dR_1}\right) \tag{17}$$

then from Equations (15), (16) and (17) we may derive an expression for Ψ_a which involves $g(R_1)$, η, f_1, Ψ_∞ and the derivatives $d\Psi_{ap}/dR_1$ and $dg(R_1)/dR_1$ which are calculable from the expressions for Ψ_{ap} and $g(R_1)$. Incorporation of the result in Equation (9) yields an expression for f_3.

Plots of f_1, f_2 and f_3 vs θ and R_1 are presented in Barlow and MacDonald's paper for various values of the parameters S and J. Increasing S results in increased values of f for all three definitions of f, whereas for f_1 and f_2, an increase in J results in a decline in f. At high surface coverages the same behaviour occurs for f_2; at low coverages the reverse is true. The calculation for f3 indicates that even for $a = 0$ redistribution has a significant effect and that for $J \geq 1$, f_3 is markedly lower than f_2.

Under some conditions f_1, f_2 and f_3 are negative; this implies that it requires more energy to remove an isolated ion from a metal than from an adsorbed array. This is a consequence of the surprising fact that for $a \neq 0$, (Ψ_a) may be greater than Ψ_∞. Plots of the normalized quantity $\Psi(Z)/\Psi(\infty)$ vs Z/R_1 show that maxima in these curves occur for certain J values and that occurrence of the maximum requires higher values of J as coverage decreases. $\Psi(Z)$ is calculated from the "cut-off" model.

---

1 C.A. Barlow and J.R. MacDonald, J.Chem. Phys. 43, 2575 (1965) (Paper 12 of this review series)

2 C.A. Barlow and J.R. MacDonald, J. Chem. Phys. 44, 202 (1966) (Paper 11 of this review series)

Critique.- Barlow and MacDonald have carefully distinguished between a number of similar definitions of the penetration parameter and have established expressions for them.

Because of the uncertainties about the value of the various parameters involved in these expressions, they are more suited to interpreting experimental ion desorption energy data than for making predictions about such energies, ϵ_{ni} which appears in S is only obtainable by comparing experiment with theory.

The authors point out that the ordered hexagonal array concept on which their calculations are based, probably loses its regularity below $\theta \sim 0.1$ so that this coverage represents a lower coverage limit for the applicability of the theory. A more serious limitation at higher coverage is posed by the uncertainty in the value of the ion charge Z. From the work of Gurney[1] it seems likely that Z is a continuous function of coverage, so that failure to include the coverage dependence of Z in the expressions for f will result in significant error. Barlow and MacDonald estimate an upper limit of $\theta \sim 0.7$ or 0.8 for the applicability of their theory although in view of the preceding considerations concerning Z, this may be optimistic.

In spite of these criticisms, however, this work perhaps represents the most careful attempt to calculate the ion array penetration coefficient for a classical model of ions adsorbed in a hexagonal array.

---

[1] R.W. Gurney, Phys. Rev. 47, 479 (1935)
(Paper 7 of this review series)

WORK FUNCTION CALCULATIONS

Vapour Pressures, Evaporation, Condensation and Adsorption

By I. Langmuir

Review.-Langmuir's contribution to the theory of work function change, ion and neutral desorption energy is made in the form of a semi-empirical procedure which rests upon experimentally determined values of the atom evaporation rate. The theories underlying Langmuir's **1933** paper are as follows:

First, he assumed that the mechanism by which equilibrium is established between vapor and bulk phase of liquids or solids was identical to that for adsorbate and substrate equilibrium. From these considerations, five important equations were derived:

$$\tau = \frac{}{\nu} \tag{1}$$

$$p = A_1 T^{3/2} e^{-b/T} \tag{2}$$

$$\frac{\sigma}{\sigma_o} = \text{constant}_1 \cdot T^{-1/2} e^{b/T} \tag{3}$$

$$\theta = \text{constant}_2 \, \alpha p T^{3/2} e^{b/T} \tag{4}$$

$$\frac{\nu_a}{e} = \text{constant } Te^{-b/T} \tag{5}$$

where

ν_a is atom evaporation rate.

ν_P is the ion evaporation rate.

I is the ionization potential of the adsorbate.

τ is the lifetime of an adsorbed molecule.

σ is the surface coverage of adsorbate in adparticles per unit area. $\sigma = \sigma_1$ when $\theta = 1$.

A is a universal constant.

b is approximately a direct measure of adsorption energy.

δ is the distance traveled by an adparticle before evaporating.

δ_o is the distance between the nearest atoms in the substrate.

a is the condensation coefficient.

θ is the relative coverage.

p, T pressure and temperature.

Secondly, by employing the Gibb's adsorption equation, a two-dimensional version of the van der Waals equation and a two-dimensional version of the Clausius virial equation, Langmuir was able to derive an expression for the spreading pressure F of the adsorbed layer in terms of the average effective dipole moment M on the adparticles, thus:

$$F' = +3.34\sigma^{5/2} M^2 + 1.53 \times 10^{-5} \sigma^2 T^{1/3} M^{4/3} I' \qquad (6)$$

where I' is an integral which is a function of M, T, σ_1, and θ; and F' is that part of the spreading pressure due to the repulsion of the dipoles. F' was obtained from Taylor's experimental work for cesium atom desorption from tungsten so that M was obtainable as a function of surface coverage. Once M was obtained, it was possible to calculate the work function change, $\Delta\phi$, from the Helmholtz equation:

$$\Delta\phi = 2\pi M\sigma \qquad (7)$$

$$\ln (2\nu_p = \ln \nu_a + \frac{e}{kT} (\phi_w - I - \Delta\phi) \qquad (8)$$

By using the Saha Equation (8), in which ϕ_w is the clean tungsten work function, for ion evaporation it was also possible to calculate rates of ion desorption from tungsten from calculated values of $\Delta\phi$. The activation energy of ion desorption is thus $\phi_w - I - \Delta\phi$ less than the neutral desorption energy. Equation (5) gives rate of atom evaporation in terms of the heat adsorption so that if b could be calculated it would be possible to calculate: (1) rates of atom evaporation, (2) rates of ion evaporation, (3) rates of electron emission for comparison with experimental data. Unfortunately, Langmuir was not able to calculate b which is a function of substrate, its surface geometry and adsorbate coverage.

Critique.- Langmuir was able to predict the variation of work function up to $\theta = 0.5$ with the aid of experimentally determined values of the neutral atom desorption rate. Beyond $\theta = 0.5$ his theoretical work function values were less than his experimental ones by an amount which increased with coverage. Moreover, the theoretical curves did not exhibit the maximum

which the experimental ones show.

Langmuir's model is a classical one and as such suffers from the same defect' as other classical treatments in which the adsorbed particles are treated as independent classical elements. The model defects only become manifest at high coverages where the individual adsorbed particles coalesce into a two-dimensional macrocrystal in which the adsorbate valence electrons occupy positions within a new adsorbate valence band. Under these circumstances the classical treatment employed by Langmuir and others is inadequate to account for work function coverage dependencies.

---

[1] J. Ross MacDonald and C.A. Barlow, Jr., J. Chem. Phys., **39**,421 (1963) (Paper 9 of this review series)

Theory of Electrical Double Layers in Adsorbed Films

By R.W. Gurney

Review.- Gurney discussed the conditions under which ionic, covalent and polar bonds are formed, in terms of the work function of the metal, ϕ, the ionization potential, I, and the extent of broadening of the valence level of the adsorbate atom as it approaches the metal surface. He pointed out that if the adsorbate atom possesses an allowed energy level near the Fermi level of the metal, this level will broaden into a band of states as the atom moves closer to the solid. Because the potential barrier between the ion core of the adsorbed particle is like the barrier between the ion cores of bulk atoms, transparent to the free electrons of the metal, an equilibrium concentration of electrons is immediately established in the vicinity of the adsorbate ion core. Whether or not this concentration is sufficient to neutralize the charge or the ion core depends on the relative positions of the metal Fermi level and the center of the new band of states associated with the adsorbate particle. Univalent adsorbates require coincidence of the Fermi and valence levels for neutrality because only in this case is the single charge on the adsorbate ion core balanced by the single electron present in the half-filled adsorbate band. Divalent adsorbate atoms acquire a single positive charge when $I = \phi$, because the half-filled adsorbate band is clearly insufficient to neutralize the doubly charged ion core of the adsorbate. When It. ϕ the univalent adsorbate atom will acquire a positive charge number between 1 and 2. These values of the charge will approach 1 and 2 for the univalent and divalent adsorbates respectively only if an insignificant portion of the adsorbate band dips below the Fermi level. Similar considerations apply in the case of complete neutralization of divalent adsorbates, although of course, 1is now greater than ϕ and only an insignificant portion of the E vs $(\Psi)^2$ curve can remain above the Fermi level. If the valence level of the adsorbate atom falls below the bottom of the conduction band, it will remain discrete when the atom is adsorbed, It may be possible, however, for the atom to acquire a supernumerary electron of which the energy level may be high enough to be broadened by the adjacent metal, Such adsorption will result in formation of a dipole layer with negative end outwards and the extent of the charge will depend once more on the degree of broadening, and the relative positions of the new energy level and the Fermi level.

Critique.- Gurney's work function theory was a valuable contribution to the understanding of the quantum mechanical nature of adsorbed particles. J.A. Becker had argued that cesium was adsorbed on tungsten as separate ions and neutral atoms because ions are obtained when cesium is evaporated from dilute layers of cesium on tungsten. Gurney's theory, however, explained how the adsorbate-bond could also be polar as in the case of polar molecules, In Gurney's view the charge number of the adsorbed particle would continuously vary between 0 and 1 as the work function of the composite cesium-tungsten surface changed.

Although Gurney has given a satisfactory qualitative description of how electropositive elements may result in a lowering of work function of metals, no quantitative estimates were made to check with experiment. Moreover, no mention is made of the fact that the center of the broadened adsorbate band will move up or down as the adsorbate atom moves in close to the metal and may not coincide with the original sharp ionization level of the adsorbate atom when it is at its equilibrium position.

Work Function Variation of Metals Coated by Metallic Films

By E.P. Gyftopoulos and J.D. Levine

Review.- Gyftopoulos and Levine have employed a phenomenological approach to develop an expression for the work function change, $\Delta\phi$, due to adsorption. $\Delta\phi$ was expressed in terms of the work functions of the metallic substrate, ϕ_m, and adsorbate, ϕ_f, and in terms of the adsorbate polarizability a, the number of sites available for adatom occupancy per unit substrate area to form a monolayer σ_f, a dielectric constant ϵ_o, the distance between the centers of the adsorbate atom and the nearest substrate atom, R, the angle 2β between the directions along R for two diagonally opposite pairs of substrate, adsorbate atoms arranged in a square lattice, and the relative surface coverage θ.

No attempt was made to establish the dependence of $\Delta\phi$ on temperature and a dynamic equilibrium situation was assumed for all degrees of coverage.

It was also assumed that the work function barrier $\Delta\phi$ could be resolved into a dipole barrier, $d(\theta)$, due to a surface double layer and into an electronegativity barrier, $e(\theta)$, the functional form of which was fixed by considering experimentally known boundary conditions for the work function behaviour in the coverage range $0 < \theta < 1$. Thus the simplest polynomial expression for $e(\theta)$ that is consistent with the experimental results, $e(1) = \phi_f$ and $(de(\theta)/d\theta) = 0$ when $\theta = 1$ and with the assumptions, $e(0) = \phi_m$ and $(de(\theta)/d\theta) = 0$ when $\theta = 0$ is:

$$e(\theta) = \phi_f + (\phi_m - \phi_f)\, G(\theta) \qquad (2)$$

where

$$G(\theta) = 1 - 3\theta^2 + 2\theta^3 \qquad (3)$$

The dipole barrier was obtained by extending to surfaces, Pauling's statement relating the dipole moment of a molecule of two dissimilar atoms to their difference in electronegativity $(x_1 - x_2)$ i.e.

$$\mu \propto (x_1 - x_2)$$

$M(\theta)$, the dipole moment per adatom was then obtained:

$$M(\theta) = M_o \frac{x(\theta) - x_f}{x_m - x_f} \qquad (4)$$

Using the Gordy-Thomas relation, [Equation (5)] between electronegativity and work function of a pure metal for the composite surface

$$\phi_e = 2.27x + 0.34 \text{ eV} \tag{5}$$

and Equation (3), $M(\theta)$ was related to $G(\theta)$ via:

$$M(\theta) = M_o G(\theta) \tag{6}$$

where M_o is the dipole moment of a single adsorbate substrate dipole at zero coverage. The effective dipole moment $M_e(\theta)$ is diminished by depolarization and Gyftopoulos and Levine used Topping's formula to account for this:

$$M_e(\theta) = \frac{M(\theta)}{1 + \frac{9\alpha\sigma_f^{3/2}\theta^{3/2}}{4\pi\epsilon_o}} \tag{7}$$

$d(\theta)$ is then

$$-\frac{4\pi M_e(\theta)\sigma_f\theta}{4\pi\epsilon_o} = -\frac{\theta G(\theta)\sigma_f M_o}{\epsilon_o\left[1 + 9\alpha\sigma_f^{3/2}\theta^{3/2}/4\pi\epsilon_o\right]} \tag{8}$$

M_o was expressed as the sum of the four perpendicular components of the dipoles, M_{fm}, formed between an adsorbate atom and each of its four nearest substrate neighbors resting in a square lattice underneath the adatom.

$$M_o = 4M_{fm}\cos\beta, \quad \cos\beta = (1 - 1/2\theta_m R2)1/2 \tag{9}$$

M_{fm} was evaluated in terms of the difference in electronegativities between the substrate and adsorbate.

$$M_{fm} = \frac{k(x_m - x_f)}{1 + \alpha/4\pi\epsilon_o R^3} \tag{10}$$

where the denominator has been included to account for self-depolarization,

Using

$$\phi_e(\theta) = e(\theta) + d(\theta) \qquad (11)$$

and the expressions for $e(\theta)$ and $d(\theta)$, we have finally for $\Delta\phi$:

$$\frac{\Delta\phi}{\phi_m - \phi_f} = 1 - G(\theta)\left[1 - \frac{0.765 \times 10^{-18}\,\sigma_f \theta \cos\beta}{\left(1 + \frac{\alpha}{4\pi\epsilon_o R^3}\right)\left(1 + \frac{9\alpha\sigma_f^{3/2}\theta^{3/2}}{4\pi\epsilon_o}\right)}\right] \qquad (12)$$

where $\mathbf{AQ} = \phi_m - \phi_e(\theta)$

Equation (12) predicts either a maximum or a plateau in the variation of ϕ_e with θ when $\theta < 1$ for some adsorbate-substrate combinations. A more rapid change of ϕ_e with θ and a greater value of $\Delta\phi$ are predicted for the more densely packed crystallographic planes.

Critique.-Since the calculation of $\Delta\phi$ by Gyftopoulis and Levine requires prior knowledge of ϕ_f and ϕ_m, the model developed by them predicts only the shape of the $\Delta\phi$ vs θ curve. It makes no prediction about the magnitude of $\Delta\phi$ at $\theta = 1$; neither does it offer any clues about the temperature dependence of **AQ** at constant θ.

Good agreement with Langmuir's data[1] was obtained if his measured value of $\sigma_f = 4.8 \times 10^{14}$ cesium atoms/cm^2 was used. However, this value is an apparent one and is greater than the actual density by the surface roughness factor which is roughly 1.3. Calculated values of $\Delta\phi$ vs θ for adsorption of cesium on the 100, 110 and a rough plane of tungsten do not exhibit the maximum which is now a well established feature of this system for the 110, 211, 100 and 111 planes.[2] The experimental results of reference 2 do suggest though that the maximum is more pronounced for the 110 and 211 planes than for the 100 and 111. In spite of the absence of a maximum in Gyftopoulos and Levine's calculations for cesium on tungsten, Equation (8) of Section I will yield a maximum if an appropriate choice of physically reasonable values of α, R, etc. is made.

The authors of this review are dubious about the assertion that ϕ can be divided into a dipole and an electronegativity barrier. We feel that $\Delta\phi$ can probably be expressed in terms of the dipole barrier or perhaps in terms of the electronegativity barrier but that it is not equal to the sum of both.

---

1 I. Langmuir and J.B. Taylor, Phys, Rev. **44, 423** (1933). Paper 6 this series.

2 R. Gomer and L.D. Schmidt, J. Chem. Phys. 45, 1605 (1966)

Work Function Change on Monolayer Adsorption

By J. Ross MacDonald and C.A. Barlow, Jr.

Review. - MacDonald and Barlow have developed a semiempirical theory of work function change which employs the concepts of effective polarizing field ϵ_1 and effective orienting field ϵ_2. ϵ_1 is a field which would produce the same polarizing effect as that produced by covalent bonding, nonpolar van der waals etc., while ϵ_2 is a fictitious normal field which would produce the actual time average orientation of the permanent dipoles perpendicular to the adsorbent surface. ϵ_1 is defined by:

$$\epsilon_1 = \epsilon_{ni} + E_{eff} \tag{1}$$

where

$$\epsilon_{eff} = 4\pi(q + q_a) + \epsilon_d \tag{2}$$

ϵ_{ni} is the value of ϵ_1 when $\theta = q = 0$. q is the average charge density of adsorbent surface and q_a is the average adsorbate layer charge density. ϵ_d is the depolarizing field. The polarization, P_1, corresponding to ϵ_1 is given by:

$$P_1 = N_v \alpha \epsilon_1 \tag{3}$$

where $N_v = \theta N_s / d$ is the number of adsorbed particles per unit volume in the thickness d. α is the polarizability of an adsorbed species. ϵ_2 is also related to ϵ_{eff}, thus:

$$\epsilon_2 = \epsilon_{n2} + n^{-2} \epsilon_{eff} \tag{4}$$

The n^{-2} factor is introduced because the effect on a given dipole of ϵ_{eff} is screened out by the electronic contribution to the high-frequency dielectric constant. The polarization resulting from ϵ_2 is given by:

$$P_2 = N_v \langle \mu(\epsilon_2) \rangle \tag{5}$$

where $\langle \mu(\epsilon_2) \rangle$ is the time averaged perpendicular component of permanent dipole when the average orienting field is ϵ_2.

$$\langle \mu(\epsilon_2) \rangle = \mu L \left[\left(\frac{\mu}{kT} \right) \epsilon_2 \right] \tag{6}$$

where L is the Langevin function.

The depolarizing field ϵ_d is obtained by summing over all discrete dipoles and is given by:

$$\epsilon_d = - \left[a\epsilon_1 + \langle \mu(\epsilon_2) \rangle \right] \mathcal{A} \delta (\theta N_s)^{3/2} \tag{7}$$

where $\delta = 1$ for the mobile case and $\theta^{-1/2}$ for the immobile. $\mathcal{A}$ is very close to 9 for both square and hexagonal arrays of adsorbate species on the surface.

Now from electrostatic theory we have:

$$4\pi (q + q_a) = F + 4\pi P \tag{8}$$

where F is the average normal field in the layer given by $V_1 = F_d$ and V_1 is the potential difference across the layer.

If q and q_a are unchanged by adsorption, work function change, AV, on adsorption is:

$$AV = -4\pi dP \tag{9}$$

and $P = P_1 + P_2$. From Equation (1) through (9) we have for AV:

$$AV = \frac{-4\pi\theta N_s}{\epsilon_{eff}} \left[a (4\pi q + 4\pi q_a) + a\epsilon_{ni} + \langle \mu(\epsilon_2) \rangle \right] \tag{10}$$

in which

$$\epsilon_{eff} = 1 + a \mathcal{A} \delta (\theta N_s)^{3/2} \tag{11}$$

$$\epsilon_2 = \epsilon_{n2} + (n^2 \epsilon_{eff})^{-1} \left[4\pi (q + q_a) - \mathcal{A} \delta (\theta N_s)^{3/2} \left\{ a\epsilon_{ni} + \langle \mu(\epsilon_2) \rangle \right\} \right] \tag{12}$$

This is an implicit equation for ϵ_2 because of the dependence of μ on ϵ_2. This formation does not hold when the dipoles are formed by adsorbed ions and their images in the conducting adsorbent* In this case, $\langle \mu(\epsilon_2) \rangle$ is replaced by $2Zed_1$, where $2d_1$ is the distance between ion and image. Application of Gauss's law leads to:

$$V_1 = 4\pi (q + q_a) d - 4\pi q_a d_i - 4\pi P_1 d \tag{13}$$

where V_1 is the potential difference across a layer of thickness d from which:

$$V = -4\pi\theta N_s \alpha \frac{\{4\pi(q + q_a) + \epsilon_{ni}\}}{\epsilon_{eff}}$$

$$- 4\pi\theta N_s (Zed_1) \left\{ \frac{2}{\epsilon_{eff}} - 1 - \left(\frac{d}{d_1} \right) \right\} \qquad (14)$$

In the above treatment of work function change, dipole imaging has been neglected; moreover, the ion-image dipoles are treated as ideal.

Note: The corrections which Barlow and MacDonald made to this paper in J. Chem. Phys. 44, 202, (1966), have been incorporated into the above equations.

Critique.-This paper contains an approximate classical treatment of the work function change due to adsorption in which it has been assumed that the image dipoles are assumed to be ideal and in which the imaging in the metal of permanent and induced dipoles have been neglected. Most of the deficiencies of this theory have been pointed out by the authors. Thus the effect of thermal motion in the plane of the adsorbent has been neglected and the only temperature effect on work function is introduced via the Langevin function which contains the permanent dipole term. Additionally, the theory only applies when the adsorbate is adsorbed into a single adsorption state. This may be satisfactory for alkali and alkali-metal adsorption but is clearly unsatisfactory for electronegative adsorption in which adsorption into a multiplicity of states is usually the rule rather than the exception. Although the electropositive adsorbates do not exhibit multiple binding modes, it seems likely that they possess variable charge numbers when adsorbed and that the residual charge on the adsorbate atom is a function of coverage. At low coverages', the binding is probably very nearly ionic for adsorbates such as potassium and cesium while at high coverages it is probably only slightly polar. A consequence of variable, nonintegral charge number Z, is that α, the adsorbed particle polarizability, is also coverage dependent. Since the present theory does not predict how Z and α vary with θ, it is unlikely to account for work function changes over a wide coverage interval even for electropositive adsorbates.

The employment in the theory of ϵ_{n1} and ϵ_{n2}, which are not calculable except by reference to experiment, precludes the possibility of predicting the value of AV at a particular coverage.

The utility of this theory may, however, exist in its capacity to interpret experimentally observed work function changes.

---

[1] R.W. Gurney, Phys. Rev. 47, 479 (1935). Paper 7 this series.

Theory of Work Function Change on Adsorption of Polarizable Ions

By J. Ross MacDonald and C.A. Barlow, Jr.

Review. -In this paper J.R. MacDonald and C.A. Barlow have corrected an earlier semiempirical formulation of the work function change' resulting from the adsorption of an array of ions or molecules. They have extended this treatment to real, instead of ideal image dipoles and have also considered the effect of the images of the dipoles induced in the adions.

From Gauss's law and Equation (33) of reference 1 is derived the expression $\psi_\infty = 4\pi q_a \beta + 4\pi P_1 d + 4\pi\theta N_s \langle \mu(\epsilon_2) \rangle$ where $\beta = d_1$. (See ref. 1) ψ_∞ is the contact potential due to adsorption. Let $\psi_\infty^o = 4\pi q_a \beta$, then $\psi_\infty = \psi_\infty^o + 4\pi\theta N_s \alpha \epsilon_1 + 4\pi\theta N_s \langle \mu(\epsilon_2) \rangle$. Note: ϵ_1 and ϵ_2 were defined in ref. 1. ϵ_d is recalculated here for polarizable ions. The depolarizing field ϵ_d was calculated by considering an infinite plane array of adsorbed elements with one element removed. All other physical properties of the layer were assumed unchanged by the removal. ϵ_d is the field acting at the charge centroid of the removed element and was calculated by Barlow and MacDonald by resolving ϵ_d into five components: ϵ_{di}; i = 1,2,3,4,5. They are:

$$\epsilon_{d1} = \frac{-Ze}{4\beta^2}$$

due to image charge of removed element,

$$\epsilon_{d2} = \frac{\alpha\epsilon_1 + \langle \mu(\epsilon_2) \rangle}{4\beta^3}$$

due to image dipoles of removed element.

$$\left| 1 + \langle \mu(\epsilon_2) \rangle \right| \sigma r_-^{-3}$$

due to contributions from all other surrounding dipoles.

$$\epsilon_{d4} = -\psi_\infty^o / 2\beta \left[0.9117 + (2\pi R_1 / \sqrt{3}\sigma)^2 \right]^{-1/2}$$

due to surrounding nonideal dipoles formed by the adion charges and their images; and finally:

$$\epsilon_{d5} = -\left(\frac{8\pi^3}{3^{3/2}\sigma^2}\right)\left[\frac{a\epsilon_1 + \langle\mu(\epsilon_2)\rangle}{\beta^3}\right]\left[1+\left(\frac{2\pi R_1}{\sqrt{3}\,\sigma}\right)^2\right]^{-3/2}$$

due to the images of all surrounding ideal dipoles. Note that in ϵ_{d4}, ψ_∞^o is defined by $\psi_\infty^o = 4\pi\theta N_s Ze\beta$ and $R_1 = r_1/\beta$ where r_1 is the nearest neighbor spacing of discrete elements.

An equation for ψ_∞ may be derived from these quantities but owing to the dependence of $\langle\mu\rangle$ on ϵ_2 is not explicit.

In this paper Barlow and MacDonald correct an earlier expression[1] for the work function change due to adsorption of polarizable ions and the result is:

$$-\Delta V = \psi_\infty = \frac{4\pi\theta N_s}{\epsilon_{eff}}\left[a\epsilon_{ni} + (2-\epsilon_{eff})\,Ze\beta\right] \qquad (1)$$

An explicit result superior to that in Equation (1) is obtainable from the Equations preceding (1) if the permanent dipole of the adion is assumed to be zero. In this case:

$$\psi_\infty = \psi_\infty^o\left[1 - g(R_1)\right] \qquad (2)$$

where

$$g(R_1) = \frac{1}{2e_1}\left(\frac{a}{\beta^3}\right)\frac{(8\pi/\sqrt{3})R_1^{-2}}{\left\{0.9117 + (2\pi R_1/\sqrt{3}\sigma)^2\right\}^{1/2}} + 1/2 - 2\left(\frac{\beta}{Ze}\right)\left(\beta\epsilon_{ni}\right) \qquad (3)$$

and

$$e_1 = 1 + \left(\frac{a}{\beta^3}\right)\left\{\sigma R_1^{-3} - 1/4 + (8\pi^3/3^{3/2}\sigma^2)\left[1 + (2\pi R_1\sqrt{3}\sigma)^2\right]^{-3/2}\right. \qquad (4)$$

---

[1] J. Ross MacDonald and C.A. Barlow, J. Chem. Phys. 39, 412 (1963) (Paper 9 this review series)

Critique.- This paper represents an added degree of sophistication to the theory presented earlier[1]. The adsorbed ions and their images are no longer treated as ideal dipoles and additionally, the images of induced dipoles are explicitly considered.

The general critique applied earlier to ref. 1 also applies to the theory incorporating the above refinements. As with the earlier theory, the utility of this one lies in fitting the experimental with the theoretical in order to

obtain values of the various parameters appearing in the expression for work function change. The fit obtained was found to be insensitive to choice of ϵ_{ni}. Unfortunately, the experimentally determined values of a and β were considerably smaller than the likely values if the data was fitted over the whole θ range. However, reasonable combinations of the parameters Z, β and a are obtained if fit is restricted to the range $0 < \theta \leq 0.6$.

---

[1] J. Ross MacDonald and C.A. Barlow, Jr., J. Chem. Phys. 39, 412 (1963) (Paper 9 this review series)

Discreteness of Charge Adsorption Micropotentials II - Single Imaging

By C.A. Barlow, Jr. and J.R. MacDonald

Review.- In their paper concerning single imaging of regular arrays of nonpolarizable ions, Barlow and MacDonald consider two problems, the first of which is the calculation (negiecting boundary effects) of the field and potential outside a complete array of ions; this is useful for calculating work function changes. The second, micropotential problem, concerns calculation of field and potential along a line perpendicular to the array through the center of a single vacancy., Ion desorption energies may be predicted from the micropotential results. Polarization effects are accounted for by incorporating a dielectric term E while possible thermal disturbances to the regularity of the adion array are neglected.

Barlow and MacDonald have carefully distinguished between a number of similar though not identical potentials that have been used in the past or which are pertinent for the calculation of work function change and the ion array penetration coefficient f. Thus we have the following local potentials:

Ψ_{aic}	Potential arising from complete adion-image array
Ψ_e	Potential contribution from excess charge $q \pm q_1$ on the electrode
$\Psi_{ic} =$	$\Psi_e + \Psi_{aic}$
Ψ_a	Potential analogous to Ψ_{aic} but pertaining to a lattice with a single vacancy
Ψ	$\Psi_a + \Psi_e$
ϕ_{iz}	Potential due the image of a charge at 0,0,Z
Ψ_i	A hybrid potential $\Psi + \phi_{iz}$
$\Psi_1 = \Psi_{(1)} - \Psi_{(Z)}$	The conventional micropotential

$\Psi_{i1} = \Psi_i(1) - \Psi_i(Z)$ The correct micropotential

$\Psi_2 = \Psi(1) - \Psi(\infty)$

$\Psi_{12} = \Psi_i(1) - \Psi_i(\infty)$

Near-field micropotentials . The enclosed brackets refer to the value of the coordinate Z.

$\Psi_{ai} = \Psi_a + \phi_{iz}$

$\Psi_{ail} = \Psi_a \, t \, \phi_{il}$

where ϕ_{il} is a special case of ϕ_{iz}, calculated for the image at 0,0,-1.

The ion vacancy is situated at the point 0,0,1 where the Cartesian coordinates X,Y,Z are expressed in terms of β, i.e., $X = X/\beta$, $Y = Y/\beta$, $Z = Z/\beta$ where β is the distance of the charge centroid of the adion array from the image plane. X and Y are measured in the adsorbent plane while Z is measured perpendicular to it.

$\Psi_a(Z)$ (and hence Ψ_{aic}) is expressed as an infinite series which, because of its slowly converging nature, must be transformed into a more rapidly converging one in order to facilitate computation. The result consists of a closed form part and a series part which can frequently be neglected especially when $r_1 \rightarrow 0$ (Z fixed) or $Z \rightarrow \infty$ (r_1 fixed), For $r_1/\beta \rightarrow \infty$ (Z fixed), however the series part is dominant and calculation lengthy. Values of Ψ_{aic}/Ψ_∞ have been calculated as a function of Z/R_1 and are plotted in Barlow and MacDonald's paper for various positions in the lattice together with a plot of Ψ_a/Ψ_∞ vs Z/R_1 for one position in the lattice. Also given are plots of Ψ_{aic}/Ψ_∞ vs R_1 for various values of Z. The plots of potential vs Z/R_1 show that the potential curves are nearly linear between Z = 0 and Z = 1 and that the potential rise which takes place as Z/R_1 increases is essentially complete when $Z/R_1 = 1$. The use of Z/R_1 instead of Z removes much of the dependence of curve shape on R_1.

If rearrangement possibilities on adsorption or desorption are excluded, then f is properly calculated from Ψ_∞ and Ψ_{i2}, instead of from Ψ_∞ and Ψ_2 because only Ψ_{i2} includes the contribution to the adsorption energy of the adsorbing ions own image. In this case, f is given by:

$$f' = -\frac{\Psi_{i2}}{\Psi_\infty} = 1 - \left[\frac{\Psi_{ai}(1)}{\Psi_\infty}\right] \qquad (1)$$

The rearrangement contribution to the energy of adsorption is derived from Ψ_{ail}; thus, the total system energy U is given as:

$$U = \left(\frac{Ze}{2}\right) \Psi_{ail}(1)\, N \qquad (2)$$

for unit area and N particles adsorbed. Z is valence of adions. The total system energy change, including rearrangement, when one adion is desorbed is:

$$\Delta U = U(N \mp 1) - U(N)$$

$$= \frac{Ze}{2}\left[\Delta N \Psi_{ail}(1) + N\Delta\Psi_{ail}(1)\right]$$

$$= \frac{Ze}{2}\left[\Psi_{ail}(1) + N\Delta\Psi_{a}(1)\right]$$

$$= \frac{Ze}{2}\,\Psi_{ail}(1)\left(1 + \eta\tau\right)$$

where $\Delta\Psi_a(1)/\Psi_a(1) = \eta\,\Delta N/N = \eta/N$ and $\Psi_a(1)/\Psi_{ail}(1) \equiv \tau$. The rearrangement work is $W = \Delta U - Ze\left[\Psi_a(1) + (1/2)\phi_{il}(1)\right]$ where the negative term is the energy of adsorption in the absence of rearrangement. The last expression simplifies to give

$$W = \left(\frac{Ze}{2}\right)(\eta - 1)\,\Psi_a(1) \qquad (3)$$

Barlow and MacDonald conclude that the rearrangement work W is significant and cannot be neglected for coverages in the range of experimental interest.

Critique. - Barlow and MacDonald have made accurate and comprehensive calculations of the potential anywhere in front of a hexagonal array of non-polarizable ions and along a perpendicular line through the center of a single vacancy in this array by transforming the slowly converging series which appears in the expressions for these potentials into a more rapidly converging one.

They have also obtained an expression for the rearrangement work which takes place on adsorption and show that it cannot be neglected in considering estimates of the ion array penetration coefficient.

Employed in these authors' theories of work function change[1] and ion adsorption energies', the above results enable accurate and rigorous calculations to be made based on the classical model of adsorption of discrete elements into positions in a fixed array.

This model suffers from the limitations outlined by Barlow and MacDonald and which are discussedin earlier critiques in this series of Barlow and MacDonald's classical approach.

---

1 J. Ross MacDonald and C.A. Barlow, J. Chem. Phys. 44, 202 (1966) Paper11 this review series.

2 J. Ross MacDonald and C.A. Barlow, J. Chem. Phys. 39, 412 (1463) Paper 9 this review series.